Summer 7-29-2022

Development of a Decellularized Hydrogel Composite and its Application in a Novel Model of Disc-associated Low Back Pain in Female Sprague Dawley Rats

David Lillyman
University of Nebraska-Lincoln, david.lillyman@huskers.unl.edu

DEVELOPMENT OF A DECELLULARIZED HYDROGEL COMPOSITE AND ITS APPLICATION IN A NOVEL MODEL OF DISC-ASSOCIATED LOW BACK PAIN IN FEMALE SPRAGUE DAWLEY RATS

by

David Lillyman

A DISSERTATION

Presented to the Faculty of

The Graduate College at the University of Nebraska

In Partial Fulfillment of Requirements

For the Degree of Doctor of Philosophy

Major: Biomedical Engineering

Under the Supervision of Professor Rebecca Wachs

Lincoln, Nebraska

July, 2022

DEVELOPMENT OF A DECELLULARIZED HYDROGEL COMPOSITE AND ITS APPLICATION IN A NOVEL MODEL OF DISC-ASSOCIATED LOW BACK PAIN IN FEMALE SPRAGUE DAWLEY RATS

David Lillyman, Ph.D.

University of Nebraska, 2022

Advisor: Rebecca Wachs

Chronic low back pain is a global socioeconomic crisis compounded by an absence of reliable, curative treatments. The predominant pathology associated with chronic low back pain is degeneration of intervertebral discs in the lumbar spine. During degeneration, nerves can sprout into the intervertebral disc tissue and be chronically subjected to inflammatory and mechanical stimuli, resulting in pain. Pain arising from the intervertebral disc, or disc-associated pain, is a complex, multi-faceted disorder which necessitates valid animal models to screen therapeutics and study pathomechanisms of pain.

While many research teams have created animal models of disc degeneration, the translation of these platforms to disc-associated pain models has been limited by an absence of chronic pain-like behavior. Further, the few models which measure disc-associated pain-like phenotypes have been established in mice, which are not amenable to surgical treatment procedures due to their small size. This deficiency drives the need for a new model of disc-associated pain where pain-like behavior is measurable and intervertebral discs are large enough for surgical procedures. These criteria promote rats as the optimal platform for a disc-associated model of chronic low back pain.

Herein, a rat model of disc-associated pain is described that displays chronic pain-like behavior, overt disc degeneration, and nerve sprouting in the intervertebral disc. In addition to the model, a novel method for measuring disc degeneration real-time, non-invasively, is delineated which exhibits remarkable precision and accuracy. Finally, a next generation treatment, derived from decellularized, porcine nucleus pulposus tissue is described which is injectable, thermally fibrillogenic, and cytocompatible. In the rat model of disc-associated pain, this biomaterial restores degenerated disc volume and dramatically decreases pain-like behavior.

In summary, this dissertation describes the development of a method for quantifying degeneration real-time, establishes a rat model of disc-associated pain, and successfully treats disc-associated pain in this model with a next-generation biomaterial.

Acknowledgements

First and foremost, I would like to thank my advisor, Dr. Rebecca Wachs. I would not be the researcher I am today without her guidance and cultivation of my scientific mind. Over the course of five years, Dr. Wachs transformed my perspective and understanding of what it means to be a member of a scientific community. She did this through listening to my interests, understanding my deficiencies, tempering my expectations, and exemplifying the characteristics of an upstanding researcher, teacher, and mentor. I would also like to thank my partner Kari, for supporting me throughout my PhD, in and outside of the research setting. Her patient and caring attitude allowed me to thrive despite a workload that felt overwhelming at times. She also improved how I present information to broader audience through considerate critique of visual and verbal information. I would also like current and past members of the Wachs ONE lab for their continuous support, feedback, and comradery. Further, I would like to thank my committee for providing critical feedback on the work which forms the basis of this dissertation and for their willingness to provide advice on tangential projects. Finally, I would like to thank my friends and family for providing a solid foundation of emotional, intellectual, and physical support throughout the pursuit of my doctoral degree.

Dedication

This work is dedicated to my grandfather, Arthur Rupprecht, without whom, I would have never pursued an advanced degree.

Table of Contents

List of Figures and Tables

List of Abbreviations

μCT – microcomputed tomography

ADAMTS – a disintegrin and metalloproteinase with thrombospondin motifs 5s

AF – annulus fibrosus

ANOVA – analysis of variance

ATP - adenosine triphosphate

BDNF - brain-derived neurotrophic factor

CCL2 - chemokine ligand 2

CCL5 - chemokine ligand 5

CCL7 - chemokine ligand 7

CXCL8 - chemokine ligand 8

LBP – low back pain

cLBP – chronic low back pain

CEP – cartilaginous end plates

CFA - complete Freund's adjuvant

CGRP - calcitonin gene-related peptide

COX - cyclooxygenase

DAPI - 4′,6-diamidino-2-phenylindole

DHI – disc height index

dNP – decellularized nucleus pulposus hydrogel

dNP+ – decellularized nucleus pulposus hydrogel w/ 2.5 mM genipin

DPBS – Dulbecco's phosphate buffered saline

DRG – dorsal root ganglia

ECM – extracellular matrix

FBS – fetal bovine serum

FDA - Food and Drug Administration

FOV – field of view

GAG – glycosaminoglycan

GRF - Gelatine-Resorcine-Formaline

HCl – hydrochloric acid

H&E – hematoxylin and eosin

IACUC – Institutional Animal Care and Use Committee

IASP – International Association for the Study of Pain

IL-1β - interleukin-1β

IL-6 - interleukin-6

IL-8 interleukin-8

IL-17 – interleukin-17

IFN-γ - interferon gamma

IVD – intervertebral disc

LBP – low back pain

L5-L6 – intervertebral disc between the L5 and L6 lumbar vertebrae

MAPK - mitogen-activated protein kinases

MCID – minimally clinically important difference

M-CSF - macrophage colony stimulating factor

MMP - matrix metalloproteinases

MRI – magnetic resonance imaging

NaOH – sodium hydroxide

NF-H – neurofilament-H

NGF – nerve growth factor

NP – nucleus pulposus

NSAID – non-steroidal anti-inflammatory drug

OCT – optimal cutting temperature

OD – outer diameter

P2X3 - P2X purinoceptor 3

PAA - polyacrylic

PBS – phosphate buffered saline

PBST – phosphate buffered saline with tween

PCA – principal component analysis

PCR - polymerase chain reaction

PEG - polyethylene glycol

PFA – paraformaldehyde

PGP9.5 - protein gene product 9.5

PGE2 – prostaglandin E2

ROI – region of interest

rt-PCR - reverse-transcriptase polymerase chain reaction

SB-16 - 3(N,N-Dimethylpalmitylammonio)-propane inner salt

SB3-10 - 3-(Decyldimethylammonio)-propanesulfonate inner salt

SD – sodium deoxycholate

SEM – scanning electron microscopy

SP - substance P

SPARC - secreted protein acidic and cysteine rich

TEM – transmission electron microscopy

TGF-β - transforming growth factor beta

TNF-α – tumor necrosis factor alpha

CHAPTER 1: Introduction

1.1 Preface

This dissertation describes the development of an animal model and therapeutic for disc-associated low back pain. To motivate and contextualize this work, the introduction begins with pain, as pain is the salient factor that drives the need for a therapy. Without pain, no patient would enter the clinic seeking a treatment.

1.2 Pain

The International Association for the Study of Pain (IASP) defines pain as an unpleasant sensory and emotional experience associated with, or resembling that associated with, actual or potential tissue damage [4]. Pain is part of the human experience and assists in weighing, alerting, avoiding and correcting actions that can lead to harm. Despite being variable and individualized, pain duration is diagnostically broken into two categories: acute and chronic. Acute pain is directly linked with tissue damage, inflammation, and the wound healing process [5]. This type of pain is essential for evolutionary survival to avoid danger and facilitate healing.

1.3 Chronic Pain

Chronic pain, or pain which outlasts the wound healing window, contains little evolutionary value, and can be viewed as a disease itself [5]. While there is not complete consensus, generally, pain that exists past the expected healing period (~three months in humans) is categorized as chronic pain [5]. Chronic pain afflicts 20% of people worldwide, imposing a tremendous burden on humankind [5]. In 2010, it was estimated that chronic pain costs the United States $560 - $635 billion each year due to health care

expenditures, days of work missed, hours of work lost, and lower wages [6]. This immense cost exceeds the economic burden of cancer and heart disease combined [7]. A partial explanation for the immense cost is that chronic pain encompasses a myriad of disorders ranging from irritable bowel syndrome to chronic low back pain [5]. However, the majority of pain burden resides in a few top contributors.

1.4 Chronic Low Back Pain

For the last three decades, chronic low back pain (cLBP) has been the leading cause of chronic pain [8-10]. Additionally, cLBP accounts for the greatest number of years lived with disability across all diseases according to the US Burden of Disease Collaborators [11]. Chronic low back pain is defined as pain and discomfort, localized between the bottom of the ribs and the crease of the buttocks, with or without leg pain, that persists beyond three months [12, 13]. This type of chronic pain can range in intensity from a mild nuisance to complete debilitation. The pain and debilitation of those who suffer cLBP imposes costs on society at the individual and economic level.

1.5 Costs of Chronic Low Back Pain

The economic cost of cLBP cannot be understated, with estimates ranging from $19.6 - $118.8 billion a year in direct and indirect costs [6]. Direct costs of cLBP include, physician services, medical devices, medications, hospital services, diagnostic testing, etc. Indirect costs of cLBP include all costs that do not involve monetary transactions but are a result of the cLBP. Examples of indirect costs include work absenteeism, decreased productivity, household caretaking, etc. [14].

Also not to be understated, is the burden of cLBP on those afflicted. A study performed in 2013 indicates patients which develop chronic low back pain display

remarkable increases in self-reported anxiety, depression, and stress [15]. Furthermore, those suffering cLBP report harmful effects on their exercise, sex life, social life, work relationships, and family relationships [16, 17]. Many studies have also reported tangential findings including decreased sleep quality and increased suicide in patients with cLBP [18-21].

Altogether, cLBP imposes costs on society that must be remedied. Part of the difficulty in treating patients with cLBP is that the pain can arise from multiple sources in the low back. This multifactorial nature of cLBP has led researchers to further explore low back skeletal structures in hopes of finding reoccurring sources of pain.

1.6 Etiology of Chronic Low Back Pain

In theory, any innervated structure of the low back is a potential source of cLBP. This knowledge has led research teams to identify fundamental structural sources of pain in hopes of developing therapies for each unique etiology. In the past 20 years, considerable effort has discovered that cLBP in humans arises from pathologies in three types of joints: intervertebral discs (IVDs), facet joints, and sacroiliac joints **(Fig. 1)** [22]. According to these studies, IVDs, facet joint, and sacroiliac joints account for 39%, 15-32%, and 13-18.5% of cLBP prevalence, respectively [23-25]. Observing that the IVD is the strongest associative factor with cLBP, it also represents the therapeutic target with largest potential impact if addressed.

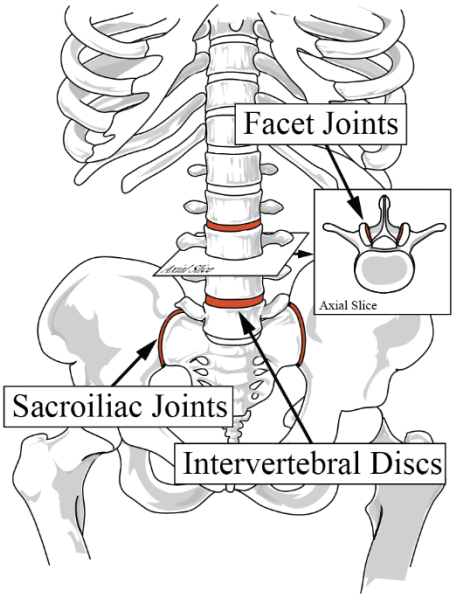

Figure 1. Sources of chronic low back pain

1.7 Disc-associated Pain

CLBP arising from the IVD is associated with many research and clinical terms. These terms include, discogenic pain, degenerative disc disease, painful IVD degeneration (IDD), and disc-associated pain. For the purpose of this dissertation, chronic pain associated with changes in, or arising from, the IVD will be referred to as **disc-associated pain**.

In humans, disc-associated pain is notoriously difficult to diagnose. Clinically it can manifest in a few different phenotypes. The three primary manifestations of disc-associated pain are radicular, non-specific, and axial cLBP **(Fig. 2)** [26].

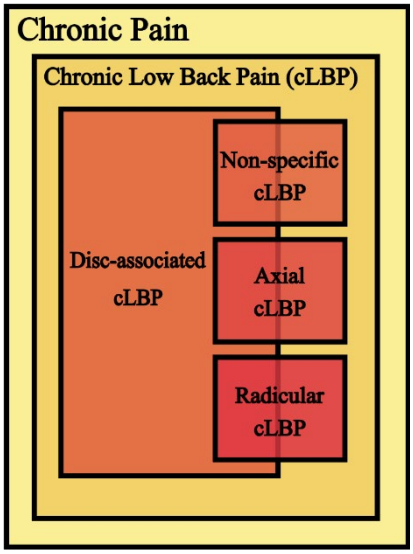

Figure 2. Types of chronic low back pain

Radicular cLBP is the most debilitating form and can involve motor deficits [27]. In most cases, radicular cLBP is caused by nerve root compression as a consequence of IVD degeneration [28].

Non-specific cLBP is cLBP that cannot be attributed to a recognizable pathology [29]. This type of pain is the most difficult to address through a causal approach because it occurs in variable regions of the body and can diminish and increase in intensity. Despite this definition, research groups have reported that disc degeneration increases the odds of presenting with non-specific cLBP by 2.18 [30]. Further, some patients that exhibit non-specific low back pain respond to procedures which alter the IVD, suggesting the IVD can be a source [31, 32].

Axial low back pain is the most common type of cLBP and is defined by pain that only localizes to the low back and occurs in a patient identifiable region on the body [33]. Axial pain is easier to treat than non-specific cLBP because pain production is localizable, and the cause can often be estimated. This type of pain worsens with certain activities like running and even at rest if an incorrect postural position is maintained [34]. Research involving 3097 individuals has indicated that disc degeneration, as measured by magnetic resonance imaging (MRI), increases the odds of self-reported low back pain by 2.24, implicating the IVD as a reoccurring source of pain [35].

The aforementioned pain conditions comprise the three main clinical manifestations of disc-associated low back pain. It should again be noted that these clinical manifestations can be indicative of disc-associated pain but are not guaranteed to be. For example, radicular low back pain can be caused by zygapophyseal joint damage, non-specific pain by osteoporosis, and axial pain by ligament tears [22, 23].

The work detailed in this dissertation focuses on axial low back pain which originates in IVD tissue. This type of disc-associated pain is thought to arise from nerve fibers which aberrantly sprout into degenerated IVD tissue. It should also be noted that the term "disc-associated pain" is not used clinically but rather is a scientific term used as a descriptor of the pain source, rather than the clinical pain phenotype.

1.8 How Disc-associated Pain is Diagnosed

Disc-associated low back pain was first described in 1970 by H.V. Crock [36]. In this seminal work, Crock described clinical features like deep-seated and dull aching back pain, referred pain, decreased physical activity, and restricted spinal movement as

characteristics of disc-associated pain. These observations hold true today and are often first line indicators a patient is experiencing disc-associated cLBP.

Today, patients which enter the clinic complaining of low back pain may be asked to complete various pain, functional and IVD morphological assessments to ascertain a diagnosis. The first and most important data collected at the clinic are body maps which allow a patient to describe the location and duration of pain. Body maps have become increasingly important in the last few years with the emphasis on individualized treatment [37]. Additionally, cLBP patients may be asked to complete questionnaires which measure various impacts of cLBP [38, 39]. These questionnaires assess both the intensity and location of pain and how the pain affects life activities like socialization, employment, etc. Functional tests employ static and dynamic measures of trunk muscle activation during movement to quantify trunk strength, flexibility, and endurance. These aspects of the trunk are measured because they are known to be impaired for many people with chronic low back pain [40-42]. The most widely used method for evaluating patient IVD morphology in the clinic is imaging via MRI [35]. This assessment is performed to determine if spinal changes, especially IVD degeneration, are present and could be a source of pain. MRI images are used to determine degenerative changes in the IVD by identifying abnormalities like a loss of nuclear signal, decreased disc height, high-intensity zones, and changes in disc contours. Interestingly, not all patients that exhibit overt signs of disc degeneration suffer cLBP [35]. This simple fact makes a diagnosis of disc-associated pain based on functional, self-reported, and IVD morphological data clinically inadequate.

Should patients screen positively across functional, self-reported, and IVD morphological measures of cLBP, further diagnosis may be pursued to determine if the IVD is the source of pain. Four associations have created diagnostic criteria for disc-associated pain [43]. All associations require intradiscal provocation for a diagnosis except for the IASP which permits anesthetization of the target disc as an alternate means of identifying the disc as the pain source. Intradiscal provocation requires insertion of a probe into the disc and injection of a contrast or pressure inducing agent to evoke pain concordant with the patient experienced low back pain. However, in recent years, this method has come under increased scrutiny because it introduces an annular tear, which is known to disrupt the function of the disc and may accelerate IVD degeneration [44, 45]. Thus, the majority of patients who experience chronic pain caused by IVD degeneration are diagnosed with axial or non-specific low back pain rather than disc-associated pain because the source cannot be directly identified.

1.9 How Disc-associated Pain is Treated

For patients diagnosed with disc-associated pain and those suffering chronic low back pain suspected to be disc-associated, four different treatment modalities can be used to alleviate suffering. These four interventions come in the form of non-steroidal anti-inflammatory drugs (NSAIDs), non-pharmacological treatments, opioids, and surgery.

NSAIDs are the first-line drug option for patients suffering disc-associated pain because of their low potential for abuse, tolerability, and cost [46]. Further, these drugs work systemically, increasing the chance they have to affect the patient pain state should the pain be non-specific. NSAIDs are anti-inflammatory drugs that exert their effect by inhibiting cyclooxygenase-1 and/or 2 (COX-1 and COX-2) [47]. In the context of disc-

associated pain, NSAIDs indirectly suppress the activation thresholds of pain-sensing nerve fibers in and around the degenerated IVD. For acute alleviation of low back pain, over-the-counter drugs like aspirin, and acetaminophen are commonly recommended [48]. Should these NSAIDs fail, selective COX-2 inhibitors like diclofenac, piroxicam, meloxicam, and celecoxib can be prescribed [49]. COX-2 inhibitors can be administered at higher effective doses than unselective NSAIDs because they pose less risk for gastrointestinal bleeding and other side effects. Unfortunately, all NSAIDs are palliative fixes for low back pain and eventually result in gastrointestinal toxicity when chronically administered. Due to this limitation, NSAIDs are recommended only for short treatment and at the lowest dose possible.

Non-pharmacological treatments may also be employed as first-line treatments for chronic low back pain. Non-pharmacological treatments for cLBP include acupuncture, exercise therapy, back schools, massages, behavioral management, physical therapy, and more [50]. Unfortunately, systematic reviews have indicated that only highly managed, combinatorial non-pharmacological treatments, like biopsychosocial rehabilitation can have any effect on the management of low back pain [51, 52]. However, because these treatments are non-invasive, cheap and have shown efficacy in combination with drug treatments like NSAIDs, they are still recommended as a first course of treatment [53].

If pain persists despite non-pharmacological and NSAID treatments, opioids may also be prescribed for cLBP. This class of drug has the most powerful analgesic capacity and is widely used for treatment of severe pain [54]. Opioids include morphine, fentanyl, oxycodone, hydrocodone, and more. All opioids exert their effect by acting on G protein-coupled receptors in the central and peripheral nervous system [55]. In this manner,

opioids act as pain signal modulators rather than direct actors like NSAIDs [56]. Opioids can be effective in treating disc-associated low back pain in the short-term, allowing patients to experience immediate alleviation after treatment [57, 58]. However, like NSAIDs, opioids are not recommended for long term treatment of pain. Opioid prescription is avoided because these drugs have high potential for abuse and are the single cause of the opioid crisis, which has plagued the United States for the last two decades. In 2015 alone, 30,000 U.S. citizens died from opioid overdose [59]. For this reason, physicians have become increasingly wary of prescribing opioids for any type of chronic pain, especially low back pain.

The last-line option for patients suffering disc-associated cLBP is surgical intervention and is particularly common for disc-associated radicular cLBP. The predominant surgical procedure applied to treat disc-associated low back pain is surgical fusion [50, 60, 61]. In 2014 alone, 347,102 spinal fusions surgeries were completed [62]. Fusion surgeries operate on two paradigms, either inducing spinal fusion between spinal facets using autologous bone or by removing degenerated IVD tissue and fusing the IVD space with a spacer and autologous bone [63]. Both options are highly invasive and ramifications include fusion failure, increased chronic pain, adjacent spinal segment degeneration, infection, etc. [64]. Despite potential complications, interbody fusions have risen as the gold standard for treating chronic disc-associated pain that does not respond to other therapies [50].

In summary, treatments for disc-associated pain that are non-invasive are inadequate long-term and invasive treatments predispose patients to a myriad of surgical complications and do not consistently alleviate pain. With this knowledge, a new

generation of therapeutics will be necessary for effective long-term treatment of this disorder. To understand what treatments could be viable, it is crucial to understand the anatomy of the IVD in a healthy and degenerated state.

1.10 Anatomy of the Intervertebral Disc

The IVD is a tripartite organ composed of a nucleus pulposus, annulus fibrosus and two end plates **(Fig. 3)**. The nucleus pulposus (NP) sits at the core of the IVD and is circumferentially enwrapped by the annulus fibrosus (AF), both of which interface with adjacent vertebral bodies on the top and bottom through cartilaginous end plates (CEPs). The interplay between these constituents allows the IVD to function as a dynamically responsive viscoelastic spacer between vertebral bodies, providing rotational and translational freedom to the spine.

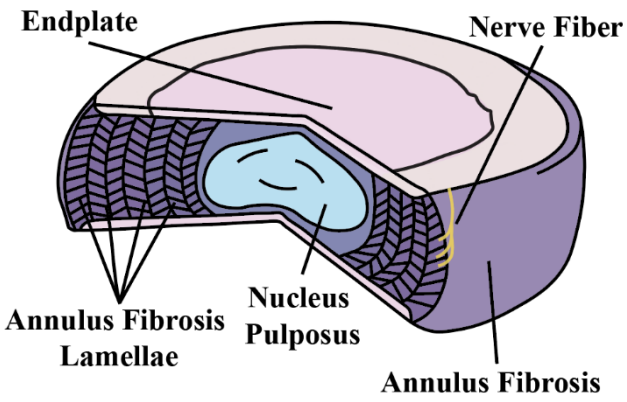

Figure 3. Overview of a healthy IVD

The core of the disc, the nucleus pulposus, forms from the notochord during embryogenesis and in a healthy state is entirely aneural and avascular [65]. At birth, the NP is highly cellularized, but by late adulthood the NP exhibits sparce cellularity [65]. The low cell density is thought to result from an absence of vasculature in the NP, which limits nutrient and oxygen abundance as the tissue grows [66]. In fact, adult NP cells contain few mitochondria, implying they rely almost entirely on anaerobic pathways to generate energy [67]. To maintain the structure of the NP, resident NP cells produce proteoglycans rich with glycosaminoglycans (GAGs), and collagen I and II [65]. Attached to a core protein backbone,

glycosaminoglycans (GAGs) like chondroitin sulfate, dermatan sulfate, heparan sulfate, and keratan sulfate comprise 30-50% of the NP dry weight [65]. These GAGs attract water into the NP matrix because they are strongly polar and negatively charged. This characteristic of GAGs causes immense swelling pressure in the NP allowing it to retain water and resist compressive loading [68, 69]. Furthermore, GAGs in the NP, like chondroitin sulfate, impart neuroinhibitory properties, disallowing nerves to aberrantly grow into the NP tissue [70]. In addition to GAGs, the NP contains collagen II along with lesser amounts of collagen IX and XI. Collagenous proteins account for 20% of the NP dry weight [65]. These proteins form the basis of the NP extracellular matrix and provide anchoring points for proteoglycans.

The annulus fibrosus compliments the NP by exhibiting remarkable elasticity and resistance against radial expansion. The AF is a highly organized structure, containing concentric rings of collagen that alternate at 30-degree angles to form a cylindrical-like ply structure that enwraps the NP [65]. The AF can be functionally split into two regions, the inner and the outer AF. The inner AF has large amounts of collagen I and II and interfaces with the NP and cartilaginous endplates. During compressive loading, the inner AF is predominantly subjected to compressive loads [65]. The outer AF is mainly composed of collagen I and is innervated and vascularized in its outermost layers [71] Under compressive loading, the inner AF is subjected to radial tensile stress as the NP and inner AF expand within its boundaries [65]. In a relaxed state, collagenous fibers in the outer AF appear as wavy or crimped and provide little resistance to motion [65]. However, in a strained state, collagenous fibers of the outer AF straighten and resist further displacement. This characteristic of the outer annulus fibrosus imparts

extraordinary rotational freedom while robustly disallowing motion that would be damaging.

The IVD is capped on the caudal and cephalic ends by cartilaginous end plates. The CEPs are thin sheets of hyaline cartilage that interface the NP and inner AF with vertebral bone [65]. The CEPs are cellularized by chondrocytes which maintain the collagen II and aggrecan-rich extracellular matrix [65]. At birth, blood vessels may traverse from the adjacent vertebra into the CEPs, providing a heavy supply of nutrients [65]. With age, these vessels disappear which has led researchers to hypothesize that this change is involved with the dramatic decline in NP cellularity with age [72]. With or without the presence of vasculature, the core function of the CEP is to permit diffusion of nutrients to the NP through channels in its central region.

1.11 Mechanics of the Intervertebral Disc

The primary function of the IVD is to provide rotational and translational degrees of freedom to the spine. In a relaxed state, the abundant GAGs in the NP impart a continuous swelling pressure which produces axial and radial strain which must be countered by the AF to maintain function [73]. In the simplest sense, the NP can be thought of as a partially squeezed sponge in a sink of water and the AF as rubber bands which wrap the sponge and keep it from completely rehydrating.

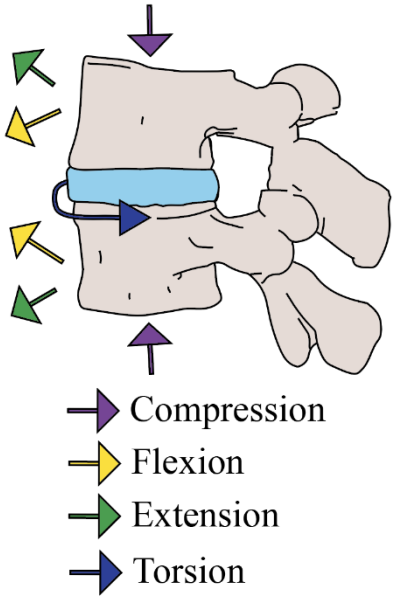

Figure 4. Overview of spinal mobility permitted by the IVD.

As part of loading, the IVD is subjected to compression, flexion, extension, and torsion **(Fig. 4)**. The IVD experiences significant

compressive pressure in all upright activities [74]. During a compression event, the NP is pressurized and immediately expands radially. As a compensatory mechanism for the expanding NP, the outer AF then bulges outward and the collagen fibers in the lamellae sheets straighten and align to provide equal and opposite resistance. When loading is prolonged and exceeds the swelling pressure of the NP, water may gradually exude from the NP. As the NP depressurizes due to water loss, it loses its ability to bear load, subjecting the AF to compressive forces which can be deleterious [65]. However, some NP depressurization is part of the healthy functioning of the IVD as it facilitates diurnal nutrient cycling by allowing the NP to pull in nutrient laden water at rest, during sleep [65].

IVDs of the spine are subjected to flexion and extension any time the spine is not in a neutral, well-aligned, position [65]. Contrasting pure compressive loading, where the AF expands radially to resist the expansion of the NP, flexion and extension result in asymmetric AF loading patterns. For example, during an exercise that involves spinal extension, the posterior AF is compressed while the anterior AF is in tension. Likewise, during lateral bending, the side of AF in the direction of the bending is subjected to compressive pressures while the side opposite to the bending is subjected to tension. It should be acknowledged that the IVD exhibits a remarkable capacity to bear spinal loading in these abnormal states. For instance, in the case of a moderate deadlift (200 – 350 lbs.), lumbar IVD are subjected to axial compressive loading in excess of 1,500 pounds, shear loading in excess of 330 pounds, and internal pressures which can exceed 2000 pounds per square inch i.e., commensurate with a pressure washer [75-77].

The final important mechanical characteristic of the IVD is its rotational freedom [65]. Torsion is imparted on the IVD during twisting motion of the trunk. When quantifying torsional mechanics of the spine, it is easier to understand when speaking about spinal motion segments, i.e., the IVD and two adjacent vertebral bodies. The maximum rotational freedom of individual motion segments is 1°–3° [65]. While this may not seem sufficient to allow the trunk rotational freedom experienced by most humans, the presence of multiple motion segments at the cervical, thoracic, and lumbar spinal levels endow the spine with significant overall rotational freedom [78]. Similar to compressive loading, the annulus fibrosus is ultimately responsible for resisting normal and deleterious strains via alignment and elongation of collagenous fibers in the lamellae.

In summary, healthy IVDs display incredible mechanical properties, permitting compression, flexion, extension, and torsion of the spine. Without IVDs, the spine would be completely rigid and would be incompatible with essentially all movement associated with natural human mobility. However, spinal stability and mobility are not maintained by the presence of IVD tissue alone. Ample nerve supply in the outer AF and surrounding ligaments is required for coordinating musculature control over the spine and monitoring the health of the disc.

1.12 Innervation of the Intervertebral Disc

In general, the IVD is described as both avascular and aneural [65]. In reality however, the healthy IVD is innervated and vascularized in the outermost rings of the AF [71]. The majority of nerves in the disc are nociceptive, i.e., they are nociceptors, which means they are responsible for initiating signals to the brain which manifest as pain [79]. To understand how disc-associated pain develops, it is vital to understand where nerves

in the disc originate from, how they behave, how they can change, and how nociception becomes pain.

1.13 Neuroanatomy of Dorsal Root Ganglia

Nerves in the IVD predominantly originate from dorsal root ganglia [80, 81]. Dorsal root ganglia (DRG) are spherical clusters of neuronal and support cells which exist bilaterally at each level of the spine [82]. These clusters represent the junction between the central and peripheral nervous system. The core function of the DRG is to transmit and modulate sensory information from the periphery to the central nervous system where it is further processed and propagated to the brain [82]. The predominant type of neuron found in the DRG is a pseudounipolar sensory neuron, meaning a single axon extends from the cell body and bifurcates into a dendritic end, which extends to a peripheral site, and an axonic end, which inserts into the dorsal horn of the spinal cord **(Fig. 5)** [83]. In general, all DRG sensory neurons functionally behave according to the same paradigm. In this paradigm, the dendritic end exists in a peripheral site where it can detect a specific set of stimulants like chemicals, heat, vibration etc. When a stimulant exceeds a certain threshold, an action potential is initiated and propagates to the axonic end where it is detected by interneurons in the spinal cord [84]. This all or nothing response allows neurons to effectively transmit sensory information from peripheral tissue to the central nervous system. DRG neurons can come in multiple phenotypes,

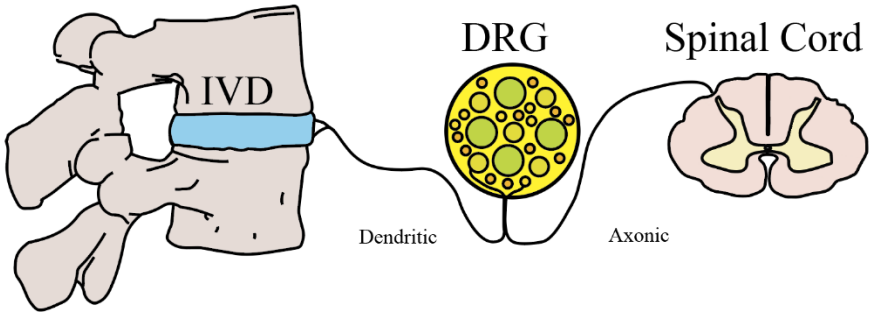

Figure 5. Overview of DRG anatomy and innervation

tailored for detecting different types of sensory information. These phenotypes include large neurons, intermediate neurons, small non-peptodergic neurons, and small peptodergic neurons [79].

Large neurons facilitate conscious and subconscious processing of joint positioning or proprioception [85]. For the spine, this perception is critical to coordinate proper musculature control.

Intermediate neurons are a subset of DRG neurons that are mechanosensitive [79]. While generally only responsive to vibration and touch, in the disc these neurons serve as pain sensing fibers for harmful mechanical stimuli that can result in permanent tissue damage [86]. Additionally, these fibers have demonstrated capacity to phenotypically switch and express substance P (SP), which can contribute to inflammatory pain hypersensitivity [87].

Small non-peptodergic neurons are a subset of sensory neurons that respond to noxious chemical and mechanical stimuli, especially under inflammatory conditions [79, 88, 89]. These neurons are primarily responsive to mechanical stimuli although they have been shown to increase their responsiveness by 4-fold to noxious chemical stimuli after inflammation is induced [88, 90]. Also, the presence of P2X purinoceptor 3 (P2X3), a receptor for adenosine triphosphate (ATP), on these neurons implicates them in the sensation of tissue damage because cells release physiologically high concentrations of ATP under acute and inflammatory stress [91].

Small peptodergic neurons, which utilize small signaling peptides like calcitonin gene-related peptide (CGRP) and substance P (SP), comprise the majority of nociceptors that involve pain signaling as well as the majority of nociceptors in the IVD [79]. These

nociceptors can be responsive to either heat, cold, mechanical, chemical or a combination of stimulants [92]. In the IVD, peptodergic neurons are the primary source of inflammatory pain because they dynamically interact with the inflammatory milieu [93]. Additionally, the peptides released by this neuronal subclass are known to act as inflammatory agents implicating them as part of the causal loop in disc-associated cLBP [94, 95].

In sum, nerve fibers in the disc which contribute to disc-associated pain are small diameter fubers, especially small diameter peptodergic neurons. These nerve fibers can be activated by a wide range of stimulants and their signaling can be further augmented by a phenomenon known as sensitization.

1.14 Sensitization of Dorsal Root Ganglia Neurons

Regardless of the neuronal subclass, all sensory neurons can have their activity modulated by a phenomenon called sensitization [96, 97]. Under the sensitization paradigm, neurons break from “same stimulus-same response” behavior and dramatically alter their activity. When sensitized, nociceptive neurons may lower firing thresholds, increase receptive fields, phenotypically switch their stimulant response profiles, spontaneously activate, and increase firing amplitude [96, 97]. The primary factors which drive sensitization are chemical mediators released by cells around neuronal fibers and cell bodies. These mediators include, but are not limited to, ATP, PGE2, nerve growth factor (NGF), macrophage colony stimulating factor (M-CSF), interleukin-6 (IL-6), interleukin-1β (IL-1β), tumor necrosis factor alpha (TNF-α), CGRP, and SP [97]. Sensitization via these factors can occur in various manners including phosphorylation of signal amplifier molecules, increasing ion channel transcription, and increasing ion

channel externalization [98]. Regardless of the way which sensitization is produced, the end result is a dramatic increase in responsiveness to stimulants. Nociceptor hypersensitivity caused by sensitization is thought to be a key source of chronic pain [99].

1.15 How Nociception and Sensitization Produce Pain

As defined by the IASP, pain requires emotional processing. For this reason, pain and nociception are distinct from each other. Nociception strictly relates to the neural detection of a stimulus that, if eventually passed into the brain, would result in pain. Similarly, sensitization does not indicate an amplified pain state. The analogous verbiage for cognitively manifested sensitization is pain hypersensitivity. For disc-associated axial cLBP, pain is thought to arise from sensitized nociceptors in and around degenerated disc tissue.

1.16 Degeneration of Intervertebral Discs

In a healthy state, IVDs are not sources of nociception nor pain due to their sparse innervation. Unfortunately, in all humans, IVDs do not remain in a healthy state over the course of life. Intrinsic healing mechanisms like the innate immune response are ill-equipped at repairing such a complex and isolated tissue like the IVD [100]. On account of this, IVDs, especially those in the low back, suffer overt degeneration over the human life span **(Fig. 6)**.

1.17 Pathophysiology of Intervertebral Disc Degeneration

IVD degeneration onset can result from natural aging or trauma and can be accelerated by environmental and genetic factors like smoking and collagen gene polymorphisms, respectively [101-103]. Irrespective of the exact cause, degeneration onset is typified by metabolic and mechanical stresses on disc cells, incompatible with tissue homeostasis that result in inflammation. Evaluation of human IVD tissue throughout the human lifespan has implicated TNF-α to be the primary initiator of disc degeneration [104]. This canonical pro-inflammatory cytokine and its cognate receptors are expressed in healthy IVD tissue and are upregulated with age and degree of degeneration [105]. Interestingly, multiple research groups have suggested that TNF-α is not the key cytokine in degenerative signaling but rather stimulates the production of IL-1β which is the master regulator of IVD catabolism [104, 106-108]. IL-1β facilitates production of inflammatory cytokines like IL-6, interleukin-17 (IL-17), interleukin-8 (IL-8), interleukin-2 (IL-2), and interferon gamma (IFN-γ). These factors in turn stimulate the creation of growth factors like nerve growth factor (NGF), brain-derived neurotrophic factor (BDNF), and transforming growth factor beta (TGF-β) to combat the ongoing catabolism [109].

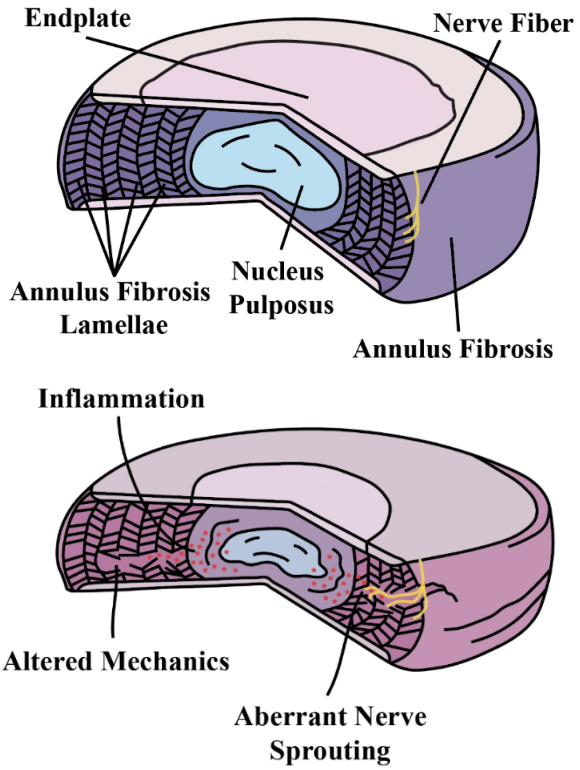

Figure 6. Overview of a healthy and degenerated IVD

Furthermore, this inflammatory soup drives the translation of chemotactic proteins like chemokine ligand 2 (CCL2), chemokine ligand 7 (CCL7), chemokine ligand 5 (CCL5), and chemokine ligand 8 (CXCL8) which recruit innate and adaptive immune cells like macrophages and T-cells, respectively [108, 110]. Additionally, two main classes of matrix degrading enzymes are produced, disintegrin and metalloproteinase with thrombospondin motifs 5s (ADAMTSs) and matrix metalloproteinases (MMPs). ADAMTSs like ADAMTS-5 are increased in response to the production of cytokines like IL-1β and degrade proteoglycans in the extracellular matrix, particularly in the NP [111]. Proteoglycan loss decreases the ability of the NP to retain water and thus resist compressive loading. Further, MMPs like MMP-2 are increased in response to production of cytokines like IL-1α and TNF-α and hydrolyze collagen in the extracellular matrix [112]. TNF-α and high amounts of TGF-β also shift NP cells to produce collagen I and decrease collagen II leading to net fibrosis. Through the concerted action of ADAMTSs and MMPs, tissue properties may decline to the point at which the disc cannot sustain loading, leading to NP herniation and annular tears. Overall, this catabolic process can persist for decades leading to aberrant nerve sprouting, and altered disc mechanics, ultimately culminating in chronic low back pain.

1.18 Innervation of Degenerated Intervertebral Discs

Amid the degenerative process, three factors enable ingrowth of nociceptive nerve fibers deep into the IVD. These factors are, a loss of neuroinhibitory GAGs, formation of annular fissures, and the production of neuronal growth factors [95, 103, 113]. The loss of neuroinhibitory GAGs like chondroitin sulfate results from the activity of catabolic enzymes, like ADAMTSs, which breakdown GAG-containing proteoglycans [106, 111,

114]. Annular fissures provide a route of minimal resistance for nerves to sprout and elongate. In fact, in humans, a preponderance of nerves is routinely observed in degenerated IVD tissue around sites of granulation and fissure [115, 116]. Finally, factors which stimulate nerve ingrowth, like NGF and BDNF, are constitutively expressed by human IVD cells amidst degeneration [117]. These factors strongly promote growth of nerves up the growth factor gradient, causing nerve fibers to penetrate the disc.

Evidence of aberrant nerve penetration has been observed repeatedly in IVD samples taken from human donors [115, 116, 118-122]. Shinohara et al. were first to visualize nerves within human degenerated disc tissue [122]. In this seminal work, nerve fibers were observed deep within the annulus fibrosus tissue, particularly around granulation tissue deposited within annular fissures. These findings have since been replicated by a number of independent research teams [118, 120, 121]. Additionally, biopsies taken from painful and non-painful IVDs exhibit significantly more nerve fibers, suggesting the aberrant penetration of fibers into degenerated tissue is the basis of disc-associated pain [120]. More recently, the type of nerve fiber within the disc has been interrogated using immunohistochemistry. This analysis has discovered that most aberrantly penetrating fibers are of the small peptodergic type [93]. However, despite a large body of literature demonstrating nerve fibers in degenerated IVD tissue, consensus that this pathology drives disc-associated pain has not been reached. For this reason, more work must be accomplished to elucidate the relationship between aberrant disc innervation and the presence and intensity of disc-associated pain.

1.19 Mechanical Properties of Degenerated Intervertebral Discs

Motion segments containing degenerative IVDs present with mechanical properties distinct from healthy segments, namely, neutral zone expansion and decreased torsional resistance [123]. The neutral zone is the range of displacement a motion segment can pass with minimal resistance and can be quantified in all planes and rotationally. Evidence in the literature indicates that neutral zone expansion may be due to a breakdown of the interconnected collagen lamellae in the annulus fibrosis [124]. Decreased resistance to torsional strain also results from compromise of the collagenous AF macrostructure. Due to tissue catabolism, hoop stresses are not passed uniformly through the rings of collagen, leading to tissue destruction and ultimately disconnection [125]. This compromise of macrostructure results in a feedback loop where increasing tissue destruction causes the remaining healthy tissue to bear a higher load, resulting in mechanical overload [125]. These facets of IVD degenerative mechanics along with an understanding of the irregular innervation of degenerated discs draw attention to the contribution of altered disc mechanics in pain generation.

1.20 Nociceptive Sources of Disc-associated Pain

Curiously, not all patients who present with clinical signs of disc degeneration experience chronic low back pain [35]. This fact has led researchers to further explore the pathogenesis of disc-associated pain. Fundamentally, disc-associated pain can manifest from three sources: nerve root compression, inflammatory factors, and mechanical factors.

Nerve root compression results in neuropathic pain [126]. The primary source of neuropathy in context of disc-associated pain is nerve root compression due to disc height

loss, which manifests clinically as radicular pain [28]. Nerve root compression can be surgically addressed by removing bone around the intervertebral foramen to alleviate compression [127]. Interestingly, nerve root compression may be treatable with a therapeutic which restores disc volume, although this concept is largely unproven.

Inflammatory factors are abundant in the degenerative process and act on non-peptodergic and peptodergic nerve fibers. For example, molecules like ATP, produced by inflammatory cells, bind purinergic receptors on non-peptodergic nerves leading to nociception [91]. Further, CGRP, which increases in abundance during degeneration, can bind receptors on peptodergic nerve fibers also leading to nociception [128]. Activation of these nerve fibers is thought to drive the dull chronic aching pain reported by disc-associated pain patients [129]. Supporting this notion, systemic treatment with anti-inflammatory drugs, like NSAIDs, can prove effective short-term in treating disc-associated pain [46, 130].

Evidence of the role of mechanical factors in disc-associated pain can be observed in the outcomes of current treatments. The treatment for disc-associated pain with highest success rate short-term is surgical fusion [60, 61, 131, 132]. Surgical fusions are routinely performed by rigidly adjoining adjacent vertebral bodies thereby introducing stability to a degenerated motion segment. In select cases, fusion patients report excellent results after surgery implying that stabilization alone can be sufficient in alleviating disc-associated pain [133]. Another, albeit less effective, treatment for low back pain are spinal stability exercises. Exercise increases the strength of core muscles like the multifidus and transverse abdominus imparting more musculature control over spinal movements. Studies have demonstrated significant pain remission short term with exercise regimes

focused on increasing multifidus cross-sectional area indicating muscular stabilization of the spine can reduce pain and disability [134, 135]. This evidence in combination with localization of aberrant sprouting along fissures provides ample evidence that altered spinal mechanics drives at least part of pain emergence in those suffering disc-associated low back pain.

These data support inflammation and altered disc mechanics as the primary contributors to disc nociception and in turn, chronic disc-associated low back pain. Knowing this, a therapeutic which addresses one or both factors stand to improve disc-associated pain through causal mechanisms. To date, the only therapies which get close to this level of efficacy are highly invasive surgical procedures. The purpose of the work described in this dissertation was to engineer a minimally invasive therapy for low back pain that was causally targeted. To accomplish this goal, a method for monitoring disc degeneration real-time was established, an animal model of disc-associated pain was created, a therapeutic was engineered, and finally, the therapeutic was evaluated *in vitro* and *in vivo*.

CHAPTER 2: Motivation

Treatments for spinal disorders have been in development since as early as the 1890s. One of the first procedures ever described was by W.T. Wilkins who removed a hernia and fused two vertebrae using carbolized silk suture [136]. Since this time, spinal procedures have been refined and today, the gold standard, spinal fusion, uses patient tissue and metal alloys to accomplish spinal fusion. In light of the drawbacks of surgical fusions and inadequacy of other treatments, research teams around the world have been working to create alternative next generation therapeutics like antibody therapies, gene

therapies, injectable biomaterials, etc. [50]. However, because these treatments are not simply constrained to inert metal alloys for fabrication, they pose more severe risk for side effects. To this end, animal models of disc degeneration and disc-associated pain have become increasingly important to evaluate the pathogenesis of disc-associated pain and screen treatments.

2.1 Models of Intervertebral Disc Degeneration

The earliest model of disc degeneration was described in 1932 and entailed an annulotomy in New Zealand white rabbits [137]. Since this time, animal models of disc degeneration have been created in mice, rats, pigs, chondrodystrophic dogs, non-chondrodystrophic dogs, goats, sheep, cows, macaques, baboons, and rhesus monkeys [138]. The induction method for disc degeneration is also highly varied including both spontaneous and induced approaches. Spontaneous mechanisms for creating disc degeneration include natural aging, specific diets, transgenic secreted protein acidic and cysteine rich (SPARC) null breeding, genetic knockout of collagen genes, and transgenic induction of HLA-B27 and human β2m genes [138]. Methods for inducing disc degeneration in animal models include, stab incision, tail bending, facet removal, cyclic compression, chronic compression, NP aspiration, chemonucleolysis, nucleotomy, cytokine injection, complete Freund's adjuvant (CFA) injection, annulotomy and more [138-140]. However, these models are only useful for elucidating pathomechanisms of disc degeneration because they do not quantify pain.

2.2 Models of Disc-associated Pain

All models of disc degeneration have pros and cons, but a massive limitation to most models is the inability to assess pain. In humans, pain, i.e., nociception

contextualized with emotional processing, can only be measured via cognitive communication. Because animals are incapable of communicating in sophisticated ways, researchers must be wary when describing pain in animals [141]. For this reason, human recognizable signs of pain in animals are referred to as pain-like behaviors. This careful terminology avoids anthropomorphizing animal behavior in an attempt to be more scientifically sound. Likewise, therapies administered to animals cannot be described as analgesics but rather must be denoted as anti-nociceptive, because analgesia relates to the suppression of pain.

Primates are the most ideal animal for studying disc-associated pain because their anatomy and physiology is closely analogous to humans and their high cognitive ability permits means for robust pain-like behavior evaluation [142-144]. Unfortunately, primates are expensive, and their cognitive abilities raise ethical questions as to the degree of suffering that is reasonable to induce in animals for the purpose of researching therapies to alleviate human suffering [145]. For this reason, primates are reserved for evaluating therapeutics that have proven effective in lower order species.

Less cognitively evolved animals, like rabbits, pigs, and goats have provided excellent utility for studying the molecular and morphological pathogenesis of disc degeneration but have failed to provide reliable measures of disc-associated pain [143, 146-149]. A partial explanation is that the aforementioned animals are prey animals which are known to exhibit pain-masking as part of evolutionary behavior to avoid predation [150]. Additionally, these animals can be difficult to handle, meaning that measures of pain-like behavior are limited to observational metrics which are notoriously noisy and require high animal numbers to provide enough statistical power to detect

differences [151]. Fortunately, since the inception of biomedical sciences, researchers have poured considerable effort into developing pain-like behavior assays in rodents that are robust and reliable [141].

Rodents are excellent for pre-clinical models because of their accelerated aging, well-defined behavioral assays, size, and cost [141]. It may be reasoned pronograde animals like rodents cannot represent the spinal loading of orthograde animals like humans. Interestingly, research suggests the orientation of the spine, whether parallel or perpendicular to gravity, does not largely impact discal pressures [75, 77, 152]. This lack of difference is further supported by the similarity of disc rheological properties among rodents, pigs, rabbits, sheep, baboons, and humans [153-156]. For models aimed at evaluating early stage therapeutics, rats are a stronger candidate than mice because rat discs are around ten times larger and thus are more amenable for injection procedures [157].

2.3 Outcomes in Rat Models of Disc-associated Pain

In rat models of disc-associated pain, success can be measured by a few key pathologies associated with IVD degeneration in humans. These metrics are gross IVD morphological decline, IVD biomechanical decline, IVD inflammation, and above all, pain-like behavior.

2.4 Measuring Gross Morphology of Rat IVDs

Gross IVD morphology can be approximated using non-invasive procedures and directly measured using tissue processing techniques. The most common analysis used to measure disc degeneration real-time is the disc height index (DHI) [158]. The DHI is a combination of measurements that normalizes the IVD height to adjacent vertebral

bodies. As described earlier, when the disc degenerates, it loses water content, leading to a decrease in height which is detected by the DHI. This metric can be quantified using any imaging modality that can contrast bony and soft tissue. In practice, X-ray images provide an easy way to repeatedly collect this information throughout the course of an animal study. However, this method is limited by observer bias and sample orientation because the location of measurements involved in collecting the DHI are not clear nor consistent. The poor accuracy and precision of this method has created a need to innovate new methods for evaluating the disc state real-time. The widely accepted method for evaluating IVDs after they are collected at the end of an animal study is histological analysis [159]. Staining with hematoxylin and eosin (H&E) is the gold standard for grading disc degeneration semi-quantitatively [160]. Research methods for grading degenerated IVDs are extensively established and described in detail for all major animal model species and humans [160-163]. H&E grading invariably involves evaluating pre-defined disc morphologies, like NP cell number, AF organization, etc., on a point scale. These grades are then summed to get a total measure of IVD degeneration. Other histological stains like fast green, Alcian blue, Safranin-O, tartrazine, toluidine blue, and picrosirius red are less commonly utilized but can be valuable if questions about specific matrix constituent like collagen and proteoglycans are of interest [164, 165]. In sum, numerous methods for non-invasive and terminal state assessment of IVDs have been described, each with their own advantages and disadvantages.

2.5 Measuring Mechanical Properties of Rat IVDs

In many rat models of disc degeneration and disc-associated pain, mechanical properties of healthy and degenerated disc are collected [2, 147, 166, 167]. To

accomplish this, IVDs are excised and fixed to devices called pots that interface with mechanical assessment apparatuses. Torsional and compressive mechanics are the two properties of IVDs routinely measured [156, 168-170]. Torsional mechanics are assessed using rheometers which apply predefined angular displacements on the disc and collect torsional resistance values. Compression mechanics are collected using systems like the ElectroForce 3300, and entail measuring the resistance to compressive displacement. Results from rat IVDs suggests degenerated discs are stiffer and exhibit expanded neutral zones although these effects are not consistently observed in all rat models [167, 171, 172]. Part of the problem in collecting robust mechanical data in rats is the small size of the IVDs, which makes potting and attachment a difficult process. Overall, outcomes of mechanical testing have been hindered by inter and intra experimental variability. However, the consistent decline of mechanical properties in degenerated IVDs suggests there is valuable data to be collected if the systems can be refined.

2.6 Measuring Inflammation in Rat IVDs

Inflammation of the IVD is measured as part of post-processing at the conclusion of many animal studies [173, 174]. Inflammation can be quantified using an array of techniques including, immunohistochemistry (IHC), western blots, polymerase chain reaction (PCR), reverse-transcriptase polymerase chain reaction (rt-PCR), and more. Widely used cytokine targets for quantifying inflammation include IL-1β, TNF-α and IL-6. The presence of these targets or their transcripts is ubiquitous across rodent models of disc degeneration albeit less data exists for disc-associated pain models [175-177].

2.7 Measuring Pain-like Behavior in Rats

Measuring pain-like behavior is essential in rat models of disc-associated pain. Without a pain-like phenotype, disc-associated pain models are simply models of disc degeneration. Fortuitously, many assays have been described which measure pain-like behavior in rats [146]. These assays can be broken into two core groups: evoked and spontaneous pain-like behavior **(Fig. 7)**. Evoked pain-like behavior assays entail direct manipulation of the animal by an observer and bias towards collecting measures of acute pain. Examples of evoked assays in rat models of disc-associated pain are pressure algometry, grip strength, von Frey, cold plate, acetone withdraw, hot plate, tail flick, and Hargreave's [146]. Pressure algometry and grip strength are the only assays in this list which directly perturb the degenerated IVD, making them the most useful and determinative in detecting disc-associated pain. All other assays listed measure signs of increased distal hypersensitivity to either tactile stimulus, heat or cold [151, 178]. Hypersensitivity to stimuli at sites distinct from the IVD can be caused by sensitization of DRG neurons and/or centrally acting interneurons and cerebral pain-related neurons [96]. Primarily, distal hypersensitivity is thought to manifest after disc degeneration because DRG which innervate the distal location also innervate the degenerated disc tissue [179, 180]. This phenomenon is known as cross-

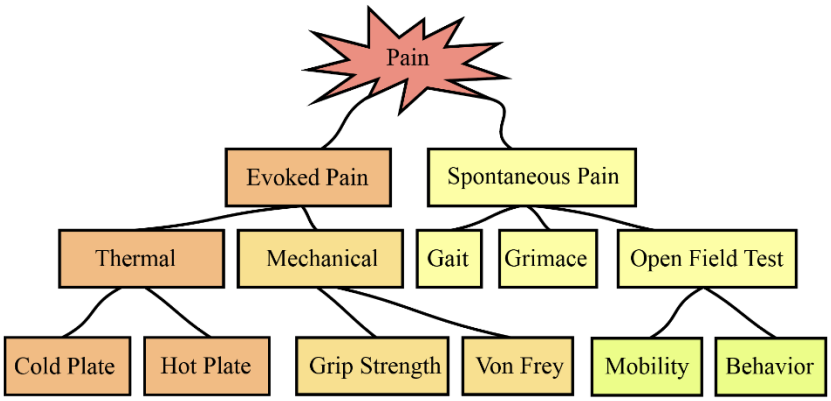

Figure 7. Breakout of pain and assays used to measure pain-like behavior in animal models of disc-associated cLBP

sensitization [181, 182]. Under the cross-sensitization paradigm, inflammatory factors in one tissue or organ phenotypically alter the entire DRG, leading to hypersensitivity in all tissue sites innervated by a single DRG body [183-185]. For example, IVD inflammation may sensitize the L5 DRG, which also innervates the hindpaw footpad, resulting in hindpaw hypersensitivity. However, assays which do not directly provoke the disc are not always indicative of disc-associated nociception nor inflammation. Large differences, especially in assays which measure thermal hypersensitivity, can be indicative of a neuropathy [186, 187]. Thus, due to human confounds and extraneous factors, the ideal method for assessing pain in animals is through pure observational methods like those involved in spontaneous pain-like behavior assays.

Spontaneous pain-like behavior assays do not require animal manipulation but rather rely on observing changes in voluntary action. These assays include the open field test, rotarod, gait, weight bearing, grimace, vocalization, and operant conditioning [141, 144, 188]. Measuring significant changes in spontaneous pain behavior assays is ideal because these assays entirely abrogate the effects of human involvement and are strongly indicative of chronic pain. However, spontaneous assays of pain are more sensitive to confounding factors than evoked pain-like behavior assays. For example, the Open Field Test can be powerfully confounded by environmental variables like, illumination, size, white noise, abrupt noise, room odors, handler odors, how an animal is transferred, etc. [189]. Scientists have drawn attention to details like these because they are known to interact with outcomes, leading to inter-lab outcome variability and replicability problems. Furthermore, confounds may have larger effect sizes on animal behavior than a given treatment, severely limiting the ability to detect differences. Despite these

limitations, measuring significant differences in spontaneous pain-like behavior assays is considered a more robust and translatable measurement of a pain-like condition than evoked measures [151].

2.8 Types of Rat Disc-associated Pain Models

Current rat models of disc-associated pain fall into two categories: spinal destabilization and direct IVD damage.

Spinal destabilization procedures like facet removal are generally paired with mild damage to the disc like annular incisions to induce disc degeneration and disc-associated pain [149, 190, 191]. The rationale behind these models is that deleterious loading can be the fundamental initiator of disc degeneration. Supporting this notion, multiple researchers have reported increased mechanical and thermal hypersensitivity after lumbar facet removal paired with annular damage [176, 192]. Additionally, these models have demonstrated overt degeneration and increases of IL-1β, TNF-α, IL-6, and SP, in the IVD tissue indicating human markers of disc degeneration are replicated [175, 176]. However, the validity of these models as pure disc-associated pain is questionable because spinal features like the facets, which are known to be sources of low back pain in humans, are also damaged [191, 193]. On account of this, spinal destabilization models of disc-associated pain are not adequate as pure models of human disc-associated cLBP.

Most rat models of disc-associated pain involve direct damage to the IVD [148, 149]. In rats, the L5-L6 IVD is the lowest lumbar IVD, analogous to the human L4-L5 IVD, the most common site of human disc degeneration [194]. Therefore, the L5-L6 disc is a common target for single level procedures in rats. The repeated IVD puncture model is the most typical model employed to create a disc-associated pain-like phenotype in rats

[173, 188, 195-198]. These models induce degeneration by repeatedly puncturing the IVD with syringe needles ranging from 18-gauge to 33-gauge. This model paradigm has yielded fair results with one model demonstrating spontaneous pain-like behavior and several demonstrating evoked pain-like behavior. Using a 10X puncture model of the L5-L6, Leimer et al., have been the only group to measure spontaneous pain-like behavior changes. In this model, animals that were injured spent less time traveling in the Open Field Test and exhibited preference for forelimbs in stride frequency as part of a gait analysis [173]. Lai et al., Muralidharan et al, Li et al, and Isa et al., have all performed puncture models and measured differences in evoked pain-like behavior like deep pressure hypersensitivity, hindpaw tactile hypersensitivity, and tail thermal hypersensitivity [176, 199-201]. However, pain-like phenotypes in these models suffer inter-study variability and repeated puncture of the disc with a syringe needle cores the tissue resulting in pathologies dissimilar from humans. More severe models of disc-associated pain utilize triple level injury of the lumbar spine, damaging the L3-L4, L4-L5, and L5-L6 IVDs and may inject inflammatory agents like cytokines or CFA into the IVD [2, 139, 199, 202, 203]. Iterations of this model have been repeatedly employed and display robust mechanical hypersensitivity indicative of disc-associated pain [2, 139, 167, 199, 203]. The Iatridis lab has utilized variations of a triple-level puncture with cytokine injection model in more than four publications, with all iterations displaying robust hindpaw tactile hypersensitivity and a minority displaying other signs of pain-like behavior like thermal hypersensitivity, increased grooming, etc. [2, 139, 167, 204]. However, these models apply a severe injury and an injection volume that represents a significant fraction of the entire disc volume and apply supraphysiological levels of

inflammatory cytokines [157, 205-208]. Furthermore, pain-like behavior has failed to manifest in female animals in dual sex studies implicating other mechanisms than IVD degeneration are at play in the production of pain-like hypersensitivity [2]. These factors implicate potential inflammatory cytokine leakage and sensitization of nervous tissue around the disc as behavioral confounds. More models have been described but these are greatly limited by factors such as relatively large needle size, spinal damage, inconsistent behavioral shifts, and inappropriate inflammatory agents [173, 176, 198, 209, 210].

In summary, numerous models of disc-associated pain have been outlined, but translatability has been limited by inconsistent pain-like behavior, severe injury, spinal damage, supraphysiological inflammatory agents, sex differences, and more. There is a need for an animal model of disc-associated pain induced through pure, single-level, mechanical injury that manifests mild pain-like behavior in evoked and spontaneous pain-like behavioral assays.

2.9 Treatments in Rat Disc-associated Pain Models

To date, numerous research groups have treated disc degeneration in rodent models with varying degrees of success. These treatments have included cell transplantation, *in situ* gene therapy, and bioactive factors [202, 211-218]. The vast majority of models are limited by the administration of treatments prophylactic or concomitant with the initiation of degeneration. Further, the majority of publications that evaluate treatments for disc degeneration fail to quantify pain-like behavior [219]. Clinically, patients do not seek treatment for disc degeneration unless the degeneration causes pain. This simple fact brings into question the validity of prior work because treatments are administered prior to pain-like manifestation which does not replicate how

human patients are treated. As of 2021, no treatment in over 100 animal model publications has achieved approval by the Food and Drug Administration (FDA) for the treatment of degenerative disc disease providing strong evidence that the prophylactic and concomitant treatment paradigms are inadequate [219]. There is a strong need to shift the treatment paradigm to that of rescue treatment, which above all replicates how humans are treated at the clinic.

Nevertheless, there is growing evidence from *in vitro* and *in vivo* work that injectable treatments for disc-associated pain have therapeutic potential [220, 221]. Specifically, focus has shifted to biomaterials as platforms for composing injectable therapies with tunable properties. These candidate materials have demonstrated promising properties on the benchtop but have yet to make an impact in an animal model of disc-associated pain.

2.10 Biomaterials for Treating Disc-Associated Pain

Hydrogel biomaterials are ideal therapeutics for IVD tissue replacement and repair due to their tunable, injectable, and conformable properties. As evidence of their profound utility, the global biomaterials market has grown to an estimated $106.5 billion as of 2019 [222]. Hydrogel biomaterials can be broken into two major classes – natural and synthetic. Synthetic biomaterials, like polyethylene glycol (PEG) and polyacrylic (PAA) hydrogels are recognized as foreign bodies by the immune system making them unideal for long term solutions [223-225]. Natural biomaterials, like collagen or hyaluronic acid hydrogels, employ native structural moieties and ligands making them more readily received by hosts.

Natural biomaterials derived from decellularized tissue have more recently entered the therapeutic arena due to several advantages [226-228]. Foremost of these advantages is their intrinsic biomimicry. When fabricated from analogous tissue sources and carefully processed, decellularized tissues maintain native proteins, microarchitecture, and immunomodulatory factors like matrix bound vesicles [229-231]. In the context of disc degeneration repair, decellularized tissues convey another advantage in that they can be enzymatically digested to create an injectable solution which is thermally fibrillogenic.

In the last decade, several research teams have developed decellularized biomaterials for treating IVD degeneration [230, 232-235]. Using methods that involve detergents, ultrasonication, freeze-thaw cycles, nucleases, and trypsin digestion, these teams have removed cellular material and other antigens from IVD tissue to create ECM scaffolds. More recently, decellularized methods have been paired with enzymatic digestion to yield solutions composed of ECM constituents [235, 236]. Because a major component of these ECM solutions is collagen, they spontaneously form collagenous hydrogels when brought to 37 °C [237]. This thermal gelation allows these formulations to be delivered to IVDs, *in vivo,* via minimally invasive injection. In fact, a decellularized biomaterial composite has proven effective at decreasing disc degeneration in a rabbit model of IVD degeneration [238]. However, the capacity of a decellularized biomaterial to alleviate disc-associated pain has not been determined. Considering disc-associated pain is driven by nociception in the disc, which may be exacerbated by mechanical instability, a minimally invasive, injectable, thermally curing biomaterial may be able to percolate into tissue defects, restore mechanics, and alleviate pain.

In order to accomplish biomaterial-tissue integration and promote long term viability of a biomaterial implant, native cells must be present to facilitate cross-linking of tissue extracellular matrix with delivered extracellular matrix components or moieties, like collagen or aldehyde groups [226]. Unfortunately, degenerated discs are characterized by their hypocellularity making cell-mediated integration slow if not non-existent [239]. To remedy this problem, chemical cross-linkers have entered the realm of biomaterial engineering as potent solutions for robust tissue integration. In the past, covalent bonding of biomaterials doped with crosslinking agents has been studied as part of the development of bioadhesives likes Gelatine-Resorcine-Formaline (GRF) glue [240]. Classical crosslinking agents like glutaraldehyde and carbodiimide, have been used to cross-link collagenous tissues to prevent degradation and promote integration of implants like PeriGuard, a bovine pericardial patch [241-243]. These crosslinking agents work by creating covalent linkages between and within collagen fibrils resulting in increased interconnectivity [241, 244]. In addition to making biomaterials more resistant to degradation, chemical cross-linkers can also dramatically increase the mechanical properties of tissues. However, the current broad guidance for adding chemical crosslinking agents to biomaterials is that of caution because cross-linkers are known to have potent cytotoxic effects and can result in biomaterial failure [245].

More recently, a naturally derived chemical crosslinking agent, genipin, has entered realm of biomaterials [246-248]. This agent, derived from the fruiting bodies of *Gardenia Jasminoides*, exhibits remarkably minimal cytotoxicity at concentrations which increase the mechanical properties of biomaterials by more than double [168, 246, 247, 249-251]. In the context of collagen, free genipin covalently bonds with lysine molecules

via nucleophilic attack. When two genipin molecules interact after each having bound with a lysine, they condense into a single covalent bridge between the two lysine residues and form an aromatic ring [251]. This structural reformation results in a blue color which can be readily observed by the naked eye. Additionally, genipin has proven cytocompatible as part of bioadhesives used to repair annular defects in IVDs. In this context the genipin crosslinked biomaterial, FibGen, exhibits superior reparative properties compared to commercially available products like BioGlue [252]. A decellularized biomaterial, doped with genipin, could dramatically improve the mechanical function and integrity of a degenerated disc, decreasing inflammation and nociceptor activation, thereby alleviating disc-associated low back pain.

CHAPTER 3: Context for Project Chapters

The primary goal of this dissertation was to engineer a therapeutic for disc-associated low back pain. Prior to any evaluation of a treatment, two systems had to be established. The first was a means to quantify disc degeneration real-time and the second was an animal model of disc-associated pain.

The first goal, described in Chapter 4, was motivated by the inadequacy of the DHI method as a real-time proxy for disc degeneration. At the outset of all animal work, it was quickly realized that the DHI method required too many subjective choices by the experimenter and could not be relied on as a robust metric for gauging degeneration longitudinally. To remedy this problem, a method for processing three-dimensional data from uCT scans to create three-dimensional renderings of the intervertebral discs was created. This system was used to non-invasively measure changes in disc volume of degenerating discs because it was known that damaging the disc would decrease the water content and volume. This method was extremely sensitive in detecting changes of the IVD and provided a state of the art means to monitor disc degeneration real time.

The second goal, described in Chapter 5, was to create novel and robust model of disc-associated pain. The problem with established models of disc-associated pain was that they either were too mild to manifest a replicable pain-like phenotype, or they were far too severe to be categorized as a model of pure disc-associated pain. Additionally, essentially all models had been created in male animals, despite cLBP being far more prevalent in women [10]. To address this deficit, a model of disc-associated pain using only mechanical injury of the L5-L6 IVD in female Sprague Dawley rats was established. This model manifested consistent and increasing chronic axial hypersensitivity and deep

pressure hypersensitivity at the L5-L6 level. Furthermore, this was the first rat model to demonstrate nerve fibers penetrating deep into degenerated disc tissue. The presence of pain-like behavior across two assays in concert with aberrant nerve sprouting solidified this model as a leader in the field of biomedical research.

The final goal, described in Chapter 6, outlines the engineering of a biomaterial derived from decellularized, healthy NP tissue, supplemented with collagen and genipin. After testing *in vitro,* this biomaterial was injected into animals which had been experiencing disc degeneration for 8-weeks. The novel biomaterial therapy increased exploratory behavior in the open field test, decreased axial hypersensitivity, and prevented the development of deep pressure hypersensitivity. Additionally, immediately after treatment, disc volumes in treated animals returned to baseline and remained at baseline for the remainder of the study, suggesting complete tissue-biomaterial integration.

CHAPTER 4: Application of microcomputed tomography to calculate rat intervertebral disc volume as a surrogate measure of degeneration

4.1 Introduction

Low back pain (LBP) is the leading cause of disability worldwide [253]. 84% of people who suffer an episode of LBP will recover, but for 16%, the pain will become chronic and disabling [254]. Chronic LBP increases risk of unemployment, depression, insomnia, suicide and costs the United States more than $100 billion each year [255-257]. Despite the immense socioeconomic burden of chronic LBP, elucidation of the causal drivers of pain remains incomplete. The most strongly associated factor with chronic LBP is intervertebral disc (IVD) degeneration [22].

The IVD is a viscoelastic organ that sits between vertebral bodies, providing spinal damping and flexibility. The IVD has three components: the cartilaginous end plates, the annulus fibrosus (AF), and the nucleus pulposus (NP) [258]. The AF, high in elastic collagen I fibers, circumferentially enwraps the NP which is rich in glycosaminoglycans and collagen II. The AF and the NP together form a thick disc which is capped on both ends by cartilaginous end plates which allow nutrient diffusion from adjacent vertebral bodies[258]. In a healthy state, negatively charged GAGs in the NP make it energetically favorable for the NP to imbibe and maintain 75% of its weight in water [68]. Maintenance of water in the NP is essential for the IVD to resist compressive loads and to dynamically cycle nutrients throughout the tissue. The tradeoff for the

phenomenal mechanics of this organ is an absence of nerves, blood vessels, and immunological access which predisposes the IVD to degeneration.

In humans, the primary causes of IVD degeneration are age, environmental factors, and trauma [102]. These factors serve to decrease nutrient flow to the IVD, triggering cellular senescence and apoptosis, creating a catabolic feedback loop resulting in IVD degeneration [259]. Two hallmarks of IVD degeneration measured regularly to diagnose disc degeneration are disc water loss and height loss. Disc water content is usually measured using MRI and quantified using defined grading schemes like the Pfirman grading system [260]. Disc height loss is thought to result from compromise of the AF which acts as a hydrostatic barrier between the hydrated NP and surrounding tissue[261]. Clinically, disc height loss is measured using X-ray imaging using a process that normalizes the IVD space to the length of adjacent vertebral bodies. This measurement, known as the disc height index (DHI), is the gold standard for assessing IVD degeneration real time using X-ray imaging [262]. While this metric is useful in humans, X-ray imaging exhibits poor spatial resolution in the sub millimeter range, limiting the utility of the DHI in rodent models, where IVDs heights range from 100 μm – 1600 μm [263-265]. Additionally, measuring DHI using radiographs is limited by error introduced by subjective choices made by experimenters concerning sample orientation, measurement selection, measurement location, etc. [158]. Despite these limitations, the DHI is widely used in rat and mouse models because no other robust method has been established [138].

Microcomputed tomography (μCT) is a relatively new imaging technique which has been developed over the past several decades [266, 267]. Unlike X-ray imaging,

which collects data from a single imaging plane, μCT employs a rotating scanner that collects data from a myriad of reference frames, permitting 3D reconstructions with high spatial resolution. This 3D imaging method is fundamentally like MRI with the caveat that μCT uses X-rays which deliver greater resolving power compared to the radio waves used in MRI. Modern μCT are capable of high-resolution scanning with spatial resolutions as low as 9 μm which vastly outperforms state of the art small animal X-ray scanners with spatial resolutions of 143 μm [268]. These μCT scans can be used to evaluate DHI through measurements in a single slice plane, but this option is suboptimal because it requires observer discernment for slice selection and disregards most of the data set. In recent years, contrast enhanced μCT has been used to precisely measure volumetric changes in degenerated IVDs in rodents, but the use of a contrast agent increases cost and time [157, 263]. Due to the limitations of using the DHI or contrast agents in small animal models of IVD degeneration, the purpose of this work was to evaluate if non-contrast enhanced μCT could be used to generate a metric of volume to assess degeneration real time in rodents.

The objective of this study was twofold: 1) develop a novel technique for quantifying IVD volume *in vivo* using μCT without the use of a contrast agent and 2) determine the ability of this technique to measure changes in IVD volume in real time in an animal model of IVD injury and degeneration. The data presented herein confirm that IVD volume as measured by μCT imaging is a reliable, precise, and sensitive metric for quantifying IVD degeneration in rodents *in vivo*.

4.2 Materials and Methods

Animals*:* 24 female, 15-week-old, Sprague Dawley rats were purchased from Envigo and housed with a 12-hour light/dark cycle and *ad libitum* access to food and water. All animal procedures were in accordance with the National Institute of Health guidelines following PHS Policy on Humane Care and Use of Laboratory Animals and approved by the Institutional Animal Care and Use Committee and the University of Nebraska – Lincoln.

µCT Data Collection: Scans of the L5-L6 IVD were collected using a Quantum GX2 µCT Imaging System. The rat lumbar spine was radiographed by placing anesthetized animals in the scanning bed in the supine position and scanning for 2-minutes with 90 kV power, 88 µA tube current, 72 mm FOV, 144 µm isotropic voxel size, and a Cu .06 + Al .05 X-ray filter. The resulting VOX files were renamed according to respective animal ID's and transferred to an external hard drive to be processed. All baseline values, week 0, were collected in a single day. Animals were also scanned at 2, 8 and 18 weeks after injury.

Disc Height Index: The disc height index was quantified according to previously described methods[167, 269, 270]. In brief, the mid-coronal disc slice image was determined by selecting the midpoint slice between the most dorsal and ventral slice that contained the disc. The IVD height was calculated using three measurements of disc height (two lateral and one midline) and six measurements of adjacent vertebral body length (two lateral and one midline x two vertebral bodies) (**Fig. 2A**). DHI = (2 x (D + E + F)) / (A + B + C + D + E + F).

***IVD Injury Surgery**:* This injury method applied herein is based on an established model of disc degeneration developed by our lab (under review). On the day of surgery, the animals were split into two groups of equal size (n = 12): sham and injured. Rats were anesthetized, and the lumbar spine was approached ventrally by dissecting through the abdominal cavity and retroperitoneum. The iliac crest was used as a landmark to reliably dissect down to the L5-L6 IVD. For injured animals, the L5-L6 IVD was punctured bilaterally with a strong point dissecting needle (Roboz, RS-6066) with an O.D. of 0.5 mm set to a length of 3 mm. The exact needle length was predetermined based on μCT data to ensure that the needle length did not exceed the diameter of the smallest L5-L6 IVD in all animals. While the needle was within the IVD, it was swept back and forth along a 90^{o} arc six times in the transverse plane to disrupt the dorsal and lateral aspects of the IVD for injured animals. A simple continuous and subcutaneous suture pattern were used to close the abdominal wall and the skin respectively. Buprenorphine SR (1 mg/kg) was administered once post-op for pain and animals were rested for two weeks following surgery. At the study conclusion, a total of two animals were excluded from the study (sham: n = 12 and injured: n = 10) due to mis-puncture confirmed by IVD volume and H&E (data not shown).

Statistical analysis: All data is presented as mean ± standard deviation. Data were analyzed using GraphPad Prism 9. Normality was assessed using a Shapiro-Wilk test. IVD volume and DHI data were analyzed using a one-way ANOVA with Dunnett's post hoc. Results were considered statistically different when $p < 0.05$.

4.3 Results

The first objective of this work was to use μCT data to create a new method for assessing the IVD non-invasively and without the use of a contrast agent. IVD volume was identified as a potential measurement primarily because it incorporated as much data from the μCT scan as possible into the outcome, unlike the DHI method which used only a single slice plane. To establish this method, Sprague Dawley rats were acquired to collect lumbosacral μCT data to create a protocol for quantifying IVD volume. Data collection was completed by anesthetizing rats using isoflurane, placing them on the scanning bed in the supine position, and scanning the lumbosacral spine using a Quantum GX2 μCT (Fig. 8A). Once data was collected, the VOX files were loaded into Analyze 14.0 (Analyze Direct), a proprietary software associated with Quantum imaging devices. All VOX files were loaded in as float files (Fig. 8B). A chosen file was then opened using the segment tool and the L5-L6 IVD was located using the iliac crest as a landmark (Fig. 8C&D.) The ventral most slice of the L5-L6 IVD space can be seen in Fig. 8E. The vertebral column was then made into an object using the semi-automatic tool for thresholding bony objects (Fig. 8F). The threshold intensity used for bone in this work was 700 Hounsfield unites (HU) [271, 272]. The bony spine object was then locked, and a new object for the IVD space was created. Starting at the ventral most slice of the L5-L6 IVD space, where both adjacent vertebral bodies can be visualized, the IVD space object was drawn using the manual draw tool (Fig. 8G). Making sure the vertebral body object was locked was important during this drawing to prevent unwanted overlap (Fig. 8H). The edge of the disc space, i.e., the width boundary, was approximated by a line of shortest length between the edges of the L5 and L6 vertebral body. The manual drawing

was continued through all slices of the L5-L6 IVD space until the dorsal edge of the spine was reached, and the vertebral bodies began to recede. The middle slice can be seen in Fig. 1I, and the last slice can be seen in Fig 8J. Finally, the semi-automatic tools for coronal and propagating objects, with smoothing enabled, were performed to smooth out the objects and reduce variability caused by imprecise drawing (Fig. 8K). The object maps were then saved, and the segment tool was closed. The same sample was next opened using the measure tool and the corresponding object map was loaded (Fig. 8L). After, the sample enabled objects tool under the 3-D tab was performed to generate the volume for object 3 which corresponds to the volume of the IVD space (Fig. 8M). This process was performed on twenty-four animals as a proof-of-concept. The average disc volume in this cohort was 4.69 mm^3 ± .58 mm^3 (Fig. 8O). These data indicated the disc volume method was a viable tool for quantitatively assessing the IVD, non-invasively, in real time, and without the use of a contrast agent.

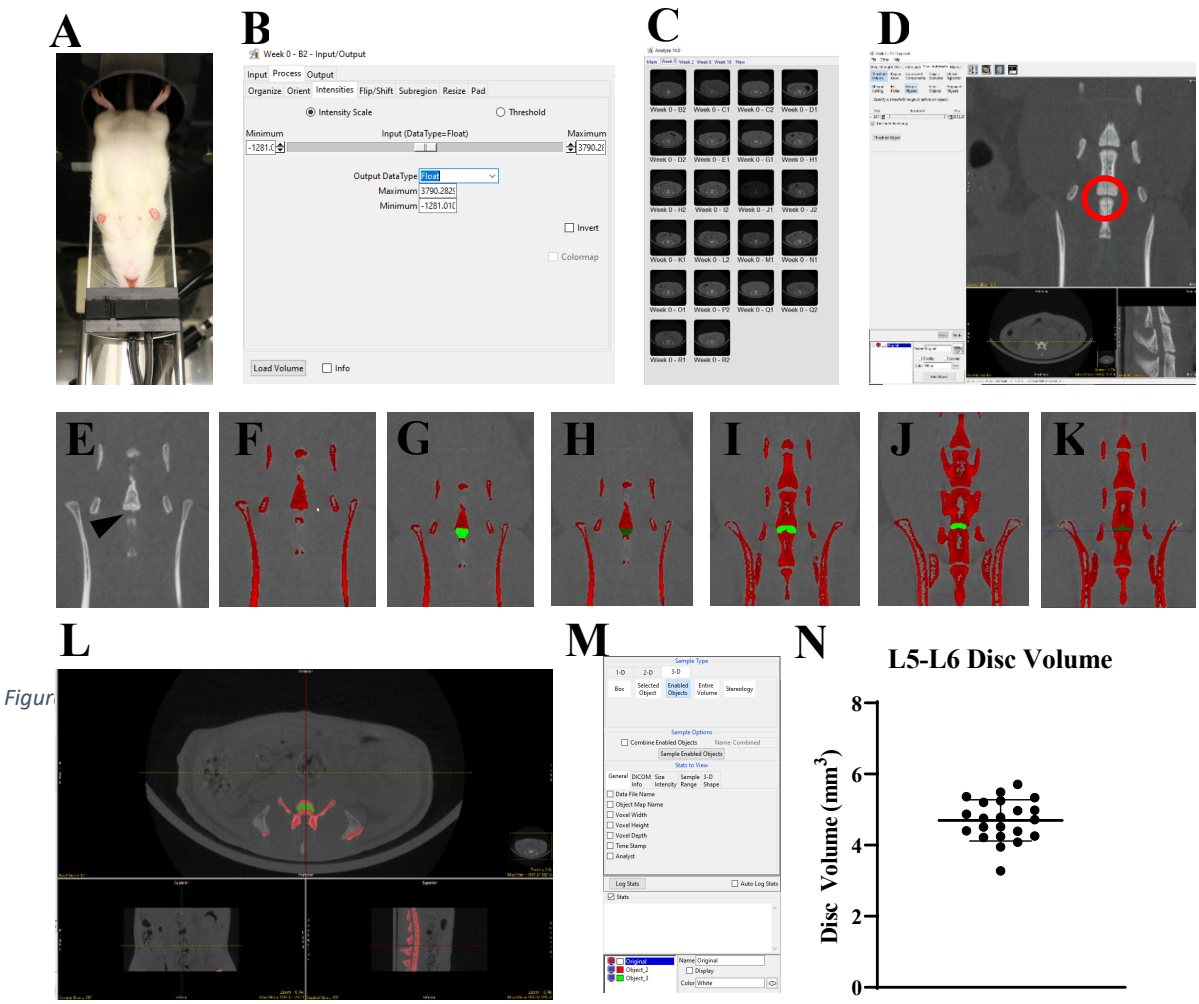

Figure 8. Overview of disc volume quantification. (A) Animals are scanned in the supine position for 2-minutes with 90 kV power, 88 µA tube current, 72 mm FOV, 144 µm voxel size, and a Cu .06 + Al .05 X-ray filter. **(B)** VOX files are loaded into Analyze 14.0 and output as a float data type. **(C)** Loaded VOX files within the main workspace are opened in the segment tool. **(D)** Loaded samples within the segment tool. **(E)** Zoomed image of the ventral most portion of the lumbosacral spine. The ventral start of the L5-L6 is in the center of the frame. The arrowhead points to the iliac crest **(F)** The bony tissue of the spine is defined as an object using the semi-automatic tool with a threshold set to 700 HU. **(G)** The bony tissue object is locked, and a new object is defined for the IVD space. The IVD object is painted in manually in the space between the L5 and L6 vertebral bodies. The bright green indicates the region being actively painted. **(H)** Locking the bony tissue object prevents overlap between this object and the IVD object. **(I)** The IVD object is continually painted in all frames where both adjacent vertebral bodies are present. **(J)** The IVD object finishes where the vertebral bodies visually rapidly separate from one another. **(K)** The object maps are propagated through all frames and smoothed using the semi-automatic tools "propagate objects" and "coronal" with the smoothing box checked. The final object map is saved, and the segment tool is closed. **(L)** The sample is opened in the measure tool and the relevant object map is loaded. **(M)** Within the measure tool, the sample enabled objects is selected under the 3-D tab, and the volume for the IVD space is output. **(N)** 24 L5-L6 IVD volumes were quantified from 24 female Sprague Dawley rats.

The second objective of this work was to test the ability of the IVD volume method to detect changes due to injury of the IVD. In this work, the DHI was used as a benchmark comparator against the disc volume method (Fig 9A-C). A commonly applied procedure for inducing IVD degeneration in animal models is mechanical trauma [167, 200]. To this end, the L5-L6 IVD was punctured in twelve of the twenty-four animals from the same cohort used to establish the process. The injury entailed using a micro-dissecting needle to perforate the AF and compromise the hydrostatic barrier of the IVD. It was expected the compromised AF barrier would result in immediate water loss and in turn height and volume loss. Confirming this notion, at two weeks post-op the IVD height index in injured animals significantly dropped from 0.098 ± 0.005 to 0.087 ± 0.011. The average DHI of injured animals was significantly different from sham at 2-weeks and 8-weeks post injury but not at week 18 (Fig. 9D). Likewise, the disc volume decreased substantially after injury from $4.90\ mm^3 \pm 0.423\ mm^3$ to $3.47 \pm 0.612\ mm^3$ and this decline was significant compared to sham at 2-weeks and 8-weeks. However, like the DHI method, disc volume did not measure a significant difference at week 18. The outcomes of this assessment revealed a 30% drop in volume and 11% drop for the DHI at 2-weeks post-injury (Fig. 9D, 9F). The disparity in these outcomes in context of proportionately equal standard deviation indicated the DHI method had less power to detect changes in the IVD compared to the volume method. Because the DHI method intrinsically includes a normalization step by involving adjacent vertebral body lengths into the calculation, it was then asked if further normalization to pre-surgery, especially for IVD volume, could increase the statistical power. Normalization of the DHI data reduced the power, resulting in no significant differences detected between sham and

injured animals at any time point (Fig. 9E). Conversely, normalization of IVD volume increased the power, resulting in larger differences between sham and injured animals. At all-time points after injury, the calculated p-value was less than .0001 which was orders of magnitude more significant than non-normalized data (Fig. 9G). These data indicate that the IVD volume method imparted greater statistical power than the DHI method in determining changes in the IVD state due to mechanical injury although both could detect changes.

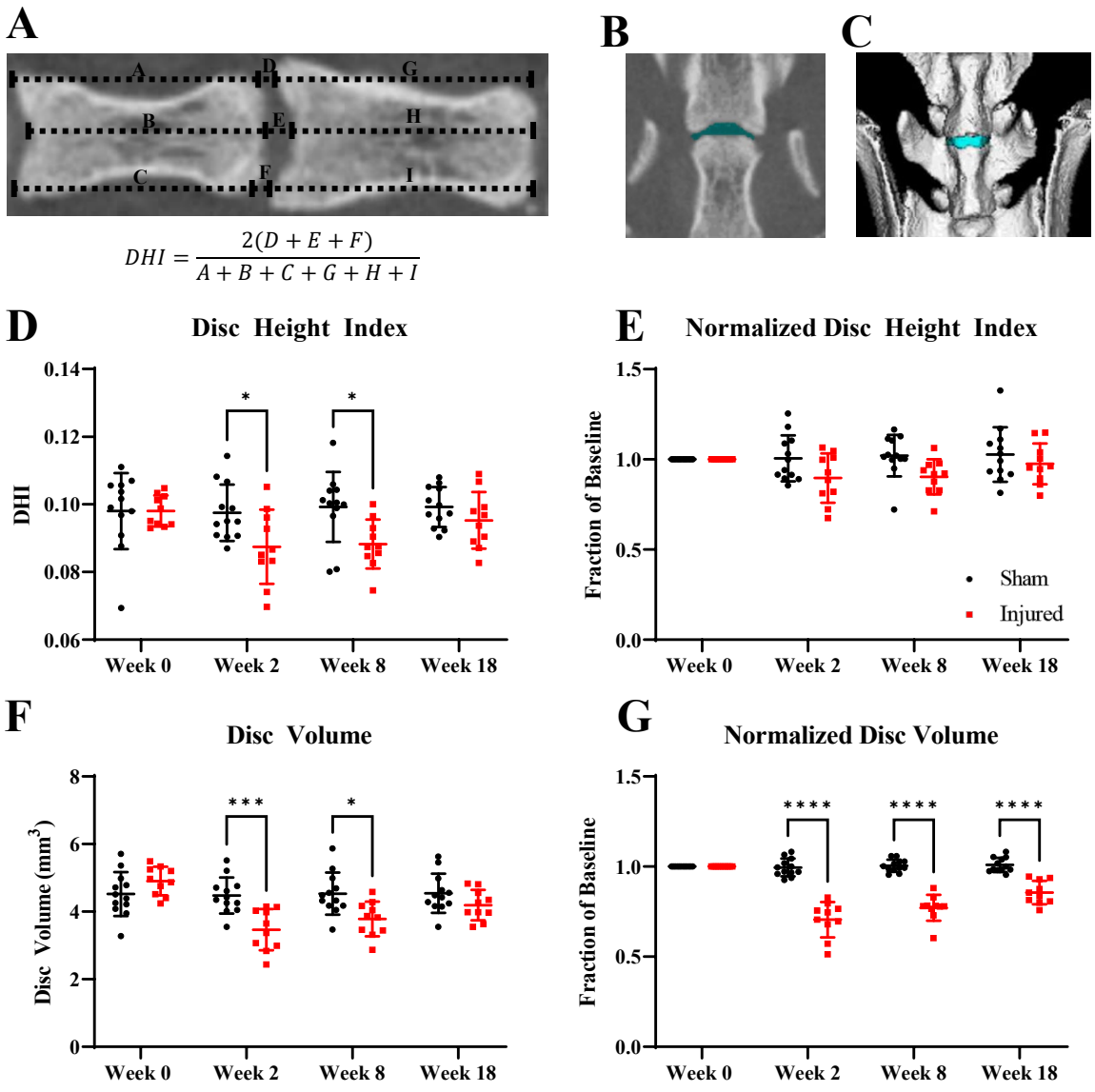

Figure. 9. **Validation of the disc volume method after disc puncture. (A)** Measurements and equation used to determine the disc height index. **(B)** IVD space painted in a single slice during the disc volume measurement. **(C)** Three-dimensional rendering of the IVD volume after all paint slices are concatenated into a single object map. The IVD is colored in teal. **(D)** Disc height index data measured at baseline, week 0, and post-injury at weeks 2, 8 and 18. The disc height index method measured a significant decrease in injured animals compared to sham in weeks 2 and 8. **(E)** Normalized disc height index data pre-op and post-op. When normalized, the disc height index method failed to detect a significant change in injured animals compared to sham. **(F)** IVD volume data at baseline, week 0, and post-injury at weeks 2, 8 and 18. The IVD volume method measured a highly significant volume decrease in injured animals compared to sham in weeks 2 and 8. **(G)** Normalized IVD volume data pre-op and post-op. When normalized, the IVD volume method detected a highly significant decrease in injured animal IVD volume compared to sham in weeks 2, 8 and 18. Data is shown as mean with standard deviation *(n = 10-12 per group)*. Significant differences between groups were assessed using a one-way ANOVA with Dunnett's post hoc. * = $P < .05$ sham vs. injured. *** = $P < .001$ sham vs. injured. **** = $P < .0001$ sham vs. injured.

4.4 Discussion

The objective of this study was twofold: 1) develop a novel technique for quantifying IVD volume *in vivo* using μCT without the use of a contrast agent and (2) determine the ability of this technique to measure changes in the IVD real time in an animal model of IVD degeneration. The Analyze 12.0 software in combination with highly spatially resolved data collected from μCT provided a means to develop a novel technique for quantifying IVD volume. This method proved sensitive at detecting changes two weeks after injury to the IVD. The application of this method in rodents *in vivo* provides a new tool for researchers to measure IVD degeneration longitudinally in a manner more precise and reliable than the DHI method and with reduced cost and time yet equal precision compared to contrast enhanced uCT.

The impetus for this work resulted from difficulties measuring DHI using μCT data in a pilot animal model of IVD degeneration of ours. During these measurements, we noted that the selected slice used to measure DHI had a large impact on the outcome. This variability was due to naturally occurring changes in IVD height across the disc. IVD height variability based on location is well characterized in literature which has used contrast enhanced μCT to show the IVD height can range from 0.4 mm to 1.6 mm depending on the location within the IVD, an increase of 400% from smallest to largest[265]. Another major drawback of the DHI method was that it used a single slice plane from the μCT data, disregarding 95% of the data set which contained the IVD. Statistically, it is generally better to sample as much of an experimental unit as possible to increase the accuracy of the ground truth approximation. Knowing the IVD was the experimental unit we were seeking to quantify, we hypothesized incorporating all slices

of the IVD into a single measurement would increase the power of the metric. We determined the best way to do this was by assessing the volume of the IVD because this outcome involved all slices that contained the IVD abrogating the effect of sampling location. A major decision at the outset of data collection was to scan all animals using a voxel size of 144 μm. This voxel size was chosen because we aimed to create a method that could be performed rapidly and repeatedly, bringing into consideration the total x-ray dosing. Despite the voxel size being relatively large compared to what the system was capable of, the extra spatial dimension alone proved efficacious in increasing the power of the volumetric method compared to the DHI. If necessary, the precision of our method could be increased in future work by increasing scan time, shrinking the FOV and reducing the voxel size. Further, the volume method was unaffected by differences in animal position evidenced by the consistency in measurements between the first study, where animals were placed in the prone position and the second study, where animals were scanned in the supine position. Understanding the relatively utility of both methods, we then questioned further about the sources and degree of error for each measurement.

Error in the DHI method can be accounted primarily by slice selection and measurement location, assuming all other parameters like imaging settings are standardized. Using μCT data, the slice selection error alone was sufficient to shift the outcome. In our work, DHI values could shift by 20% between slices indicating a large potential for single measurement interobserver variability. On the other hand, error in the volume method can be accounted primarily by selection of the start and end slice of the IVD space. Error introduced by painting within each slice was not a considerable concern because smoothed object propagation interpolated the edges of all objects and served to

normalize this variability across all samples. In our work, the first slice was defined as the slice in which 10 pixels of each vertebral body, defined by the bony spine object, was visually present. The final slice was defined as the slice in which vertebral bodies began to diverge. In our data sets, the IVD generally spanned 20 slices meaning incorrect selection of the start and end slice by one slice could introduce around 10% error, half of the DHI method. Of note, the start and end slice contained a fraction of the of the IVD space compared to interior slices suggesting this 10% error rate is an upper bound. These estimates of error terms indicate the DHI method is more prone to error introduced through experimenter subjectivity via slice selection and intrinsic process variability compared to the IVD volume method.

Another foundational principle of statistics is that error is normally distributed within data sets given a sufficiently large sample size. This phenomenon is readily observed in our data sets because both DHI and IVD volume sham animal averages at post-op closely matched pre-op averages despite having compositionally different error terms. The fact that IVD volume had drastically increased power in detecting differences due to injury suggests outcomes from this method were less diluted by error intrinsic to the process **(Fig 9E&F)**. We believe this decrease in the dilutionary effect of error was a direct result of sampling the entire experimental unit i.e., the IVD, in the volume method. A limitation of the volume method is that it is directly affected by radial IVD expansion, a phenomenon known to occur with degeneration [273]. The DHI method is not directly affected by this problem because no measurements of width are incorporated into the DHI outcome. Although the DHI method does not measure width, radial expansion might indirectly impact the location of lateral height measurements, potentially skewing

degenerated IVD values. Work will need to be done in the future to determine how much of a dilutionary effect radial expansion has on the outcome because data in this area is lacking.

Considerable work has been performed over the past decade using contrast-enhanced μCT to characterize and measure various aspects of rodent IVDs to provide insight into the pathobiology of IVD degeneration [157, 263, 265, 274]. Contrast agents leverage the anionic charge of small molecules of in combination with the anionic charge of GAGs to imbue contrast proportional to the concentration of GAGs in the IVD. Unfortunately, these contrast agents are costly, exceeding $1,000/50 mg in the case of Ioversol (Sigma), require infusion, and take time to clear the system making them unideal for repeated use. For simple measurements of disc volume, the high contrast afforded by contrast-enhanced μCT is not necessary because contrast is only required along the margins of the disc, between bone and soft tissue. For this reason, we speculated the disc volume could be measured with similar precision to that observed in prior work without the use of contrast enhancement. In both of our studies the standard deviation was 14% of the average which is lower than prior contrast enhanced work [275]. The consistent lower proportion of error in our data suggests our method is equally reliable and precise compared to methods which use contrast enhanced μCT.

In summary, we have developed a method that uses μCT data to compute IVD volume to assess IVD state changes in real time, non-invasively, and without the use of a contrast agent. The head-to-head comparison of the volumetric method with the DHI which is the gold standard for quantifying IVD state changes, suggests our method was more sensitive at detecting differences after injury to the IVD in live animals. Future

work is needed to evaluate the utility of this metric longitudinally and to assess if the contribution of radial IVD expansion significantly affects measure outcomes. We hope this method will be a useful tool for researchers that have a need to assess IVD state *in vivo*.

The work described in Chapter 4, constitutes a scientific paper which is currently under review in Computer Methods in Biomechanics and Biomedical Engineering: Imaging & Visualization.

DJ. Lillyman, F. Lee, EC. Barnett, TJ. Miller, RA. Wachs. Application of microcomputed tomography to calculate rat intervertebral disc volume as a surrogate measure of degeneration. Computer Methods in Biomechanics and Biomedical Engineering: Imaging & Visualization

CHAPTER 5: Axial hypersensitivity is associated with aberrant nerve sprouting in a novel model of disc degeneration in female Sprague Dawley rats

5.1 Introduction

Low back pain (LBP) is the leading cause of disability worldwide [253]. 84% of people who suffer an episode of LBP will recover, but for 16%, the pain will become chronic and disabling [254]. Chronic LBP (cLBP) increases risk of unemployment, depression, insomnia, suicide and costs the United States more than $100 billion each year [255-257]. Despite the immense socioeconomic burden of cLBP, elucidation of the causal drivers of pain remains incomplete. The most strongly associated factor with chronic LBP is intervertebral disc degeneration, known as disc-associated pain [22]. Unfortunately, treatments for disc-associated cLBP exhibit poor long-term efficacy [61, 276, 277]. The failure of current treatments can be attributed to a poor understanding of the pathobiology underpinning disc-associated pain and a lack of pre-clinical animal models to screen therapeutics.

In a subset of human patients with disc-associated pain, pathological changes in the disc are thought to drive nociception and in turn pain. In these patients, degenerated discs exhibit four important characteristics: 1) extracellular matrix (ECM) breakdown, 2) hypocellularity, 3) aberrant nerve sprouting and 4) inflammation [79, 113, 114, 116, 118, 205, 278, 279]. ECM breakdown and hypocellularity result from deleterious nutrient deficiency and altered biomechanics incompatible with tissue homeostasis [259]. CLBP disc samples also exhibit high levels of pro-inflammatory mediators and a preponderance

of nerves suggesting inflammation and nerve sprouting are involved in LBP genesis [116, 118, 280]. These four factors provide empirical targets for an animal model of painful disc degeneration.

To be successful, animal models of pain must achieve three criteria: construct validity, face validity, and predictive validity [281-283]. Construct and face validity relate to the replicative accuracy of disease induction and phenotype respectively. Predictive validity describes how well treatment efficacy in a model translates to human efficacy. For a disc-associated LBP model, construct and face validity require pain genesis to relate to pathological shifts in the disc, like nerve sprouting, and for the phenotype to manifest similar to the disability and pain observed in humans. In theory, accurate construct and face validity endow a model with degeneration analogous to the human disease state, making treatments translatable, thereby imparting predictive validity. It is vital these criteria are achieved in animal models that seek to provide insight for human disease mechanisms and treatments.

Rodents are excellent for pre-clinical models because of their accelerated aging, well-defined behavioral assays, size, and cost [141]. It may be reasoned pronograde animals like rodents cannot represent the spinal loading of orthograde animals like humans. Interestingly, research suggests the orientation of the spine, whether parallel or perpendicular to gravity, does not largely impact discal pressures [75, 77, 152]. This lack of difference is further supported by the similarity of disc rheological properties among rodents, pigs, rabbits, sheep, baboons, and humans [153-156]. For a model aimed at evaluating early stage therapeutics, rats are a stronger candidate than mice because rat

discs are around ten times larger and thus are more amenable for injection procedures [157].

In efforts to create a model of disc-associated cLBP in rats, various research groups have induced disc degeneration with methods such as multi-level injury, cytokine injection, spinal destabilization, and large gauge needle puncture, but the transition from a model of degeneration to a model of chronic LBP has been limited by acute time frames, absence of pain-like behavior, animal sex variability, animal age, and confounding secondary effects [173, 176, 198, 200, 203, 209, 210]. Given the state of cLBP research, there is a need for a valid rat model of disc-associated pain that is analogous to human disease progression, nociception, pain-like behavior, chronicity, and disc degeneration phenotype.

The objective of this work was to develop a novel rodent model of LBP that comprehensively recapitulates the underpinning pathobiology of disc degeneration and the emergence of pain observed in humans. Due to the similarity between our data and the clinical presentation of disc-associated cLBP, this model provides value as a platform for evaluating treatments and exploring the pathobiology of disc-associated cLBP.

5.2 materials and Methods

Animals: 36 female, 15-week-old, Sprague Dawley rats were purchased from Envigo and housed with a 12-hour light/dark cycle and *ad libitum* access to food and water. On the day of surgery, the animals were split into three groups of equal size (n = 12): sham, 1-scrape and 6-scrape. After surgery, all animals were weighed and assessed on a weekly basis for overall health. Sample sizes were chosen to ensure sufficient power to detect a 30% decrease in grip strength in injured animals compared to sham animals assuming a

standard deviation that was 26% of the mean. At the study conclusion, a total of 3 animals were excluded from the study (sham: n = 12, 1-scrape: n = 11, 6-scrape: n = 10) due to mis-puncture confirmed by disc volume and H&E data. All animal procedures and assays were in accordance with the National Institute of Health guidelines following PHS Policy on Humane Care and Use of Laboratory Animals and approved by the Institutional Animal Care and Use Committee and the University of Nebraska – Lincoln.

Surgical Procedure and Injury: On the day of surgery, rats were anesthetized, and the lumbar spine was approached ventrally by dissecting through the abdominal cavity and retroperitoneum. The iliac crest was used as a landmark to reliably dissect down to the L5-L6 disc. For sham animals, the L5-L6 was visualized only, and the surgical site was closed in the same manner as injured animals outlined below. For injured animals, the L5-L6 lumbar disc was punctured bilaterally with a strong point dissecting needle (Roboz, RS-6066) with an O.D. of 0.5 mm set to a length of 3 mm. The exact needle length was predetermined based on μCT data to ensure that the needle length did not exceed the diameter of the smallest L5-L6 disc in all animals. While the needle was within the disc, it was swept back and forth along a 90^{o} arc once or six times in the transverse plane for 1-scrape and 6-scrape animals respectively. A simple continuous and subcutaneous suture pattern were used to close the abdominal wall and the skin respectively. Buprenorphine SR (.75 mg/kg) was administered once post-op for pain and animals were rested for two weeks following surgery to enable healing. All animals displayed mild pica behavior, i.e., bedding consumption, after surgery but this behavior resolved within 72 hours.

Disc volume: The L5-L6 disc volume was quantified using the Quantum GX2 μCT Imaging System and Analyze 13.0 (Analyze Direct). In short, the rat lumbar spine was radiographed by placing anesthetized animals in the supine position and scanning for 2-minutes with 90 kV power, 88 μA tube current, 72 mm FOV, 144 um voxel size, and a Cu .06 + Al .05 X-ray filter. VOX files were then removed from the μCT computer and analyzed in Analyze 13.0. To begin processing, raw VOX files from the μCT scans were processed using a high pass threshold to remove all non-bony signal. After the scans were reduced to only bony tissue using the software filter, the intervertebral disc space was colored in every coronal plane where the adjacent vertebral bodies were present using a manual draw tool. The slices of colored intervertebral disc space between the L5 and L6 vertebral bodies were then concatenated, smoothed using a built-in function and saved as an object map. The volume of the object map of these concatenated colored planes was quantified using a built-in software analysis. This quantification was based on a previously established method developed in our lab (under review).

Behavioral tests: For all behavioral tests, animals were acclimated prior to the study commencement to the assay apparatuses and experimenters over the course of three weeks with at least 1 hour of acclimation to each assay apparatus prior to any data collection. All assays except grip strength were performed under red light to minimize animal stress. No more than two behavioral assays were performed on a given day. Experimenters were blinded to animal treatment and all animals were assigned to groups by an unblinded observer.

Von Frey mechanical hypersensitivity: Hypersensitivity to punctate mechanical stimulation in both hind paws was quantified using an electronic von Frey aesthesiometer

(IITC, 2391) with a rigid tip with an outer diameter of 0.8 mm. Briefly, four animals at a time were allowed to acclimate for 15 minutes in clear acrylic chambers placed on a metal grid (IITC, 410). Withdraw threshold was assessed bilaterally by sequentially applying the probe to the right hind paw of all animals followed by the left hind paw of all animals. This process was performed 5 times with approximately 5 minutes of rest between each test for a total of 10 values (5 left, 5 right). The withdraw threshold was calculated by taking the combined left and right average of the final 4 measurements (8 subsamples for each animal). All withdraw thresholds were log transformed to achieve normality and then normalized to baseline to reduce variability.

Grip strength axial hypersensitivity: Hypersensitivity to axial strain was quantified using a grip strength apparatus (Columbus Instruments, 1027SR). All animals were allowed to acclimate to the testing room for 15 minutes prior to testing. Animals were picked up by grasping the hind quarter and then allowed to grip a metal wire mesh attached to the grip strength force sensor. The experimenter's grip was then transitioned to the base of the tail and the animal was gently pulled backward until it released the metal wire mesh. This process was repeated three times and the average max force (N) was used as the grip strength. All withdraw grip strength thresholds were log transformed to achieve normality and then normalized to baseline to reduce variability.

Pressure algometry deep tissue hypersensitivity: Hypersensitivity around the L5-L6 motion segment was measured using an electronic von Frey aesthesiometer (IITC, 2391) with a blunt tip. All animals were allowed to acclimate to the testing room for 15 minutes prior to testing. Each animal was sequentially hooded inside a clean cotton t-shirt such that the entire animal was covered. The animal was then loosely constrained by one

experimenter while another experimenter applied the blunt probe to the dorsal L5-L6 skin and slowly increased the pressure until the animal exhibited a nocifensive response. The L5-L6 skin area was ascertained by palpating along the caudal spinal curvature to locate the area of skin directly superficial to the spinous processes just caudal of the iliac crest. Positive responses included rolling, rapid movement, and vocalization. Two measurements were collected for each animal and the average was used as the deep tissue pressure threshold. All animal thresholds were normalized to baselines to reduce variability.

Open field test: Spontaneous pain-like behavior was evaluated using the open field test with custom built acrylic 2'x2'x2' black, opaque arenas. All animals were allowed to acclimate to the testing room for 15 minutes prior to testing. Animals were individually placed in arenas illuminated by overhead red lighting and allowed to explore for 30 minutes while recorded by an overhead low-light camera (ALPCAM). The middle 20 minutes of each video was analyzed using Ethovision (Noldus) for total distance traveled, time spent rearing unsupported, time spent rearing supported, time spent grooming, max velocity, average turn angle, and max turn angle. All data were normalized to baselines to reduce variability.

Motion segment processing: At the study conclusion, L5-L6 discs were resected, fixed, decalcified, embedded, and sectioned to provide motion segment sections for histological and immunohistochemical processing. In brief, animals were euthanized using CO_2 overdose with cardiac puncture as a secondary measure, and the lumbar spine was resected, and cleaned using bone cutters. The L5-L6 motion segment was isolated from the cleaned spine using a fine-tooth hand saw. After, motion segments were placed in a 6-

well plate with 5 mL of 4% paraformaldehyde (PFA) at room temperature for 24 hours with agitation. After fixation, motion segments were washed 3 x 15 minutes with 1X PBS and decalcified for 18 hours in 3 mL of Immunocal (StatLab 1414-32) at room temperature on an orbital shaker plate at 250 RPM. Decalcified segments were then washed 3 x 15 minutes with 1X PBS and cryoprotected using an overnight 30% sucrose soak. Finally, sections were embedded in Optimal Cutting Temperature Compound (Tissue-Tek) and sectioned in the sagittal plane at 15 µm and 40 µm thicknesses.

Histological processing: 15 µm sections from L5-L6 motion segments were processed using H&E according to standard protocols. In short, sections were post fixed for 15 minutes with 4% PFA, washed with 1X PBS, and stained with hematoxylin. Following hematoxylin staining, sections were washed with 1X PBS, differentiated using acid alcohol, blued with a sodium acetate solution, dehydrated using an alcohol gradient, counterstained with eosin, dehydrated with xylenes and mounted using Permount (Fisher Scientific SP15-100). Three motion segment sections from each animal were stained using the aforementioned process and each motion segment was imaged by collecting and stitching two images taken with a 10X objective on a Zeiss Axio Observer A1 Inverted Microscope (Carl Zeiss Microscopy, Inc.).

Immunohistochemistry: 15 µm and 40 µm sections from L5-L6 motion segments were processed using IHC to visualize inflammatory cytokines and nerve fibers respectively. Both assessments employed the same IHC protocol but used different primary and secondary antibodies. Sections were post-fixed with 4% PFA for 15 minutes, washed 2 x 5 minutes with 1X PBS, 2 x 5 minutes with PBST (1X PBS + 0.01% Tween-20), blocked for one hour with blocking buffer (1X PBS + 3% goat serum + 0.3% Triton X-100), and

incubated in blocking buffer with either 1:100 mouse-derived anti-rat TNF-α (Santa Cruz SC-52746) or 1:500 mouse-derived anti-rat NF-H (Abcam ab528399), 1:100 rabbit-derived anti-rat PGP9.5 (Abcam Ab108896), and 1:1000 chicken-derived anti-rat peripherin (Novus NBP1-05423) for 16 hours. After primary incubation, sections were washed 3 x 15 minutes with PBST and incubated in blocking buffer for one hour with 1:500 goat-derived anti-mouse AF488 (Abcam Ab150177) and, in the case of nerve IHC, anti-rabbit AF555 (Abcam B150086) and anti-chicken AF647 (ThermoFisher A21449). Following secondary incubation, sections were washed 3 x 15 minutes in PBST and incubated with DAPI (ThermoFisher D1306) 1:1000 in PBS for 15 minutes followed by a 3 x 5-minute wash in 1X PBS and then mounted using Prolong Gold (ThermoFisher P36930). Three motion segment sections from each L5-L6 disc were processed using the aforementioned method and the entire motion segment images were created by stitching 6 tiles collected on a Cytation 5 (BioTek) at 4X magnification in the following channels or emission/excitations: brightfield, 377/447 (DAPI), 445/510 (AF488), 531/593 (AF555), and 628/685 (AF647).

Image Analysis: H&E, nerve fiber IHC, inflammatory cytokine IHC, and cellularity outcomes were evaluated on three sections from each animal for a total of ~99 images for each process. Three blinded observers were employed for H&E and nerve fiber scoring. H&E sections were graded according to a rubric delineated by Lai et al. 2021 excepting NP cell morphology [160]. To accomplish this process, disc morphology was broken into NP shape, NP area, NP cell number, NP cell morphology, NP-AF border appearance, AF lamellar organization, AF tears/fissure/disruptions and endplate disruptions/microfractures/ossification. Each of these sub criteria was evaluated on a 0-2

basis, with 0 implying a healthy tissue and 2 implying a degenerated tissue. Observers were trained on example H&E images until the interobserver agreement exceeded 75%. For nerve fiber and inflammatory cytokine IHC, the disc was split into 7 zones: dorsal ligament, dorsal AF, NP, ventral AF inner two thirds, ventral AF outer one third, granulation, and ventral ligament (**Fig 10.**). These zones are outlined in Fig. 1. For nerve fiber IHC, each zone was scored a 0, 1 or 2 based on the presence of 0, 1-3, and 4+ nerve fibers respectively. For nerve IHC scoring, nerve fibers within the ligamentous tissue served as ground truths for immunopositivity. A fiber was recognized as either a cross section, represented by a circular area of intense immunopositivity, or a longitudinal section, defined by a tract of immunopositivity. Further, for nerve IHC grading, graders were asked to verify immunopositivity observed in PGP9.5 by comparing to NF-H and peripherin immunopositivity. All images were individually scored on a high dynamic range IPS display by three blinded evaluators and each final animal score was calculated by taking an average of all three motion segments across the three observers. Cell counting for cellularity and inflammatory cytokine IHC analyses were processed by a single blinded observer using ImageJ. DAPI images were processed in ImageJ according to standard methods to approximate number of cells [284]. For inflammatory cytokine IHC, total number of cells and area of each zone was quantified using ImageJ using the same method as DAPI counting with two exceptions. For inflammation quantification,

the particle maximum area set to 200 μm^2 and the intensity threshold for 8-bit image conversion was set to 50-infinity.

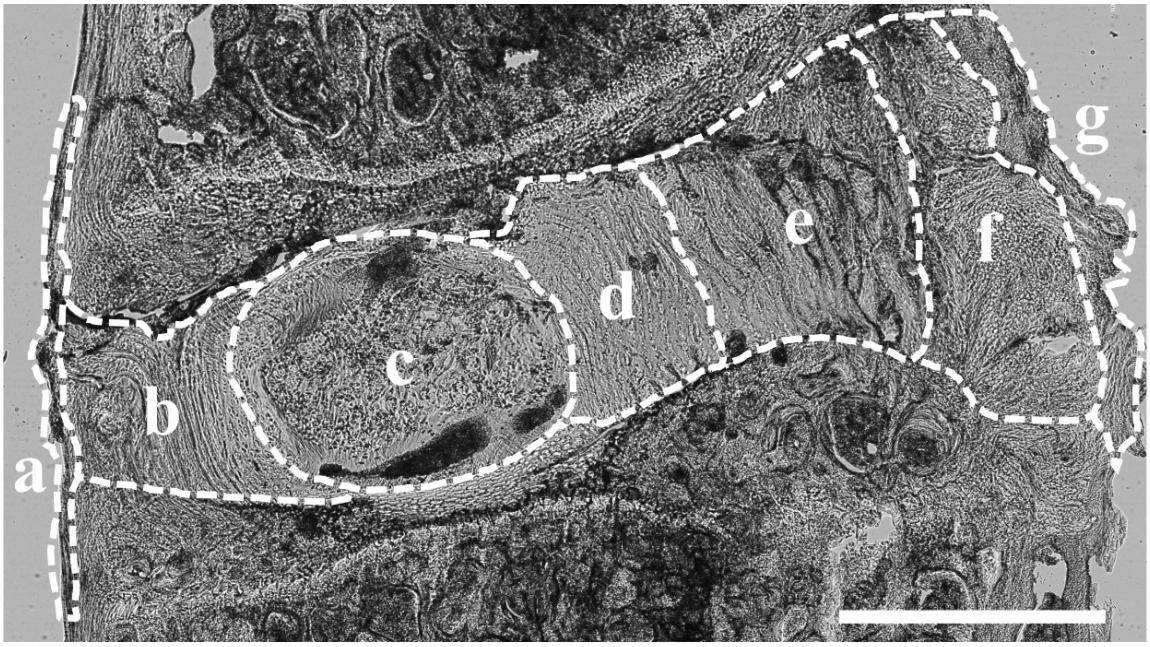

Figure 10. **Disc breakout by regions.** Region specific quantification for IHC analysis was accomplished by breaking the disc into seven regions. These regions are overlaid on the brightfield image: a = dorsal ligament, b = dorsal AF, c = NP, d = ventral AF inner 2/3, e = ventral AF outer 1/3, f = granulation, g = ventral ligament. Scale bar = 1 mm. [3]

Correlation and Principal Component Analysis: The Pearson correlation analysis and principal component analysis (PCA) were performed in GraphPad Prism 9. For both analyses, week 18 μCT and behavioral data were used. The data used from the H&E, disc nerve, and disc cellularity were the disc only values, i.e., the combination of the AF and NP values (Fig 5E, 6E, 7E). The disc inflammation data was composed only of the average number of TNF-α positive cells in the AF (Fig 8E). The ligament cellularity was composed of the ventral and dorsal ligament cell number average. A visual overview of the data used can be seen in **Table 1**. For the grip strength vs. nerve score analysis, week

16 and week 18 grip strength data was average to get a better approximation of the mean and this data was correlated to the disc (NP + AF) nerve score. All animals from all treatments were included in both the correlation and PCA data. The data across the three treatments represented a spectrum of degeneration and thus associative analyses like the Pearson correlation and PCA were particularly useful in identifying what consequences of disc injury related to one another at the 18-week time point.

Outcome	Disc Volume	Grip Strength	Von Frey	Pressure Algometry	Distance Traveled	Summed H&E	Disc Nerve	Ligament Cellularity	Disc Cellularity	Disc TNF-α
Data	Week 18	Week 18	Week 18	Week 18	Week 18	Sum of all individual H&E scores	Sum of NP and AF scores	Ligament cellularity only score	Average of NP and AF cellularity	Average of AF TNF-α+ cells

Table 1. Overview of the data included in the Pearson correlation and PCA. [3]

Statistical analysis: All data is presented as mean ± standard deviation. Data were analyzed using GraphPad Prism 9. Normality was assessed using a Shapiro-Wilk test. Behavioral and disc volume data were analyzed using a two-way ANOVA with Dunnett's post hoc. Each region in cellularity and inflammation data was analyzed using a one-way ANOVA with a Dunnett's post hoc. H&E and nerve IHC was analyzed using a Kruskal-Wallis test with a Dunn's post hoc. Results were considered statistically different when $p < 0.05$.

5.3 Results

Model overview

Sprague-Dawley rats were selected because of their outbred genetics, and well characterized assays for pain-like behavior assessment [146]. To date, the overwhelming majority of rodent models of disc degeneration and LBP have been created in male animals [146, 285]. In contrast, female animals were chosen for this study because LBP

is 30% more prevalent in aged women than men [286]. Animals were injured at 18-weeks of age to ensure all animals had reached osseous maturity such that growth related bony remodeling would not confound the model [287]. In humans, disc degeneration rarely occurs prior to osseous maturity emphasizing the importance of a correct skeletal growth state. This study entailed three weeks of acclimation and baseline data collection, surgery, and 18 weeks of observation **(Fig. 11A)**. During surgery, the L5-L6 disc was visualized in all animals via a ventral approach after dissecting through the abdominal wall and retroperitoneum **(Fig. 11B)**. The L5-L6 disc was the target for injury because it is analogous to the L4-L5 disc in humans which is the most common level of disc degeneration [194]. For injured animals, a hard point micro-dissecting needle was used to bilaterally puncture and disrupt the macrostructure of the disc **(Fig. 11C)**. The needle was rotated along a 90-degree arc in the transverse plane once for animals in the 1-scrape injury and six times for animals in the 6-scrape injury. This injury resulted in bilateral, complete annular fissures along with internal macrostructure disruption from the scraping motion. Annular fissures have been described as major contributors and predictors of progressive lumbar disc degeneration and LBP in humans [101].

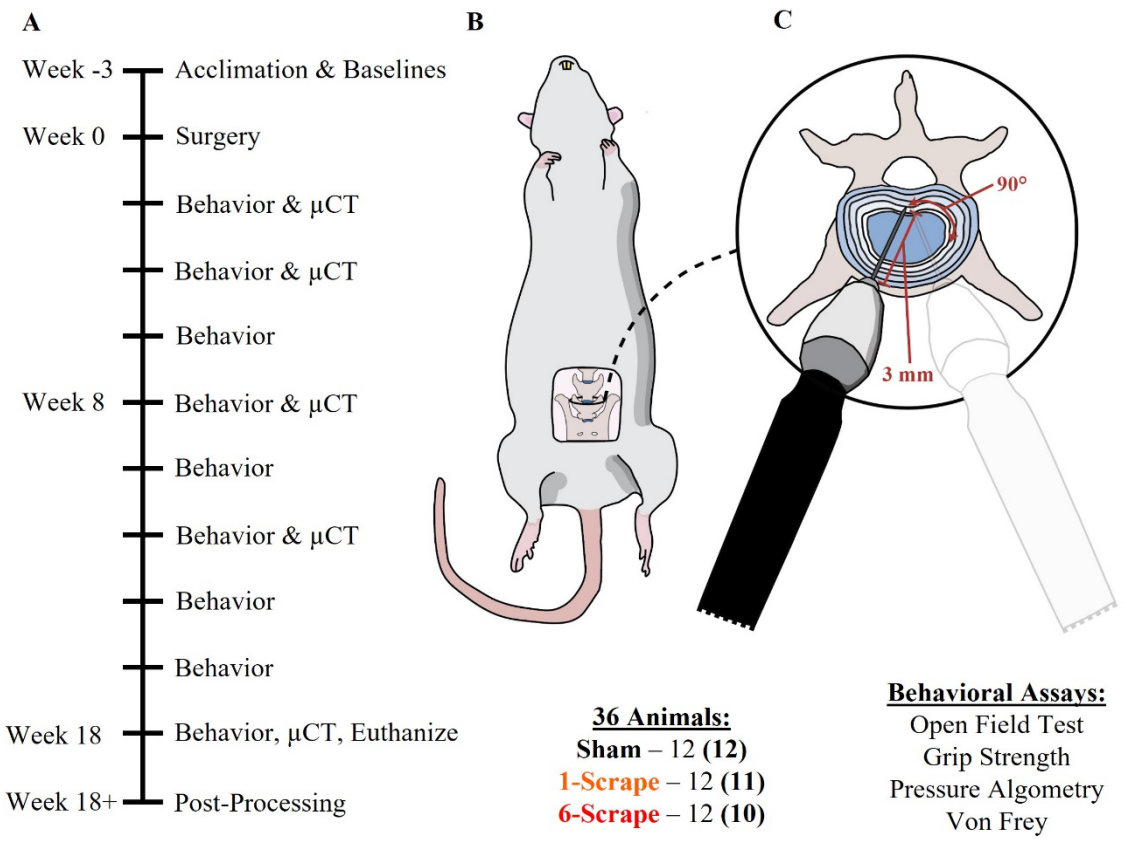

Figure. 11. Animal study overview. (A) Timeline of the study. Animals were acclimated for 3 weeks before collecting baselines. Behavior testing was done every other week and µCT was performed on weeks 0, 2, 4, 8, 12, and 18. **(B)** Graphic of the surgical process. The L5-L6 intervertebral disc was approached ventrally through the abdomen. **(C)** Graphic of the important aspects of the injury process. The needle was inserted to a depth of 3 mm and swept back and forth in the transverse plane along a 90° arc – this process was performed bilaterally. The transparent needle represents the contralateral location of needle insertion. One animal from the 1-scrape and two animals from the 6-scrape group were excluded from the study due to mis-puncture. Final animal number per group is shown in bold in parenthesis. [3]

Injury results in disc volume loss

To evaluate disc degeneration in real time, microcomputed tomography (μCT) was used to calculate the L5-L6 disc volume at 0, 2, 4, 8, 12, and 18 weeks. This method entailed masking the intervertebral disc space between the L5 and L6 vertebral bodies to create a 3D reconstruction of the disc for which the volume was calculated **(Fig. 12A&B)**. Disc volume in both 1-scrape and 6-scrape groups drastically dropped after surgery and remained significantly decreased compared to sham at all measured time points up to week 18 **(Fig. 12C)**. The disc volume method detected highly significant differences between sham and injured animals at weeks 2, 4, 8 and 12 ($p < 0.0001$ - 0.0097). These data confirmed the 1-scrape and 6-scrape injury compromised the hydrostatic equilibrium the disc, resulting in persistent decreased disc volume.

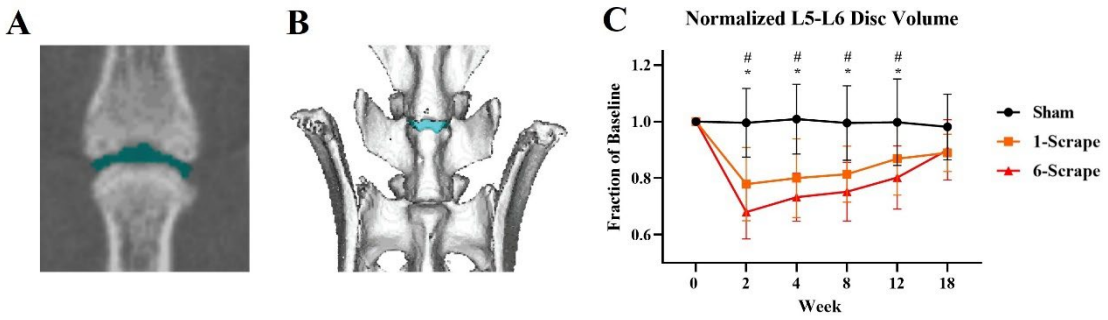

Figure. 12. Disc volume significantly decreases after injury. (A) 2D rendering with the L5-L6 intervertebral disc space colored in blue. Approximately 20 of these colored slices were concatenated to make the final object map for which the volume was determined. **(B)** 3D rendering of the rat lumbosacral spine with the L5-L6 disc object map colored in blue. **(C)** Normalized L5-L6 disc volume of all animal groups. Both injured groups displayed significantly decreased disc volumes compared to sham through week 12. Significant differences were not observed in week 18 due to the gradual increase of disc volume in injured animals occurring after week 2. Data is shown as mean with standard deviation (n = 10-12 per group). # = $p < 0.05$ sham vs. 1-scrape. * = $p < 0.05$ sham vs. 6-scrape. [3]

Injury produces hypersensitivity in evoked pain-like behavior

A battery of pain-like behavior assessments was performed on a biweekly basis to assess the impact of disc injury on animal function. Grip strength, pressure algometry, and von Frey assays measured evoked pain-like behavior, entailing direct manipulation of the animal by an experimenter whereas the open field test measured spontaneous pain-like behavior, involving only observation.

The grip strength assay specifically assessed grip strength impairment mediated by axial strain hypersensitivity **(Fig. 13A)** [288]. Of note, axial hypersensitivity is commonly observed in patients suffering disc-associated LBP and has been observed in mouse models of spontaneous and induced disc degeneration [289-292]. 1-scrape animals exhibited significantly greater hypersensitivity compared to sham only in weeks 12 and 16 whereas 6-scrape animals exhibited increased hypersensitivity in week 6 and at all time points from week 10 to 18 **(Fig. 13B)**. The differences observed in grip strength demonstrated axial strain in injured animals resulted in increased axial pain-like behavior.

Hypersensitivity to deep pressure was determined using a modified pressure algometry assay **(Fig. 13C)** [293]. This assay was employed because deep pressure hypersensitivity has been previously described as highly determinative of LBP in humans and has been used in another model of painful disc degeneration [200, 294]. Weeks 2 and 4 data were not included because animals displayed strong aversive responses to the assay in these weeks. Injured animals exhibited significantly increased hypersensitivity compared to sham animals only at week 10 for 1-scrape and in week 16 (week 18 $p = 0.052$) for 6-scrape animals **(Fig. 13D)**. This assay was successful in detecting

differences between the sham and injured animals but the failure of sham to return to baseline indicated the measurement was influenced by both surgery and injury.

The von Frey assay was performed to measure referred hypersensitivity and to rule out radiculopathy confounds **(Fig. 13E)**. Radiculopathy development was a concern because the needle used to injure the disc could have errantly damaged spinal roots. Fortunately, unilateral differences in withdraw threshold were not observed indicating the model was not confounded by spinal root lesions. Referred hypersensitivity in the hind paw was anticipated in this model because L5 DRG neurons innervate the hind paw footpad and the dorsal and dorsolateral outer AF, implicating cross-sensitization as a contributor to pain-like behavior [179, 181, 182, 295, 296]. Sham animals consistently had higher withdraw thresholds than injured animals, but these differences failed to reach significance at all time points except for week 14 between sham and 1-scrape. These data indicated referred hypersensitivity in the hind-paw did not develop after disc injury, complementing and contrasting prior models in female and male rats, respectively [2, 139].

The open field test was performed to evaluate changes in spontaneous pain-like behavior **(Fig. 13G)**. LBP increases movement disability in humans so it was presumed animals suffering disc-associated pain may exhibit similar changes [297]. No significant differences were observed at any time point in all quantifications including total distance traveled, time spent rearing unsupported, time spent rearing supported, time spent grooming, max velocity, average turn angle and max turn angle **(Fig. 13H & data not shown)**. During analysis, it was determined that a slight difference in box illumination due to the arenas not being symmetrically arranged under the overhead lighting affected

the roaming behavior **(Fig. 13G)**. The data collected from this assay could be improved in the future by addressing this confound.

These pain-like behavior data indicate the 1-scrape and 6-scrape injury resulted in hypersensitivity to axial strain and pressure but did not result in detectable changes in referred hypersensitivity, radiculopathy, nor changes in spontaneous open field behavior.

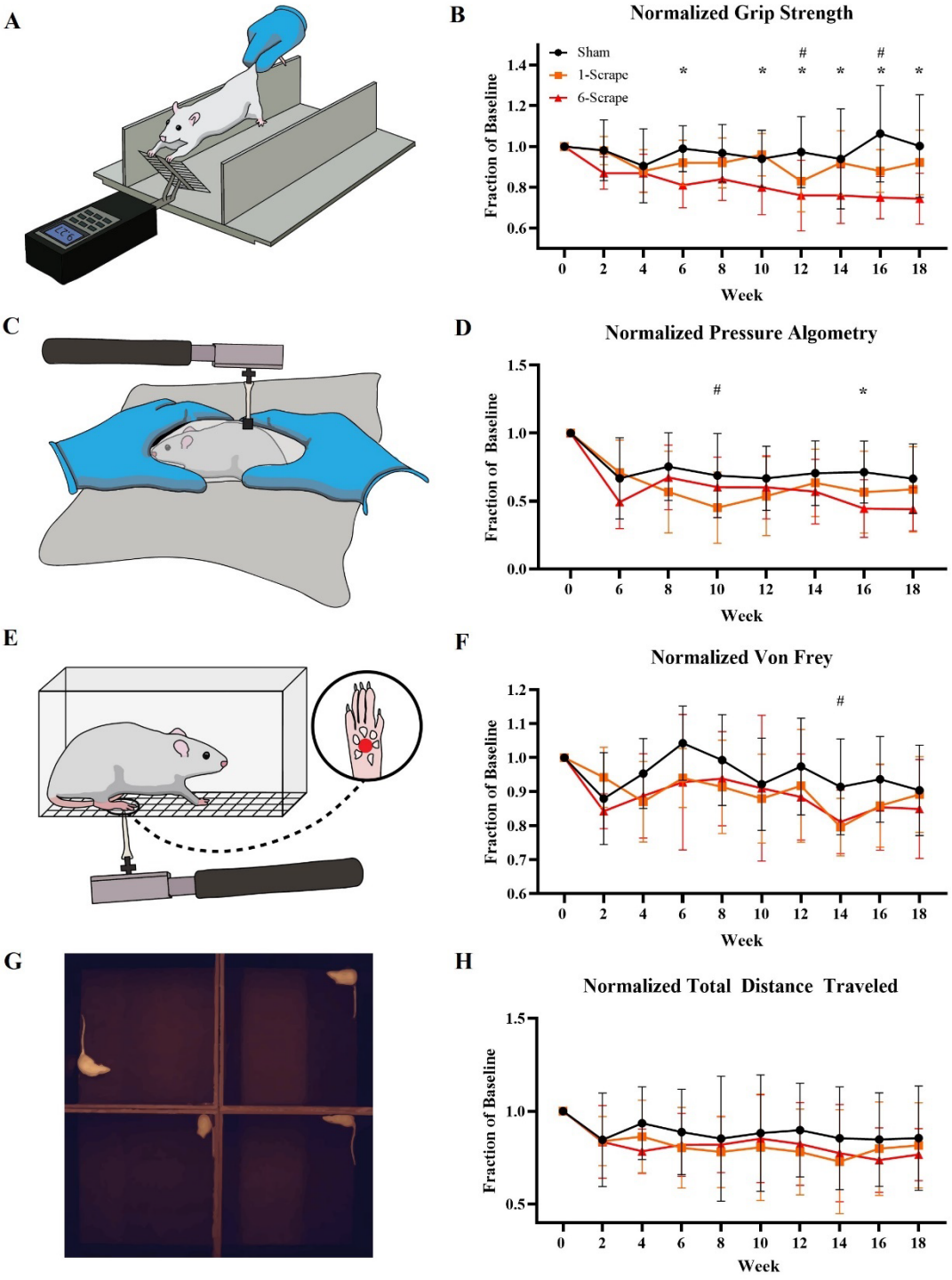
A
B
Normalized Grip Strength
Sham
1-Scrape
6-Scrape
Fraction of Baseline
Week
C
D
Normalized Pressure Algometry
Fraction of Baseline
Week
E
F
Normalized Von Frey
Fraction of Baseline
Week
G
H
Normalized Total Distance Traveled
Fraction of Baseline
Week

Figure. 13. Disc injury results in evoked pain-like behavior hypersensitivity. Evoked pain-like behavior assays: grip strength **(A&B)**, pressure algometry **(C&D)** von Frey **(E&F)**. (B) Normalized grip strength data. 6-scrape animals developed significant hypersensitivity compared to sham animals that persisted for 8 weeks. 1-scrape animals displayed hypersensitivity compared to sham in weeks 12 and 16. (D) Normalized pressure algometry data. 6-scrape animals exhibited significant deep pressure hypersensitivity compared to sham animals in weeks 16 but not week 18 ($p < .052$). 1-scrape animals exhibited significant hypersensitivity in week 10 compared to sham. (F) Normalized combined left and right hind-paw von Frey data. The average injured animal thresholds were consistently lower than sham animals but failed to reach significance except in week 14 compared to 1-scrape. **(G)** Screen capture of animal spontaneous pain-like behavior measured in the open field test. **(H)** Total distance traveled by the animals in the open field. No significant differences were observed. Data is shown as mean with standard deviation (n = 10-12 per group). # = $p < 0.05$ sham vs. 1-scrape. * = $p < 0.05$ sham vs. 6-scrape. [3]

Injury results in disc degeneration and ECM breakdown

At the study conclusion, all animals were euthanized, and motion segment sections were stained with hematoxylin and eosin (H&E) to grade morphological signs of disc degeneration according to a previously established method [160]. NP cell morphology was omitted from the criteria outline by Lai et al. because section thickness (15 μm) made grading this feature unfeasible. Sham animal discs contained healthy, GAG rich NPs and AFs with regularly spaced, uniform lamellae **(Fig. 14A)**. All animals displayed signs of end plate ossification highlighted by the arrowhead in box II, presumably due to natural aging **(Fig. 14A-II)**. Both 1-scrape and 6-scrape animals exhibited less hematoxylin staining in the NP compared to sham, indicating a loss of glycosaminoglycans and cell nuclei **(Fig. 14B&C)**. Hypertrophic cells identified by enlarged nuclei were visible in the AF of injured animals close to hypocellular tissue around the needle tract **(Fig. 14B-III arrowhead & Fig. 14C-V)**. All degenerated discs contained granulation tissue between the ventral margin of the disc and ventral ligament **(Fig. 14B & Fig. 14C-V arrowhead)**. Interestingly, multiple animal motion segments across both injury groups contained ongoing herniations, one of which can be seen in box IV **(Fig. 14B-IV)**. To score each section, NP shape, NP area, NP cell number, NP border

appearance, AF lamellar organization, AF tears/fissure/disruptions and endplate ossification were graded on a 3-point scale. Individual criteria for H&E scores measured significantly increased degeneration in all criteria between injured and sham animals except the end plate **(Fig. 14D)**. Summated scores also confirmed significantly increased overall degeneration in injured animals **(Fig. 14E)**. In summary, the H&E data demonstrated the 1-scrape and 6-scrape injury induced disc degeneration as measured by an established semi-quantitative protocol.

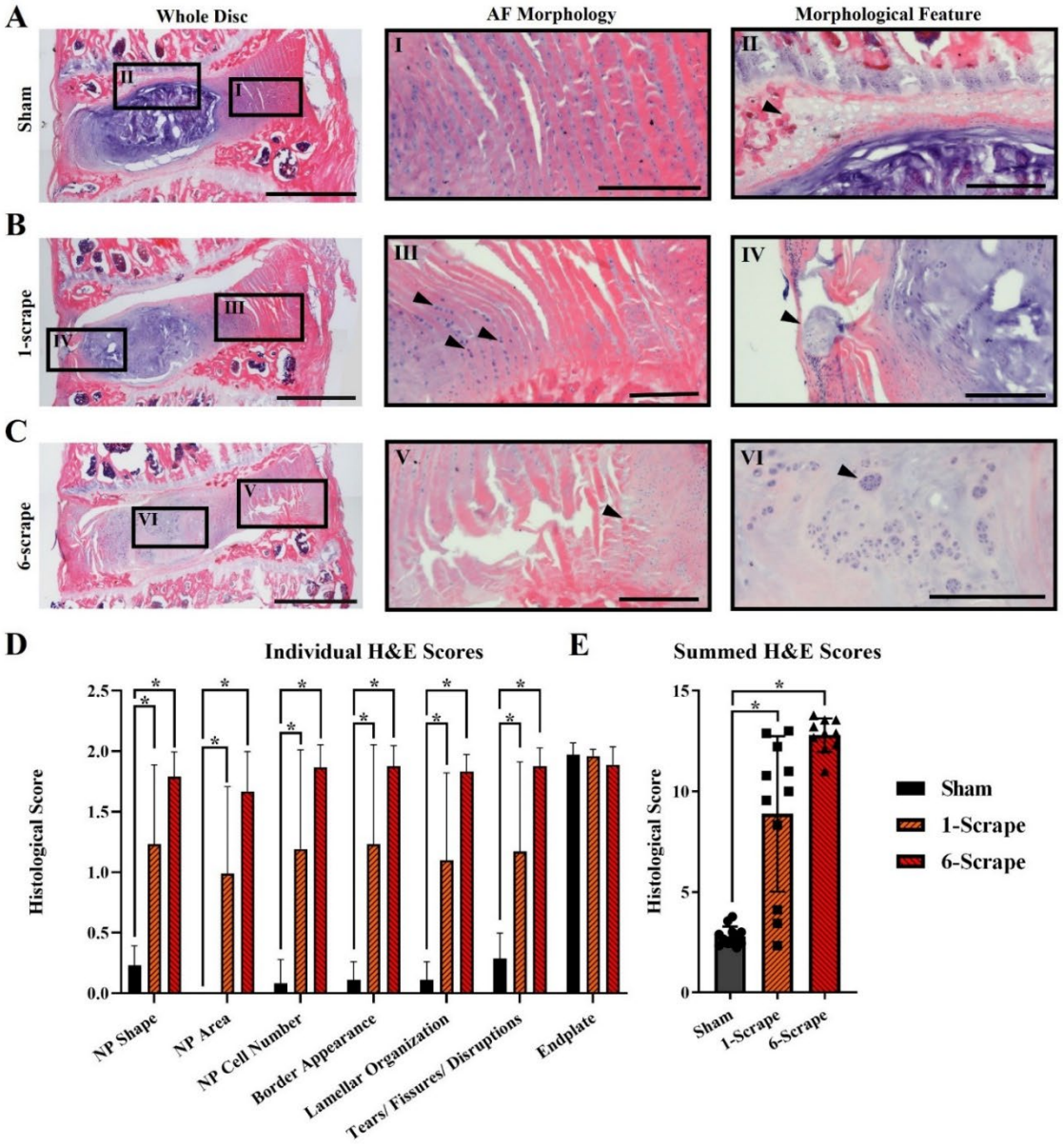
A
Whole Disc
AF Morphology
Morphological Feature
Sham
II
I
I
II
B
1-scrape
III
IV
III
IV
C
6-scrape
V
VI
V
VI
D
Individual H&E Scores
Histological Score
2.5
2.0
1.5
1.0
0.5
0.0
NP Shape
NP Area
NP Cell Number
Border Appearance
Lamellar Organization
Tears/ Fissures/ Disruptions
Endplate
E
Summed H&E Scores
Histological Score
15
10
5
0
Sham
1-Scrape
6-Scrape
Sham
1-Scrape
6-Scrape

Figure. 14. Injury to the disc results in disc degeneration. Representative H&E images from the sham group **(A)**, 1-scrape group **(B)**, and 6-scrape group **(C)**. (A) ROI box I draws focus to appearance of a healthy AF structure present in sham animals. All animals exhibited endplate degeneration as highlighted by the arrowhead in ROI box II. (B) ROI box III focuses on the hypocellularity and disruption of the AF in 1-scrape animals. Arrowhead points to hypertrophic cells in the AF. ROI box IV highlights cellular infiltrate present around an ongoing NP herniation. Evidence of these herniations were found in injured discs across both 1-scrape and 6-scrape animals (C) The ROI box V arrowhead points to granulation tissue present on the ventral margin, between the AF and ventral ligament in 6-scrape animals. ROI box VI shows the hypocellularity of degenerated NP tissue and the arrowhead points to a group of NP cells sequestered in a lacuna. Disc image scale bar = 1 mm. ROI box scale bar = 250 μm. **(D)** Summary of the H&E scores broken down by individual criteria. 1-scrape and 6-scrape scores were significantly higher compared to sham in all categories except end plate. 6-scrape injury resulted in 50% higher average H&E scores compared to 1-scrape, but this failed to reach significance ($p < .09$) **(E)** Summed averages of the individual H&E scores. 1-scrape and 6-scrape scores were significantly higher than sham. The bimodal distribution of scores in the 1-scrape animal group was accounted for by partial healing of the injury defect in three of the 1-scrape animals. Data is shown as mean with standard deviation (n = 10-12 per group). * = $p < 0.05$ sham vs. 6-scrape. [3]

Injury results in disc hypocellularity

Another important aspect of human disc degeneration is disc hypocellularity [298]. As a proxy for cells, nuclei were counted using an automated analysis of DAPI staining. The NP areas in sham animal sections were densely packed with cells and the AF displayed bands of cells consistent with the lamellar structure **(Fig. 15A)**. Conversely, injured animal sections exhibited sparce cellularity in the AF, particularly around the site of needle insertion **(Fig. 15B-IV & Fig. 15C-VI)**. The NP of 6-scrape and 1-scrape sections contained nuclei sequestered to lacunae as noted by the arrowheads in boxes III and **V (Fig. 15B&C)**. Granulation tissue, dense with cells, was present in almost all injured animals and can be seen at the arrowhead in box VI **(Fig. 15C)**. To quantitatively assess differences, nuclei number was counted using the same region scheme as the nerve IHC analysis. Compared to sham animals, 1-scrape disc tissue was significantly less cellular in the ventral AF but was more cellular in the ventral ligament **(Fig. 15D)**. 6-scrape animals displayed significantly higher cellularity in both ligaments but significantly lower cellularity in all regions of the disc compared to sham animals **(Fig. 15D)**. The average cellular density of the ventral AF, NP and dorsal AF was also

computed, and both injured groups exhibited significantly lower cell density compared to sham **(Fig. 15E)**. This cellularity analysis confirmed the 1-scrape and 6-scrape injury created a disc environment incompatible with cell survival, like that observed in humans.

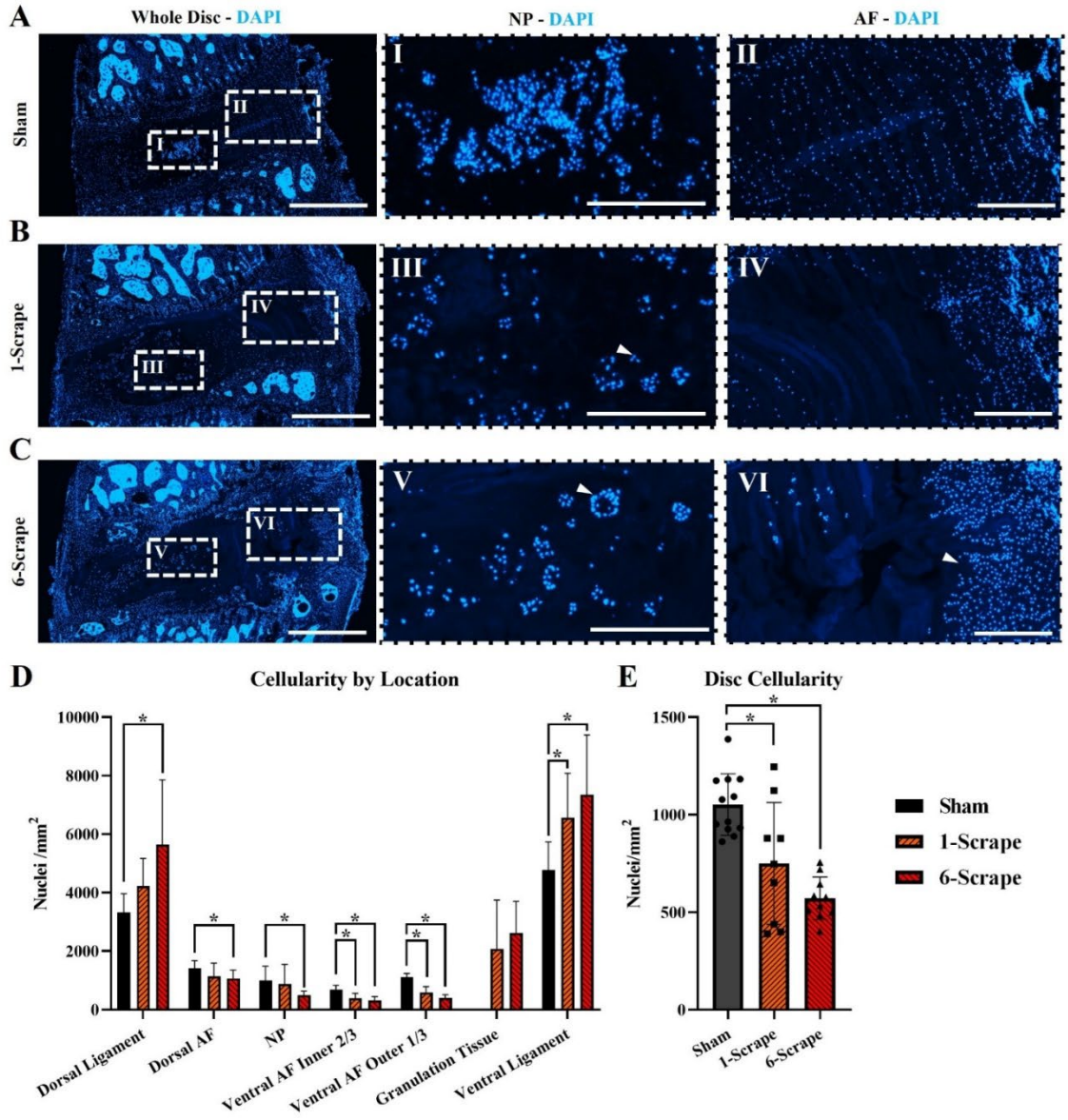

Fi

Figure. 15. Degenerated discs are hypocellular. Representative cellularity (DAPI) images from the sham group **(A)**, 1-scrape group **(B)**, and 6-scrape group **(C)**. (A) Sham animals exhibited dense cellularity in the NP and AF as shown in ROI boxes I & II. (B) 1-scrape animals displayed NP hypocellularity with cells predominantly isolated to lacunae (arrowhead), box III. Box IV highlights the AF hypocellularity. (C) 6-scrape animals exhibited widespread hypocellularity. Box V focuses on the loss of cells in the NP and highlights the isolation of remaining cells to lacunae (arrowheads) like box III in 1-scrape animals. Finally, box VI emphasizes the hypocellularity of the AF around the needle tract and the presence of thick granulation tissue (arrowhead) between the ligament and ventral AF. Whole disc image scale bar = 1 mm. ROI box scale bar = 250 μm. **(D)** Summary of the cellularity scores broken down by zones. 6-scrape ligamentous tissue was hypercellular compared to sham. All disc zones in 6-scrape animals were hypocellular compared to sham. 1-scrape sections exhibited hypocellularity in the ventral AF and hypercellularity in the ventral ligament. **(E)** Average of the NP and AF cellularity averages. Disc tissue from 1-scrape and 6-scrape animals was significantly more hypocellular than sham tissue. Data is shown as mean with standard deviation. Two animals from the 1-scrape were excluded due to a lack of usable sections (n = 9-12 per group). Significant differences between groups were assessed using a one-way ANOVA. # = $p < 0.05$ sham vs. 1-scrape. * = $p < 0.05$ sham vs. 6-scrape. [3]

Injury increases nerve sprouting into the disc

To assess if aberrant nerve sprouting coincided with disc degeneration, like in humans, motion segment sections were processed using immunohistochemistry (IHC) to visualize PGP9.5 (pan neuronal marker), the heavy chain of neurofilament (NF-H), and peripherin (small diameter fiber marker). NF-H and peripherin were included to differentiate nerve fibers, but after processing and validation in DRG sections, it was discovered that unphosphorylated NF-H is expressed across most fiber types in rats limiting its ability to differentiate fibers, and this phenomenon was further suggested by neurobiology research [299-302]. Expectedly, all animals exhibited consistent immunopositivity in the dorsal and ventral ligaments as these structures require innervation for proprioception [303]. Sham animal sections displayed little immunopositivity for any neuronal marker within the disc, but when present, nerves were predominantly in the outer layers of the dorsal AF as noted by an arrowhead **(Fig. 16A)**. In contrast to sham animals, 1-scrape and 6-scrape animal sections exhibited positivity in all regions of the disc, especially in the dorsal and ventral outer one third AF **(Fig. 16B&C)**. Unlike 1-scrape sections, nerve fibers in 6-scrape scrape samples were

commonly observed deep in the tissue along the border of the NP **(Fig. 16C)**. Advancement of nerves fibers into the interior disc structures in this model directly parallels human data in which nerves are observed to penetrate from the peripheral AF into the disc interior [116, 118]. Significantly higher nerve scores were present between injured and sham animals in all regions apart from the ligamentous tissue. Summation of disc only nerve scores, i.e., ventral AF, NP, and dorsal AF, affirmed an overall increase in innervation of injured discs compared to healthy discs **(Fig. 16E)**. The observations and quantifications made from nerve IHC data strongly suggest the 1-scrape and 6-scrape injury along with subsequent degeneration created a neuro-permissive environment throughout the disc, allowing aberrant nerve sprouting into all disc regions.

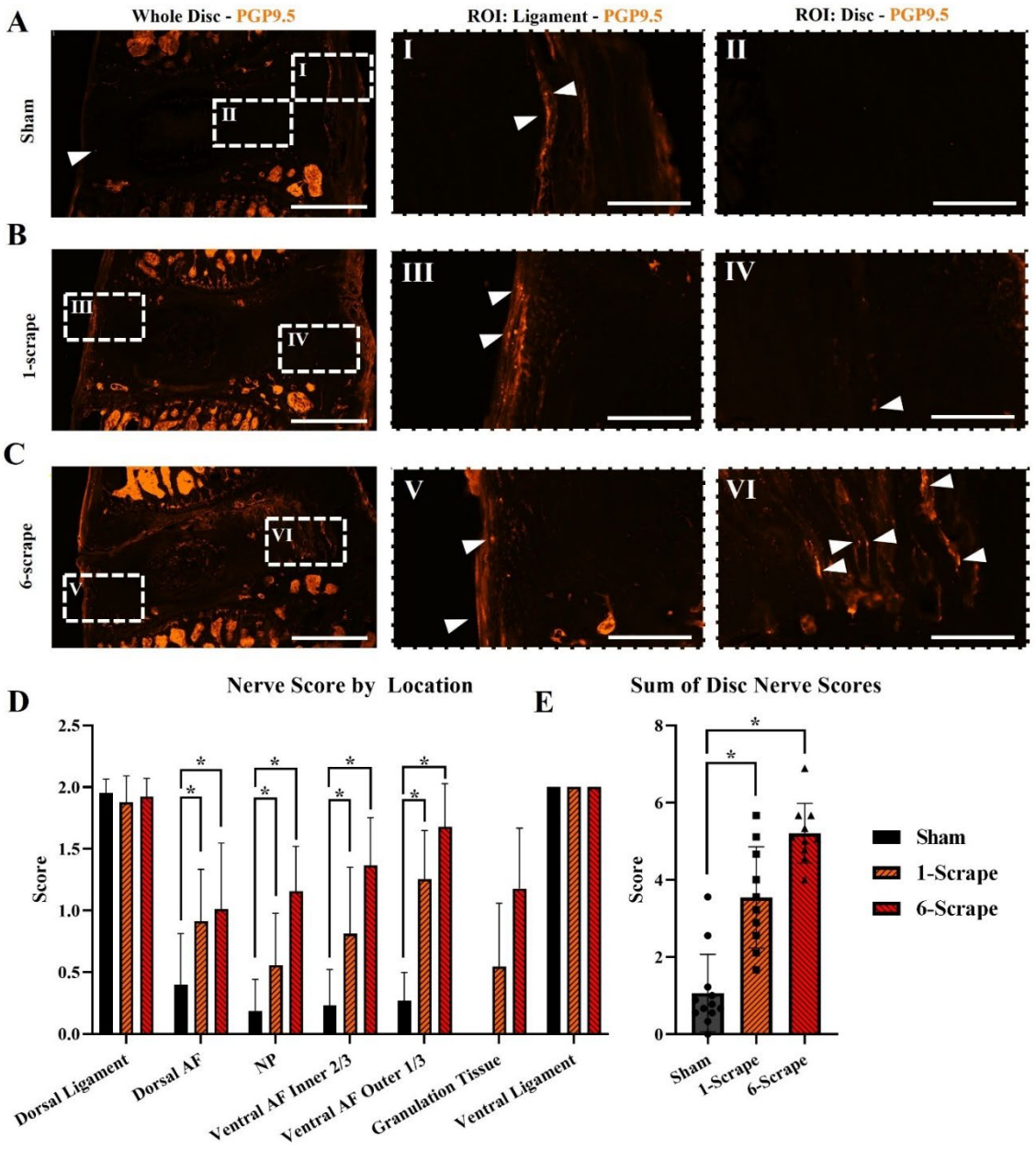
A
Whole Disc - PGP9.5
ROI: Ligament - PGP9.5
ROI: Disc - PGP9.5
Sham
I
II
B
1-scrape
III
IV
C
6-scrape
V
VI
D
Nerve Score by Location
Score
Dorsal Ligament
Dorsal AF
NP
Ventral AF Inner 2/3
Ventral AF Outer 1/3
Granulation Tissue
Ventral Ligament
E
Sum of Disc Nerve Scores
Sham
1-Scrape
6-Scrape

Figure. 16. Nerves sprout into degenerated discs. Representative nerve (PGP 9.5) images from the sham group **(A)**, 1-scrape group **(B)**, and 6-scrape group **(C)**. Arrowheads point to nerve fibers. PGP9.5 immunopositivity in the ligamentous tissue was used as ground truth for nerve fiber quantification. (A) Box I highlights the presence of nerve fibers located in the ventral ligament of a sham section in sham animals. Very rarely were nerve fibers observed in the discs of sham animals as shown in box II. (B) Box III shows a handful of fibers located in the dorsal ligament of 1-scrape animals. Box IV highlights the presence of a nerve fiber in the ventral AF of a 1-scrape animal. (C) Box V highlights multiple nerve fibers found in the dorsal AF of a 6-scrape section. Box VI exhibits a multitude of nerve fibers in the ventral AF of a 6-scrape animal. Whole disc image scale bar = 1 mm. ROI scale bar = 250 μm. **(D)** Evaluation of nerve fibers by location and treatment. 1-scrape and 6-scrape animals contained significantly more nerves than sham animals. **(E)** Summation of the NP and AF nerve scores. Both 1-scrape and 6-scrape nerve scores were significantly greater than sham. Data is shown as mean with standard deviation. One animal from the 1-scrape was excluded due to a lack of usable sections (n = 10-12 per group). The ventral ligamentous tissue in all animals contained 4+ nerves resulting in a standard deviation of zero. # = $p < 0.05$ sham vs. 1-scrape. * = $p < 0.05$ sham vs. 6-scrape. [3]

Injury results in disc cell TNF-a expression

Increased inflammation is consistently observed in disc samples from patients suffering LBP suggesting it is a contributing factor to disc-associated pain [280, 304, 305]. To assess inflammation in this model, TNF-α was visualized in disc sections using immunohistochemistry and TNF-α+ cells were counted. 1-scrape and 6-scrape disc cells exhibited immunopositivity for TNF-α especially in the ventral AF and granulation tissue (Fig. 17B-IV & Fig. 17C-VI). Significantly increased cellular inflammation was observed in the ventral AF and ventral ligament of 6-scrape animals compared to sham (Fig. 17D). The dorsal and ventral AF tissue values were then summated to get a total disc approximation of TNF-α positivity (Fig. 17E). The NP was excluded from this sum due to the abnormal staining pattern which is discussed later. 6-scrape AF tissue contained significantly more TNF-α positive cells than sham discs. In conclusion, these data confirmed the injury and subsequent degeneration promoted production of TNF-α, indicative of inflammation, but further work is needed to validate these results and to determine the inflammatory state of healthy NP.

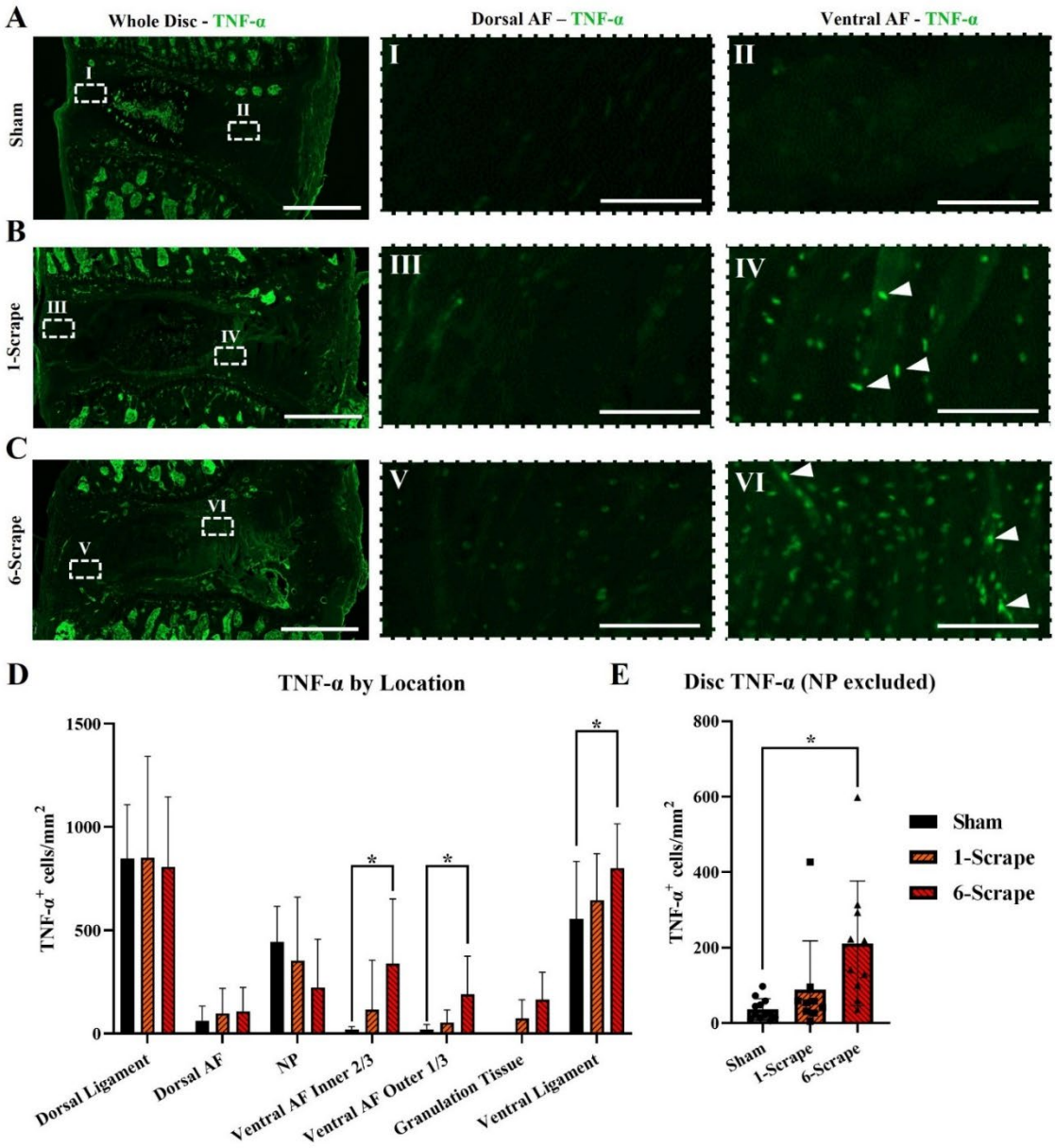
A
Whole Disc - TNF-α
Dorsal AF – TNF-α
Ventral AF - TNF-α
Sham
I
II
B
1-Scrape
III
IV
C
6-Scrape
V
VI
D
TNF-α by Location
TNF-α+ cells/mm2
1500
1000
500
0
Dorsal Ligament
Dorsal AF
NP
Ventral AF Inner 2/3
Ventral AF Outer 1/3
Granulation Tissue
Ventral Ligament
*
E
Disc TNF-α (NP excluded)
800
600
400
200
0
Sham
1-Scrape
6-Scrape

Figure. 17. Degenerated disc cells express TNF-α. Representative TNF-α images from the sham group **(A)**, 1-scrape group **(B)**, and 6-scrape group **(C)**. (A) Sham animal NPs stained extensively with TNF-α although it remains unclear if this is true immunopositivity. Sparce immunopositivity was observed in the dorsal and ventral AF of sham animals as seen in box I & II respectively. (B) 1-scrape sections contained immunopositive cells predominantly in the ventral AF, box IV, although some immunopositive cells were observed in the dorsal AF, box III. 1-scrape and 6-scrape NPs contained immunopositive areas, but this staining was fainter than sham NPs. (C) Boxes V & VI highlights immunopositivity in the dorsal and ventral AF tissue of 6-scrape animals. Arrowheads in both (B) and (C) point to cells which were strongly immunoreactive for TNF-α. Whole disc image scale bar = 1 mm. ROI scale bar = 100 μm. **(D)** Summary of the TNF-α cellular quantification broken down by zones. Significantly more TNF-α+ cells were found in 6-scrape ventral AF and ligamentous tissue. **(E)** Disc total averages, excluding NP, of TNF-α+ cell scores. Disc cellular TNF-α was significantly higher in 6-scrape animals compared to sham. Data is shown as mean with standard deviation. Two animals from the 1-scrape group were excluded due to a lack of usable sections (n = 9-12 per group). Significant differences between groups were assessed using a one-way ANOVA. # = $p < 0.05$ sham vs. 1-scrape. * = $p < 0.05$ sham vs. 6-scrape. [3]

Pain-like behavior was significantly correlated with post-processing outcomes

A Pearson correlation analysis in GraphPad Prism 9 was performed to determine how disc volume, grip strength, von Frey, pressure algometry, distance traveled, H&E, disc nerves, ligament cellularity, disc cellularity, and disc inflammation were associated with one another at 18-weeks. Semi-quantitative and ordinal data sets were included in this analysis because for each semi-quantitative or ordinal data point, nine measurements were averaged making all the data semi-continuous and thus useful for comparison. Twenty significant correlations were revealed among the ten selected assessment outcomes **(Fig. 18A)**. The analysis revealed that important facets of disc degeneration hypothesized to contribute to disc-associated pain in humans, like disc volume loss and nerve sprouting, were significantly correlated with pain-like behavior. The relationship between the average of the final two collections of grip strength and nerve score was highly significant ($p < .0004$) with a moderate correlation of -0.59 **(Fig. 18B)**. A principal component analysis was also performed in GraphPad Prism 9 to impute factors contributing the most variability in the model's 18-week data set. Because this analysis is agnostic to treatment status, it was able to provide insight into what factors most strongly

contribute to data point distribution in a blinded manner. Principal component 1 accounted for 42% of variability across all selected data sets. Assessments which were successful in detecting robust differences between injured and sham animals split along principal component 1 suggesting this component is related to injury **(Fig. 18C)**. The correlation and principal component analysis provided crucial insight into how nerve sprouting was tied to disc-associated pain-like behavior and confirmed most assessments were accurate in detecting differences due to injury. Further, the highly significant correlation between grip strength and nerve sprouting implies this model was successful in producing a degenerative disc pain-like phenotype.

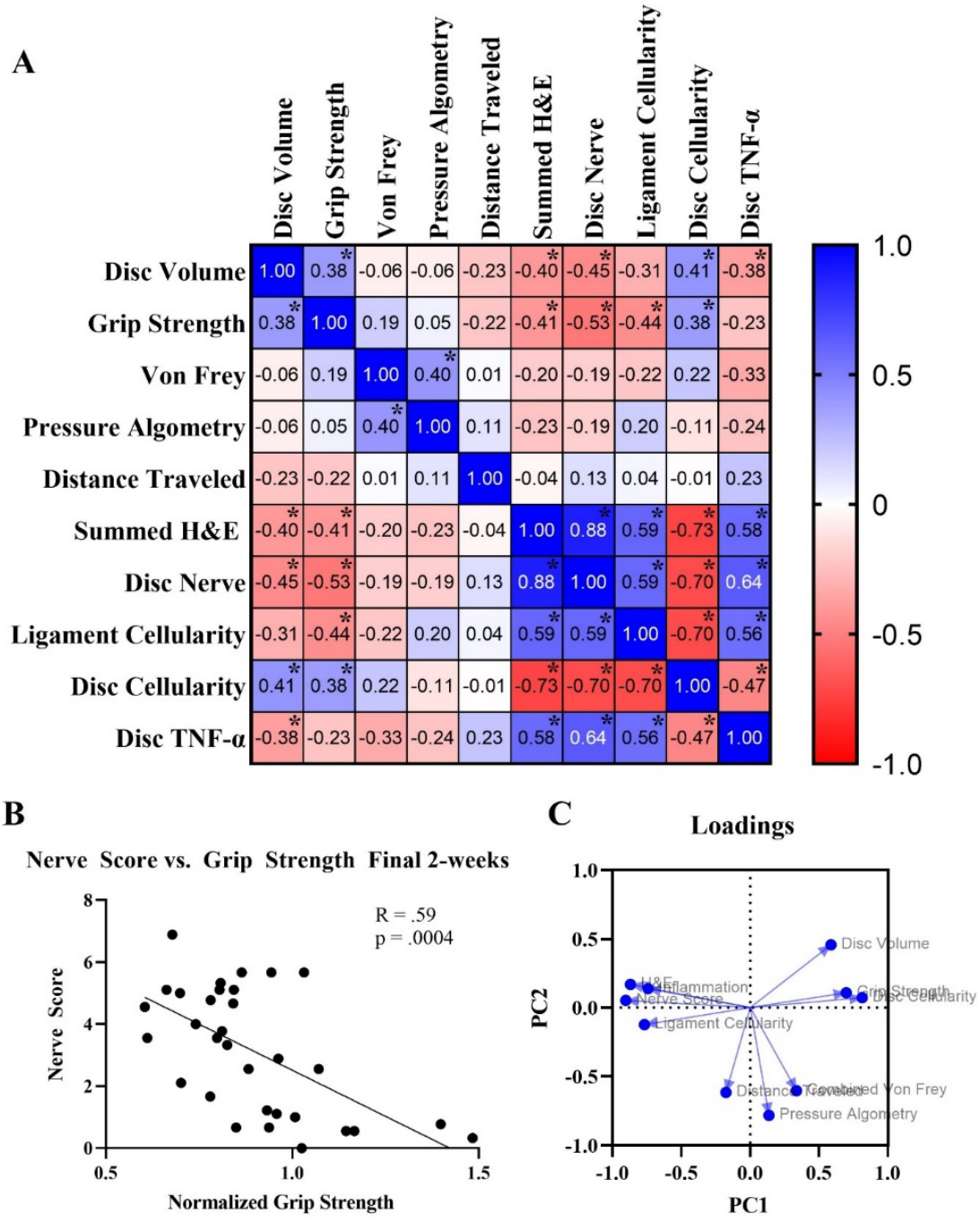

Figure. 18. Relationships between data sets. (A) Correlation matrix of various behavioral and post-processing analyses. Strong correlations were found between grip strength and disc nerve score and among various post-processing outcomes. **(B)** Association between nerve score and the average grip strength in the final 2-weeks. This relationship was highly significant and moderate in strength. **(C)** PCA loadings of the top two principal components. H&E, inflammation, nerve score, and ligament cellularity skewed negative along PC1. Disc volume, grip strength and disc cellularity skewed positive along PC1. Pressure algometry, Von Frey, and distance traveled skewed negative along PC2. PC1 was assumed to be injury due to the distribution of assessments which were metrics of degeneration along this axis. Significant correlations between groups were assessed using a correlation analysis in Prism 9. * = $p < 0.05$. [3]

5.4 Discussion

This work provides the basis of an animal model of disc-associated pain that accurately approximates the human condition. The chronic pain-like behavior, which was correlated with disc degeneration and nerve fiber sprouting, presents strong evidence this model was successful in creating a pain-like phenotype that resulted from pathological shifts in the disc. Additionally, four important characteristics of human degenerative discs, namely, ECM breakdown, hypocellularity, inflammation and aberrant nerve sprouting were manifested in our model, demonstrating comprehensive model validity.

Special consideration was given at the beginning of this study to develop a degeneration induction mechanism that replicates a traumatic event. The needle puncture procedure was refined using sixty rat motion segments (data not shown) to create a traumatic fissure which perforated the AF and resulted in a degenerative phenotype highly analogous to the human clinical presentation of a radiating annular tear (Fig. 11C) [306]. Assessing changes in the disc due to injury using μCT was important as a litmus test for injury success and to track changes in the disc real-time. At two-weeks post-injury, the volumetric method developed in our lab (under review), detected a highly significant decrease of disc volume in injured animals compared to controls confirming successful disc injury.

Provided the knowledge that injury decreased disc volume, the next important question was if injury and ongoing degeneration resulted in pain-like behavior changes. Patients suffering LBP experience movement evoked pain, indicating mechanical agitation of the spine can exacerbate nociception [307, 308]. The highly significant (week 16 & 18 $p < .0001$) and substantial reduction in grip strength between 6-scrape and sham

animals across eight time points implied disc injury resulted in hypersensitivity to axial strain. We believe the grip strength assay was sensitive to degenerative changes because the L5-L6 motion segment is the most caudal spinal structure with significant degrees of freedom involved in this assay. The L6-S1 motion segment is relatively translationally locked because it is fused to the sacrum and iliac, both of which have multiple stabilizing muscle attachments. The immobility of L6-S1 suggests the axial stress imparted on the spine by the pulling motion disproportionately affects the L5-L6 motion segment because musculature is not present to partially distribute the load. Supporting this hypothesis, we observed a distinct increase in spinal curvature above the L5-L6 motion segment in all animals during the grip strength assay. Given the abundance of nerves in degenerated discs and these features, it is likely the axial strain led to increased nociceptor depolarizations in degenerated discs, causing cognitive or spinal reflex mechanisms to release the grip plate at a lower threshold compared to sham. Also, the persistent and progressive decrease in 6-scrape grip strength suggested underlying pathological shifts due to injury drove hypersensitivity rather than acute effects. To our knowledge, no other rat model of disc degeneration has measured increased axial hypersensitivity to this extent longitudinally. Pressure algometry was performed to provide another metric of evoked pain-like behavior. Unlike grip strength, this assay provoked the disc through shear and axial strain. Similar to a prior model of repeated disc puncture [200], pressure algometry detected differences between sham and injured animals at multiple time points, implying nociceptors in the degenerative tissue were activated by shear strain albeit less so compared to axial strain. In difference to well established models of disc degeneration [139], we failed to detect signs of referred hypersensitivity measured by the von Frey

assay. The presupposition behind this assay was that dichotomizing neurons innervating both the hind paw and the degenerated disc could be phenotypically altered by the inflammation present in the degenerated disc giving rise to hind paw referred hypersensitivity. Despite sham exhibiting higher thresholds than injured animals at all time points except week 2, these differences failed to reach significance suggesting referred hypersensitivity was not strongly present. The discrepancy between our model and other models could be due to sex differences in pain, degree of injury, pain masking and innervation especially considering another study witnessed similar results with von Frey characterization on female rats after disc injury [2]. Further, sham animals exhibited higher withdraw thresholds compared to injured animals at all time points, indicating we may have lacked sufficient statistical power to detect differences. The final method used to gauge pain-like behavior was the open field test which did not measure any significant difference.

The disc volume and behavior data suggested injury resulted in pathological disc changes, but these pathologies were unknown. To elucidate the factors underpinning the behavioral changes, we quantified four key aspects of degeneration found in disc samples from LBP patients: ECM breakdown, hypocellularity, aberrant nerve sprouting, and inflammation. The first assessment employed was H&E analysis which is the gold standard for measuring disc degeneration and incorporates multiple metrics of ECM breakdown. End plate ossification present in all animals was consistent with previous literature which observed endplate calcification in 94% of sand rats at the equivalent spinal level and age [309]. Unexpectedly, all healthy NP lacunae stained with eosin (pink) which can be seen in Figure 4A-II, albeit slightly masked by dark hematoxylin

(purple) staining. This unexpected staining indicates that NP lacunae in rats are different in charge and composition than the surrounding ECM. Additional insight was provided by H&E concerning the radial expansion and volume increase of degenerated discs noted in μCT. For healthy discs, the vertebral bodies always terminated in line with the ventral AF. However, depending on the severity of degeneration, granulation tissue up to 500 μm thick was present between the outer edge of the AF and the ventral ligament in injured discs, paralleling granulation tissue found in human degenerated discs [310]. In all cases, the granulation tissue was flanked caudal and cranial and sometimes further ventrolateral by bony deposition suggesting it was load bearing. Gradual deposition of this granulation tissue may have been the factor that drove disc volume increase following injury.

Similar to human data, degenerated discs in our model were hypocellular with large swaths of the ventral AF in injured animals completely devoid of nuclei. Hypocellular tissue predominantly expanded around the site of needle puncture in the AF, indicating secondary aspects of the tissue defect inhibited cellular survival. One possible explanation for this hypocellularity is that matrix catabolism resulted in deleterious loading patterns, causing apoptosis through the MAPK pathway [311-313]. Also like human degeneration, there was cellularized granulation tissue around the ventral surface of the disc [314]. We presume the increased cellularity in the ligamentous tissue of injured animals was a result of infiltrating fibroblasts into the granulation zone.

Nerves in the disc were quantified because aberrant nerve sprouting is hypothesized as a source of painful disc degeneration. In our model, nerve sprouting was ubiquitous across degenerated discs. Because three sections were analyzed for each animal, some nerve fibers could be visualized passing between sections, confirming with

high certainty the immunopositivity was indicative of nerve fibers. When present in degenerated discs, nerves were enriched around annular fissures and in areas of clear tissue disruption which directly compliments human data [116, 118, 120, 315]. This bias in locality may be accounted for by cytokines like NGF, which is known to be produced by degenerating disc cells and stimulates neuronal ingrowth [316]. The proximity of nerves to the disrupted tissue may have predisposed them to activation during mechanical aggravation.

Inflammation proved to be the most difficult to analyze in our model. Strong staining of the NP with TNF-α contradicted literature that has quantified this cytokine in degenerated and healthy discs [304]. Of note, the areas of healthy NP that were immunoreactive with the TNF-α antibody precisely aligned with the areas of healthy NP that unexpectedly stained with eosin in H&E suggesting electrostatic interactions may have driven false-positivity [317]. Abnormal IHC staining of the NP has been observed in rodents previously suggesting this staining is a false positive [291]. We also witnessed this phenomenon infrequently with other antibody targets but failed to see this phenomenon with secondary only controls. Despite these obstacles, we believe counting TNF-α^+ cells was sufficient to gather an approximation of discal inflammation.

After analysis of individual data sets, we then evaluated how week 18 and post-processing data sets related to one another and how well our assessments measured differences due to injury. To answer these questions, we performed a correlation and principal component analysis to impute relationships between data sets and contributors of variance respectively. The correlation value of 0.88 between nerve score and H&E suggested disc breakdown was intrinsically tied to the production of a neuropermissive

environment. The notion that disc volume can serve as a proxy of degeneration was validated by the significant correlation of -0.40 between H&E and disc volume. Greatly important to the validity of this work was the significant correlation of -0.59 between nerve score and grip strength. This moderate relationship provides evidence that nerve presence could be the basis for disc-associated pain. This relationship was limited by the contribution of nociceptive fibers in the granulation and ligamentous tissue, as well as changes in the facet joints, end plates, and paraspinal muscles which were not a part of the nerve score but could have contributed to overall axial hypersensitivity. The role of nerve infiltration in pain development could be further elucidated in the future by assessing this relationship longitudinally. The principal component analysis revealed PC1 accounted for 42% of variability across all data sets used in the correlation analysis. The Eigenvector of this component was more than double that of PC2, suggesting it was an overwhelming contributor to assay variance. Assays which measured differences due to treatment tended to cluster on each end of the PC1 axis, indicating this component was related to treatment.

This work has a few limitations in addition to those already mentioned. First, only female animals were employed making it unclear how sexual dimorphism may relate to the onset of disc degeneration and pain. Further, animals were housed randomly implicating affect contagion as a possible confounding factor in behavioral data [318]. Finally, predictive validity was not measured to verify that the pain could be alleviated via treatments which have efficacy in humans. Work is ongoing to address these limitations in future use of this model.

In summary, construct validity was intrinsic to this model because degeneration induction mimicked an annular radiating tear, which occurs in 50% of human discs by age 35 [306]. Face validity was robustly upheld by significant increases in axial hypersensitivity, deep pressure hypersensitivity, disc degeneration, inflammation, hypocellularity and aberrant innervation. Therapies with known effects, like opioids, must be tested in the future to verify predictive validity. We hope this model will provide utility for the advancement of translatable therapeutics and basic science around LBP which is an immense problem that plagues modern society.

The work described in Chapter 5, constitutes a scientific paper which was published in the Journal of Orthopedic Research Spine [3].

Lillyman, D. J., Lee, F. S., Barnett, E. C., Miller, T. J., Alvaro, M. L., Drvol, H. C., & Wachs, R. A. (2022). Axial hypersensitivity is associated with aberrant nerve sprouting in a novel model of disc degeneration in female Sprague Dawley rats. JOR Spine, e1212. https://doi.org/10.1002/jsp2.1212

CHAPTER 6: Extracellular matrix hydrogel derived from porcine nucleus pulposus restores disc volume and alleviates axial hypersensitivity

6.1 Introduction

Low back pain (LBP) is the leading contributor to disability worldwide [253]. The majority of those who suffer an episode of LBP recover, but for some, the pain persists and becomes debilitating [254]. Chronic LBP imposes a tremendous socioeconomic burden on the world by increasing risk of unemployment, depression, insomnia, suicide, and healthcare expenditures [255-257]. The predominant etiology for this condition is pain arising from the intervertebral disc (IVD), termed disc-associated pain [22]. Patients suffering disc-associated low back pain exhibit pathological changes in their IVDs, including, hypermobility, inflammation, and innervation [103, 118, 319]. Despite the understanding of these fundamental aspects of disc-associated pain, more than half of patients fail to achieve remission after treatment [131, 133-135, 254, 277, 320]. For select patients, IVD fusion and stabilization therapies can be effective short term in reducing pain and disability [60, 61, 133, 276, 321, 322]. The remission these patients experience suggests IVD mechanics may be a key therapeutic target for disc-associated pain. Herein we describe a novel biomaterial which increases injured IVD rheological properties *in vitro and* restores disc volume and alleviates axial hypersensitivity in female Sprague Dawley rats, *in vivo*.

The IVD is a cartilaginous tissue that acts as a joint between vertebral bodies of the spine and is predominantly aneural [79]. Due to age, injury, environment and/or

genetics, cells of the IVD can become stressed, upending tissue homeostasis into catabolism [102, 103]. IVD catabolism is defined by a pro-inflammatory milieu consisting of cytokines, chemokines and enzymes such as TNF-α, IL-1β, IL-6, CCL2, CCL5, MMPs and ADAMTs [114, 280, 323, 324]. These factors recruit and activate immune cells and break down the extracellular matrix, resulting in inflammatory persistence and biomechanical decline [325]. Coinciding degeneration, a loss of neuroinhibitory proteoglycans and formation of annular fissures creates a neuro-permissive environment, allowing nerves to aberrantly penetrate the IVD [79]. While the presence of nerves within degenerated IVD is the basis for pain, there is considerable evidence that altered biomechanics drives nociception, poising hypermobility as the primary causative agent in disc-associated pain [319, 326]. In fact, spinal destabilization alone can produce disc-associated pain-like phenotypes in animals [140, 191, 326-328]. Further, patients treated with IVD stabilizing treatments like surgical fusion, which rotationally and translationally lock the IVD, or spinal stability exercises which impart stronger musculature control over spinal movements, often report pain remission in the short term [60, 61, 132, 133].

We have recently described an animal model of disc-associated low back pain in rats that exhibits overt IVD degeneration and pain-like hypersensitivity. Pain-like behavior in this model is detected during actions which apply strain on the degenerated IVD implying mechanical perturbation as a driver of pain-like behavior. Further, analysis of degenerated IVD morphology revealed the presence of radiating annular tears suggesting degeneration in our model compromises IVD mechanics and macrostructure like what is observed in humans [76, 101, 154, 329]. This knowledge provided the

impetus to engineer a therapeutic that restores IVD tissue mechanical properties to improve pain-like behavior.

The objective of this work was to create a biomaterial capable of annealing macro and microscopic defects in the degenerated IVD tissue in hopes of stabilizing degenerated IVD and in turn lessening disc-associated low back pain. Our lab has developed a novel biomaterial, decellularized nucleus pulposus hydrogel (dNP), derived from decellularized healthy IVD material, that is spontaneously fibrillogenic, cytocompatible, and neuroinhibitory. We modified the constituent concentrations of this biomaterial and added a collagen crosslinker, genipin, to create a robust hydrogel capable of integrating with degenerated IVD tissue. Herein, we demonstrate this biomaterial, dNP+, is cytocompatibility, and is effective at restoring IVD volume, disc mechanics, and alleviating axial hypersensitivity when administered 8-weeks after degeneration is initiated.

6.2 Materials and Methods

Whole disc decellularization: Whole disc decellularization was accomplished using a previously established protocol [235]. In short, cervical spines from commercial line Landrace/Yorkshire/Duroc young female pigs (~200 days of age) were aseptically collected and frozen (-80 °C) following humane slaughter at the United States Meat Animal Research Center Abattoir (Clay Center, NE, USA; USDA Material Transfer Agreement). The spines were then cleaned aseptically and the NPs of the C2-C7 intervertebral discs were surgically removed. NPs were decellularized using a series of detergent and buffer washes as outlined before. Finally, decellularized NPs were

lyophilized (FreeZone 4.5 L Freeze Dryer (7750020, Labconco)) and stored at -80 °C until use.

Digestion and preparation of dNP: The creation of the dNP followed a previously described method with a few exceptions. First, lyophilized decellularized NP was comminuted via cryogenic pulverization using a steel mortar and pestle and liquid nitrogen. 20 mg/mL of comminuted dNP was digested using 1 mg/mL of pepsin (P6887, Sigma-Aldrich) in 0.05 N HCl for 44 hours at 300 rpm using a magnetic stir bar. Following digestion, all steps for making dNPs were performed on ice, until incubation at 37 °C. 10X PBS was added first to the preparation to ensure a final concentration of 1X PBS after following component additions. Next, volumes to ensure 6 mg/mL dNP digest and 6 mg/mL collagen I (Ibidi, 50201) were added to the 10X PBS. The digest was then neutralized with 5 M NaOH to pH ~7.4. Finally, genipin (TCI Chemicals, G0458-25MG) at a stock concentration of 400 mg/mL in DMSO was added to the neutralized dNP solution to yield concentrations ranging from 0 mM to 20 mM. The final formulation used *in vivo* consisted of: 1X PBS, 6 mg/mL collagen, 6 mg/mL dNP and 2.5 mM genipin. Throughout this manuscript, this final formulation is referred to as dNP+.

Gelation kinetics: The rate at which the dNPs achieved complete fibrillogenesis and were cross-linked by genipin was assessed using an absorbance assay. Collagen fibrillogenesis was measured using absorbance at 405 nm as previously described [235]. Genipin cross-linking was measured using absorbance at 610 nm. This wavelength was chosen because genipin produces genipin blue, which has high absorbance at 610 nm, as part of the cross-linking process [249]. To measure these two absorbances longitudinally, 50 μL of dNPs with genipin concentrations of 0, 0.1, 0.5, 1, 2.5, 5, 10, and 20 mM were

prepared and pipetted in duplicate into a 96 well plate. The plate was then placed into a microplate reader, pre-heated to 37 °C and the absorbance was read once every two minutes for 12 hours at 405 and 610 nm. A total of n = 3 different preparations were evaluated with two technical replicates in each preparation.

Gel rheological characterization: Rheological analysis of dNPs was performed to evaluate how genipin crosslinking affected mechanical properties. Rheology testing was performed on gels using an Anton Paar MCR 302 with sand blasted plates. Briefly, dNP gels were formed by pipetting 100 uL of the gel solutions into 8-mm diameter silicone molds (666305, Grace Bio-Labs). The gels were sandwiched between glass slides within the molds to prevent desiccation and incubated at 37 °C for 24 hours to allow for complete fibrillogenesis and cross-linking. After gelation, the gels were soaked in 1X PBS for 30 minutes to reach a replicable osmotic equilibrium. An amplitude sweep was conducted to determine the storage and loss modulus across strains analogous to human movement [330]. This characterization entailed measuring the storage and loss moduli across a strain range from 0.1-1.66% at an angular frequency of 5 Hz. This angular frequency was chosen because it is analogous to the compressive cycling frequency during movement [170, 331]. The average storage and loss modulus from 0.137-0.477% strain was computed as the storage and loss modulus for each gel. Gels were fabricated and tested in duplicate, and this process was repeated three times (n = 3).

Motion segment rheological characterization: Rheological analysis of rat motion segments was performed to evaluate how treatment with dNP+ affects disc mechanics after injury in an *ex vivo* setting and 8-weeks after administration in the animal model. Rheological assessment was performed on motion segments using an Anton Paar MCR

302 rheometer with sand blasted plates. Briefly, motion segments were excised from cadavers and potted in custom 3D printed pots using Loctite 401. For the *ex vivo* work, L4-L5, L5-L6, and L6-S1 motion segments were used. After pot fixation, motion segments were allowed to equilibrate overnight in 1X PBS at 4 °C. To analyze, motion segments were brought to room temperature and attached to the rheometer base plate and probe using labeling tape. An amplitude sweep was then conducted to determine the storage and loss modulus across strains analogous to human movement [330]. This characterization entailed measuring the storage and loss moduli across a strain range from 0.1-1.66% at an angular frequency of 5 Hz. The average storage and loss modulus from 0.137-0.477% strain was computed as the storage and loss modulus for each motion segment. For the *ex vivo* work, PBS and dNP+ motion segments were then injured using the six-scrape injury method described in the injury surgery methods. These motion segments were equilibrated again overnight and mechanically assessed the following day using an amplitude sweep with the previously described parameters. Once the post-injury values were collected, the PBS and dNP+ motion segments were injected with 1X PBS or dNP+ respectively. All motion segments were placed in a humidified incubator for 8 hours at 37 °C followed by overnight equilibration in 1X PBS at 4 °C. All motion segment rheology was assessed a final time and all values were normalized against baseline. Non-injured motion segments were included in the *ex vivo* work as additional controls.

Cytotoxic Assessment of dNP+: To evaluate the cytotoxicity of dNP+ *in vitro,* human NP cells were cultured on top of dNP+ gels. In brief, P3 human NP cells (4800, ScienCell) were cultured in a T75 flask (CLS430641U, Sigma Aldrich) coated with 15

μg of Poly-L-Lysine (0413, ScienCell) using Complete Nucleus Pulposus Cell Media (4801, ScienCell) till confluent to prepare NP cells for treatment plating. 48-well plates were prepared for treatment culture by coating with either nothing (PS) or with 10 μL of 6 mg/mL collagen gel, 6 mg/mL collagen + 6 mg/mL dNP gel, or 6 mg/mL collagen + 6 mg/mL dNP + 2.5 mM (dNP+) genipin gel. The coatings were gelled for 8 hours at 37 °C in a humidified incubator and then equilibrated for 12 hours in 1X PBS. NP cells were plated on top of the treatments at a density of 7,500 cells/cm^2 and cultured for 48 hours in phenol free Complete Nucleus Pulposus Cell Media (4801-prf, ScienCell). After the 48 hours expired, each well was washed three times with 1X PBS and incubated with 200 μL 2 μM Calcein AM (ThermoFisher C3100MP) and 4 μM Eth-1 (ThermoFisher E1169) in 1X PBS for 30 minutes. A kill well was included for each donor as a positive control for Eth-1 staining. The cells were then washed three times with 1X PBS and imaged on a Cytation 5 (BioTek) at 10X. Imaging parameters were uniform across all samples and four images were taken from each well, deconvoluted, and analyzed using Gen 5 software to evaluate cell number and size in each channel. Viability was calculated using the following calculation: (# Calcein+ objects / (# Calcein+ objects + # Eth-1+ objects) x 100. Cytocompatibility was evaluated using three unique human NP cells donors, n = 3, with three technical replicated each.

Animals: All animal procedures and assays were in accordance with the National Institute of Health guidelines following PHS Policy on Humane Care and Use of Laboratory Animals and approved by the Institutional Animal Care and Use Committee and the University of Nebraska – Lincoln. Thirty-six female, 15-week-old, Sprague Dawley rats were purchased from Envigo and housed with a 12-hour light/dark cycle and

ad libitum access to food and water. On the day of surgery, the animals were split into three groups of equal size (n = 12): sham, PBS, and dNP+. After surgery, all animals were weighed and assessed on a weekly basis for overall health. After injury surgery, one sham animal had to be terminated due to surgical complications. After treatment surgery, one dNP+ animal was excluded due to incorrect treatment injection.

Injury Surgery: Animals were injured according to a previously described method. In brief, on the day of injury surgery, rats were anesthetized, and the lumbar spine was approached ventrally by dissecting through the abdominal cavity and retroperitoneum. For sham animals, the L5-L6 was visualized only, and the surgical site was closed in the same manner as injured animals outlined below. For PBS and dNP+ animals, the L5-L6 lumbar disc was punctured bilaterally with a strong point dissecting needle (Roboz, RS-6066) with an O.D. of 0.5 mm set to a length of 2.75 mm. The exact needle length was predetermined based on μCT data to ensure that the needle length did not exceed the diameter of the smallest L5-L6 disc in all animals. While the needle was within the disc, it was swept back and forth along a 90^{o} arc six times in the transverse plane. A simple continuous and subcutaneous suture pattern were used to close the abdominal wall and the skin respectively. Buprenorphine SR (.75 mg/kg) was administered once post-op for pain and animals were rested for two weeks following surgery to enable healing. All animals displayed mild pica behavior, i.e., bedding consumption, after surgery but this behavior resolved within 72 hours.

Treatment Surgery: On the day of surgery, rats were anesthetized, and the L5-L6 disc was approached using the same method as the injury surgery. For sham animals, the L5-L6 was visualized only, and the surgical site was closed in the same manner as treated

animals. For PBS and dNP+ animals, the L5-L6 lumbar disc was injected through the midline using a 30-gauge needle (BD, 305106) with a rubber stopper (WidgetCo, 7-R0000000-EPDM-RS) fixed at 2 mm attached to a 10 µL microsyringe (Hamilton, 80001). PBS animals were injected with 2.5 µL of 1X PBS and dNP+ animals were injected with 2.5 µL dNP+. The needle length was predetermined based on µCT data to increase the probability that the therapeutic was delivered to the NP space. The injection site was sealed with Vetbond (3M, 1469c). A simple continuous and subcutaneous suture pattern were used to close the abdominal wall and the skin respectively. Buprenorphine SR (.75 mg/kg) was administered once post-op for pain and animals were rested for two weeks following surgery to enable healing. All animals displayed mild pica behavior, i.e., bedding consumption, after surgery but this behavior resolved within 72 hours.

Disc volume: The L5-L6 disc volume was quantified using the Quantum GX2 µCT Imaging System and Analyze 13.0 (Analyze Direct). In short, the rat lumbar spine was radiographed by placing anesthetized animals in the supine position and scanning for 2-minutes with 90 kV power, 88 µA tube current, 72 mm FOV, 144 µm voxel size, and a Cu .06 + Al .05 X-ray filter. VOX files were then removed from the µCT computer and analyzed in Analyze 13.0. To begin processing, raw VOX files from the µCT scans were filtered using a high pass threshold of 700 Hounsfield units to remove all non-bony signal. After the scans were reduced to only bony tissue using the software filter, the intervertebral disc space was colored in every coronal plane where the adjacent vertebral bodies were present using a manual draw tool. The slices of colored intervertebral disc space between the L5 and L6 vertebral bodies were then concatenated, smoothed using a built-in function and saved as an object map. The volume of the object map of these

concatenated colored planes was quantified using a built-in software analysis. This quantification was based on a previously established method developed in our lab.

Behavioral tests: For all behavioral tests, animals were acclimated prior to the study commencement to the assay apparatuses and experimenters over the course of three weeks with at least two hours of acclimation to each assay apparatus prior to any data collection. All assays were performed under red light to minimize animal stress. Two sets of baseline behavior measurement were collected and averaged to obtain a better estimate of the mean with particular consideration that all measurements after baseline would be normalized to the baseline values. Three experimenters performed behavioral tests, and all were blinded to animal treatment. All animals were randomly assigned to treatment groups.

Grip strength axial hypersensitivity: Hypersensitivity to axial strain was quantified using a grip strength apparatus (Columbus Instruments, 1027SR). All animals were allowed to acclimate to the testing room for 15 minutes prior to testing. Animals were picked up by grasping the hind quarter and then allowed to grip a metal wire mesh attached to the grip strength force sensor. The experimenter's grip was then transitioned to the base of the tail and the animal was gently pulled backward until it released the metal wire mesh. This process was repeated three times and the average max force (N) was used as the grip strength. All withdraw grip strength thresholds were log transformed to achieve normality and then normalized to baseline to reduce variability.

Pressure algometry deep tissue hypersensitivity: Hypersensitivity around the L5-L6 motion segment was measured using an electronic von Frey aesthesiometer (IITC, 2391) with a blunt tip applied to the skin superficial the L5-L6 IVD. All animals were allowed

to acclimate to the testing room for 15 minutes prior to testing. Each animal was sequentially hooded inside a clean cotton t-shirt such that the entire animal was covered. The animal was then loosely constrained by one experimenter while another experimenter applied the blunt probe to the dorsal L5-L6 skin and slowly increased the pressure until the animal exhibited a nocifensive response. The L5-L6 skin area was ascertained by palpating along the caudal spinal curvature to locate the area of skin directly superficial to the spinous processes just caudal of the iliac crest. Positive responses included rolling, rapid movement, and vocalization. Two measurements were collected for each animal and the average was used as the deep tissue pressure threshold. All animal thresholds were normalized to baselines to reduce variability.

Open field test: Spontaneous pain-like behavior was evaluated using the open field test with custom built acrylic 2'x2'x2' black, opaque arenas. All animals were allowed to acclimate to the testing room for 15 minutes prior to testing. Animals were individually placed in arenas illuminated by overhead red lighting and allowed to explore for 30 minutes while recorded by an overhead low-light camera (ALPCAM). The middle 20 minutes of each video was analyzed using Ethovision (Noldus) for total distance traveled, time spent rearing unsupported, time spent rearing supported, time spent grooming, max velocity, average turn angle, and max turn angle. All data were normalized to baselines to reduce variability.

Diclofenac treatment: Diclofenac was administered to all animals at 15-weeks to validate pain-like behavior could be alleviated via analgesic mechanisms used in humans. To accomplish this, diclofenac (MilliporeSigma, 1188800-200MG) was dissolved in 1X PBS at 5 mg/mL and administered intraperitoneally at 10 mg/kg. Diclofenac was

administered by an unblinded observer that did not participate in behavioral quantification. Grip strength was performed thirty minutes after the administration of diclofenac. No signs of toxicity were observed in any animal.

Statistical analysis: All data is presented as mean ± 95% CI. Data were analyzed using GraphPad Prism 9. Normality was assessed using a Shapiro-Wilk test. Cytotoxicity, cell area, and cell count were assessed using a one-way ANOVA with Tukey's post hoc. Behavioral and disc volume data were analyzed using a two-way ANOVA with Dunnett's post hoc. Motion segment rheology was evaluated using a student's t-test. Results were considered statistically different when $p < 0.05$.

6.3 Results

Study overview

The central proposition of this work was that a painful degenerated disc could be transitioned to a painless state using a hydrogel fabricated from decellularized tissue **(Fig 19A)**. The success of this proposition hinged upon delivery and maintenance of the hydrogel within the degenerated disc. This criterion motivated the inclusion of a tissue crosslinker, genipin, to form inter-collagenous covalent bonds between the hydrogel and the degenerated disc tissue. The first arm of this work focused on engineering a genipin crosslinked hydrogel derived from decellularized NP tissue and collagen type I **(Fig 19B)**. To accomplish this, cervical NPs were dissected, decellularized, comminuted, digested, neutralized, and supplemented with 6 mg/mL collagen to form a dNP gel. Additionally, dNP gels were supplemented with 0 – 20 mM genipin to measure the variable effects of genipin crosslinking on select outcomes. These outcomes consisted of gelation kinetics, rheological properties, cytotoxicity, and *ex vivo* capacity to augment

disc mechanics. Work done in this first arm suggested a 6.0 mg/mL dNP + 6.0 mg/mL collagen I + 2.5 mM genipin hydrogel, termed **dNP+**, was the best candidate for *in vivo* evaluation. To test the therapeutic *in vivo,* disc degeneration was induced in female Sprague Dawley rats and progressed for 8-weeks **(Fig 19C)**. At 9-weeks, injured animals were treated with dNP+ or 1X PBS, and pain-like alleviation was measured over the following 6 weeks.

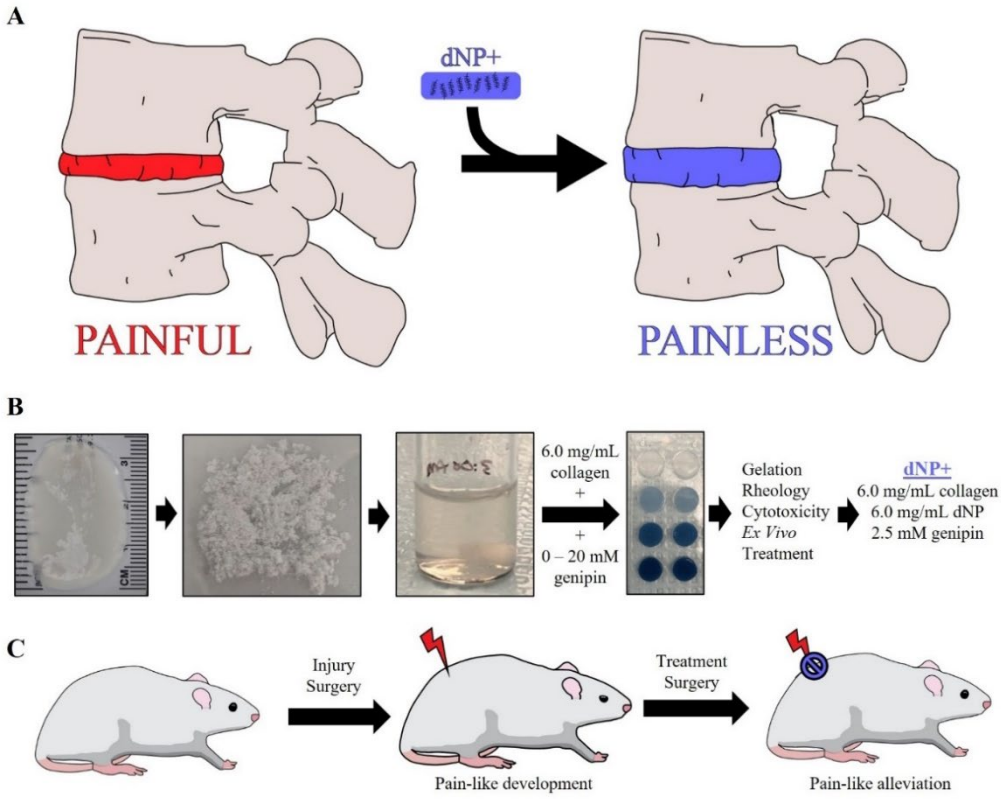

Fig. 19. Study overview. (A) The central proposal of this work was that a treatment for disc-associated pain could be fabricated from a mixture of decellularized healthy porcine NP tissue, collagen and genipin. This therapeutic would theoretically be tissue integrating, spontaneously fibrillogenic, cytocompatible, and biomechanically restorative leading to pain-like behavior remission. **(B)** The first arm of this work entailed testing decellularized nucleus pulposus gels supplemented with 6.0 mg/mL collagen and genipin from 0 – 20 mM. Testing of these gels (dNPs) included gelation kinetics, rheology, cytotoxicity, and *ex vivo* capacity to restore injured disc mechanics. **(C)** The outcomes of the first arm determined the optimal formulation to test *in vivo* was 6.0 mg/mL dNP + 6.0 mg/mL collagen + 2.5 mM genipin, referred to in this manuscript as **dNP+**. To test this therapeutic, disc degeneration was induced in female Sprague Dawley rats and allowed to progress for 8 weeks. At 9 weeks post-injury, half of injured animals were treated with dNP+ and the other half with 1X PBS. Throughout the *in vivo* arm, disc volume and pain-like behavioral metrics were collected to monitor effects of disc injury and treatment.

dNP hydrogels spontaneously gel and crosslink

Considering a core criterion of this therapeutic was to be thermally fibrillogenic after injection into a ~37 °C tissue, gelation kinetics were first to be determined. When incubated at 37 °C, all dNP gels completed collagen fibrillogenesis in under 15 minutes **(Fig. 20A&B)**. The rapid gelation indicated these gels would be suitable for an injection procedure because fibrillogenesis would complete in the time required for wound closure and awakening. Crosslinking mediated by genipin took considerably longer than collagen fibrillogenesis with most formulations hitting 75% max 610 nm absorbance by four hours **(Fig. 20C&D)**. Of note, the cross-linking process appears relatively stochastic with higher genipin concentrations beginning crosslink formation earlier than lower concentrations. Also, higher concentrations of genipin resulted in a greater final absorbance, indicating increasing degrees of crosslinking occurred with increasing genipin concentrations. It should also be noted that the asymptotic limit of absorbance seen at 610 nm for the 10 mM and 20 mM genipin dNP hydrogels could be due to limitations of the plate reader, true nature of the gel absorbance, or both. All gels were homogenous in appearance and did not desiccate during the 12-hour collection window **(Fig. 20E)**. These data showed genipin hydrogels complete fibrillogenesis in under 15 minutes and that the majority of genipin crosslinking activity completed in 4 hours in all formulations.

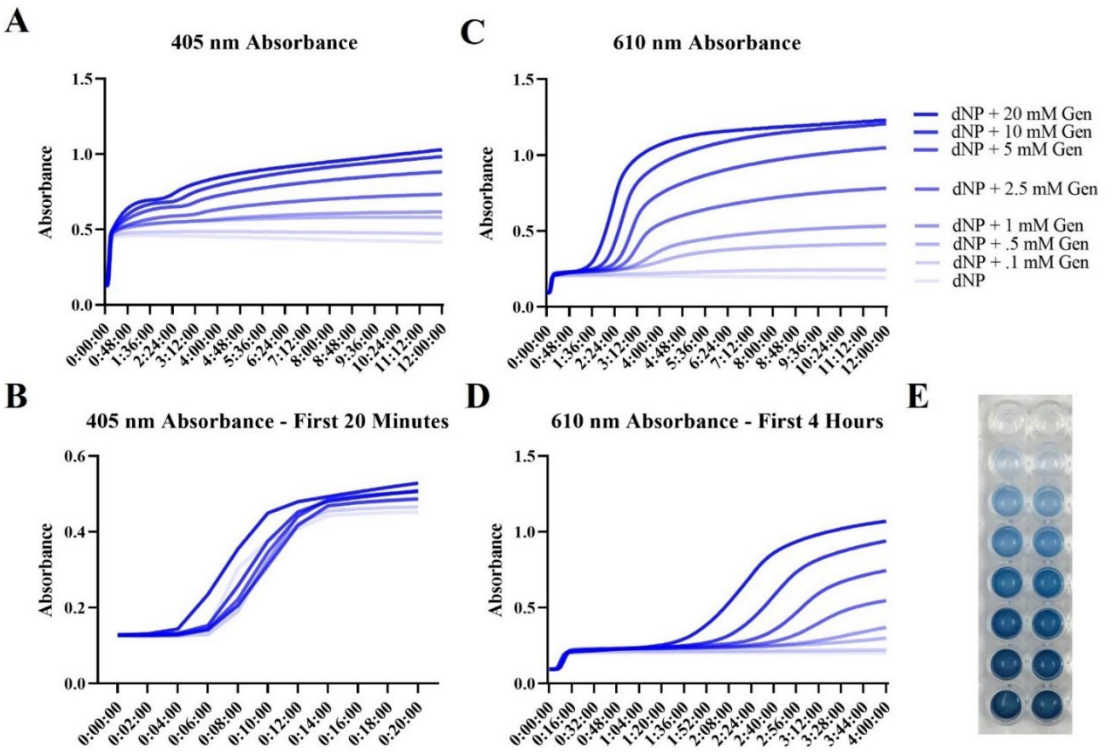

Figure. 20. dNP hydrogels spontaneously gel and crosslink. (A) Absorbance of dNP gels at 405 nm over 12 hours of incubation at 37 °C. All gels exhibited rapid fibrillogenesis in the first 20 minutes of incubation as highlighted in **(B).** The continual increase of absorbance at 405 nm after 2 hours was largely due to light absorbance by genipin blue, produced during crosslinking. **(C)** Absorbance of dNP gels at 610 nm over 12 hours of incubation at 37 °C. As part of the crosslinking reaction, genipin forms genipin blue, which absorbs light at 610 nm. 20 mM genipin dNP gels were the first to exhibit a dramatic increase in absorbance although all genipin supplemented gels increased in absorbance at 610 nm. The final absorbance values for 10 mM and 20 mM dNP gels were similar, suggesting all crosslinking sites were exhausted at around 10 mM genipin. The final absorbance of 2.5 mM genipin was at the midpoint between 20 mM and 0 mM. **(D)** All gels exhibited genipin crosslinking initiation between 1:30:00 and 3:30:00. **(E)** Visual appearance of the dNP hydrogels after 12 hours of incubation at 37 °C. Error bars are left off for clarity.

Genipin increases dNP rheological properties

Each dNP formulation was measured using a rheometer for storage and loss moduli **(Fig. 21A)**. The average storage and loss modulus for 0 mM genipin gels was 709.81 ± 44.0 Pa and 118.19 ± 8.68 Pa respectively **(Fig. 21B&C)**. The addition of genipin markedly increased storage and loss moduli with 20 mM genipin increasing the storage modulus more than 10-fold (11271 ± 3248.0 Pa) compared to 0 mM gels (709.81 ± 44.0). Despite the remarkable increase of gel mechanics due to genipin, the moduli of all gels was still several orders of magnitude lower than native disc tissue (5.8 – 42.7 MPa) [332]. The average storage and loss modulus for the 2.5 mM genipin dNP gel were 2244.6 ± 208.60 Pa and 210 ± 30.976 Pa respectively. Interestingly, the dNP hydrogels suffered increasing variability at genipin concentration of 5 mM and above. It is unclear what drove this increase in variability as duplicate variability and inter experimental variability were both present at these higher concentrations. Unlike the gelation kinetic data, the rheological properties did not reach an asymptotic limit indicating that cross-linking sites were not exhausted at high genipin concentrations. Overall, these data

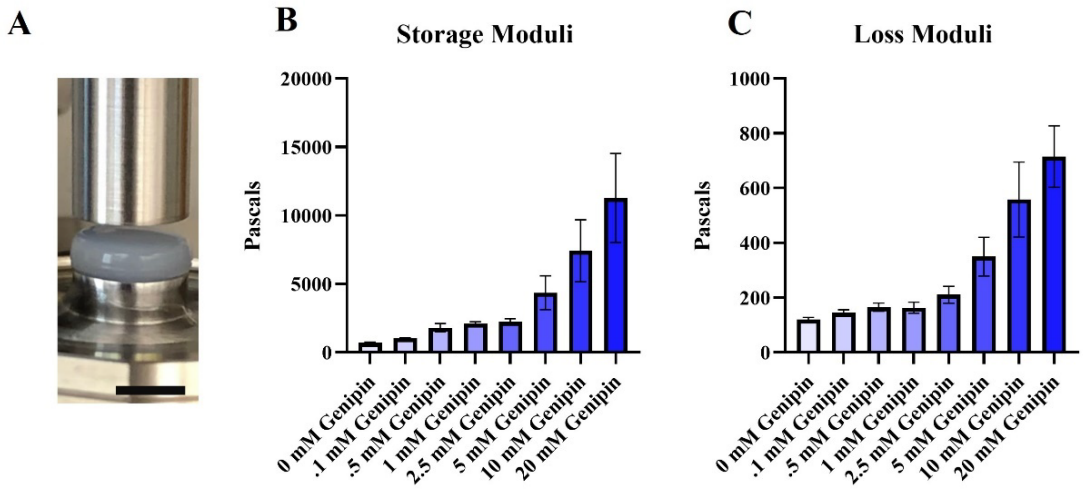

Figure. 21. Genipin increases dNP rheological properties. (A) Image of a dNP hydrogel on the rheometer. Scale bar = 4 mm. **(B)** Storage moduli of the dNP with various concentrations of genipin. These values represent the elastic resistance to torsional strain. The variability increased dramatically with genipin concentrations greater than 5 mM. **(C)** Loss moduli of the dNP with various concentrations of genipin. These values represent the viscous resistance to torsional strain. Like the storage moduli, variability increased dramatically when genipin concentrations exceeded 5 mM. Data is shown as mean with standard deviation. Gel fabrication was performed in duplicate in three separate experiments (n = 3).

confirmed genipin increases dNP mechanical properties and that 2.5 mM genipin was the highest concentration usable to maintain replicable fabrication outcomes.

dNP+ increases injured motion segment rheological properties

Two additional necessities for dNP+ were injectability and capacity to alter disc mechanics. These two aspects were tested *ex vivo* using motion segments excised from female Sprague Dawley rat cadavers (Envigo). The injection process is overviewed on a potted motion segment in **Fig. 22A** with the gel dyed green for ease of visualization. To determine how well dNP+ restores disc mechanics, the rheological properties of potted motion segments were assessed at baseline, after 6-scrape injury, and after treatment **(Figure 22B&C)**. Undamaged controls were included at all time points. All data was normalized to pre-injury baselines so that motion segments from L4 to S1 could be pooled without dramatically increasing the variability. Injury decreased the storage modulus of motion segments by around 50% compared to baseline. Treatment with dNP+ significantly restored the modulus by 15% compared to post-injury ($p < .05$). These data confirmed dNP+ alone could increase disc mechanical properties after acute injury.

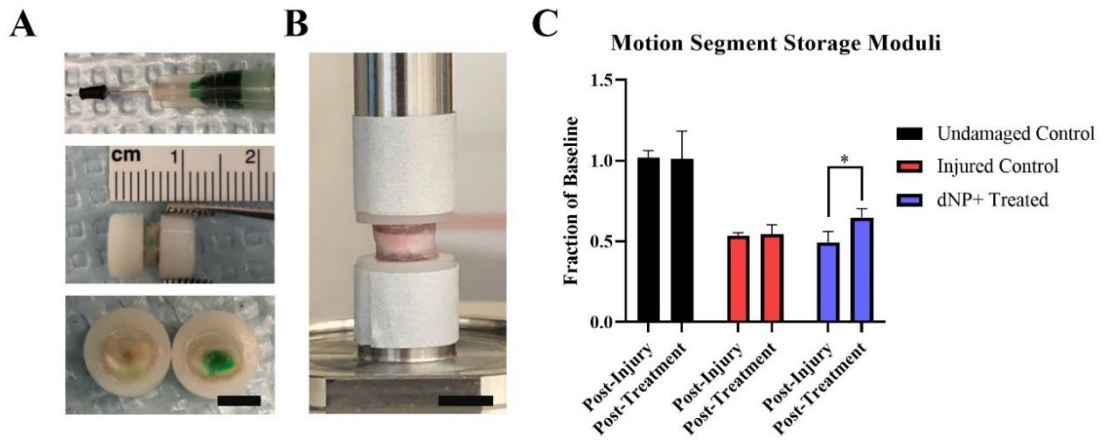

Figure. 22. dNP+ increases injured motion segment rheological properties. (A) Overview of the injection process. In the top image, the 30-gauge needle is shown with a rubber stopper set at 2 mm from the needle tip. The rubber stopper was fixed to the needle to make injection into the NP space easier. The middle image shows a potted motion segment injected with dNP gel dyed green. Evidence of injection can be seen by the faint green dye on the surface of the annulus fibrosus. In the bottom image, an injected motion segment was transected to display the presence of dyed dNP hydrogel injectate in the disc. **(B)** An image of a potted motion segment fixed to the rheometer. **(C)** Motion segment storage moduli from undamaged, injured, and dNP+ treated motion segments. The average storage modulus of undamaged control motion segments did not change over the course of the experiment. Injury decreased the average storage modulus by 50%. Treatment with dNP+ significantly rescued the storage modulus by 15% compared to post-injury. Data is shown as mean with standard deviation (n = 3 per group). Significance is denoted by * = $p < 0.05$

dNP+ is cytocompatible

To understand if the dNP+ hydrogel was cytotoxic, human NP cells were cultured on top of dNP+ for 48 hours and viability was determined using Calcein AM and Eth-1. Polystyrene, collagen, and collagen + dNP substrates were included as controls **(Fig. 23A-C)**. All treatments exhibited minimal cell death as noted by the absence of Eth-1 fluorescence **(Fig. 23A-D)**. When quantified, the viability for polystyrene, collagen, collagen + dNP, and dNP+ treatments was 96.37 ± 1.91%, 96.54 ± 1.66%, 96.15 ± .91%, and 94.75 ± 5.61% respectively **(Fig. 23E)**. Cell size was also quantified to assess how each substrate impacted cellular morphology **(Fig. 23F)**. The collagen + dNP control which represented a less stiff substrate compared to polystyrene caused the cells to adopt

significantly smaller morphology compared to polystyrene. However, this effect was partially reversed with the addition of 2.5 mM genipin in the dNP+ treatment. Rheological data indicated 2.5 mM genipin made the hydrogel stiffer which likely caused the cells to adopt a more elongated morphology. Finally, total cell count was measured to understand if dNP+ had a negative effect on cellular proliferation **(Fig. 23G)**. Analysis of the cell counts indicated dNP+ did not significantly decrease cellular proliferation compared to collagen + dNP although the difference narrowly missed significance ($p < .052$). These results demonstrated that dNP+ is not cytotoxic to human NP cells but the trend toward decreased cellular proliferation suggested concentrations of genipin above 2.5 mM might be harmful to cell growth and perhaps viability.

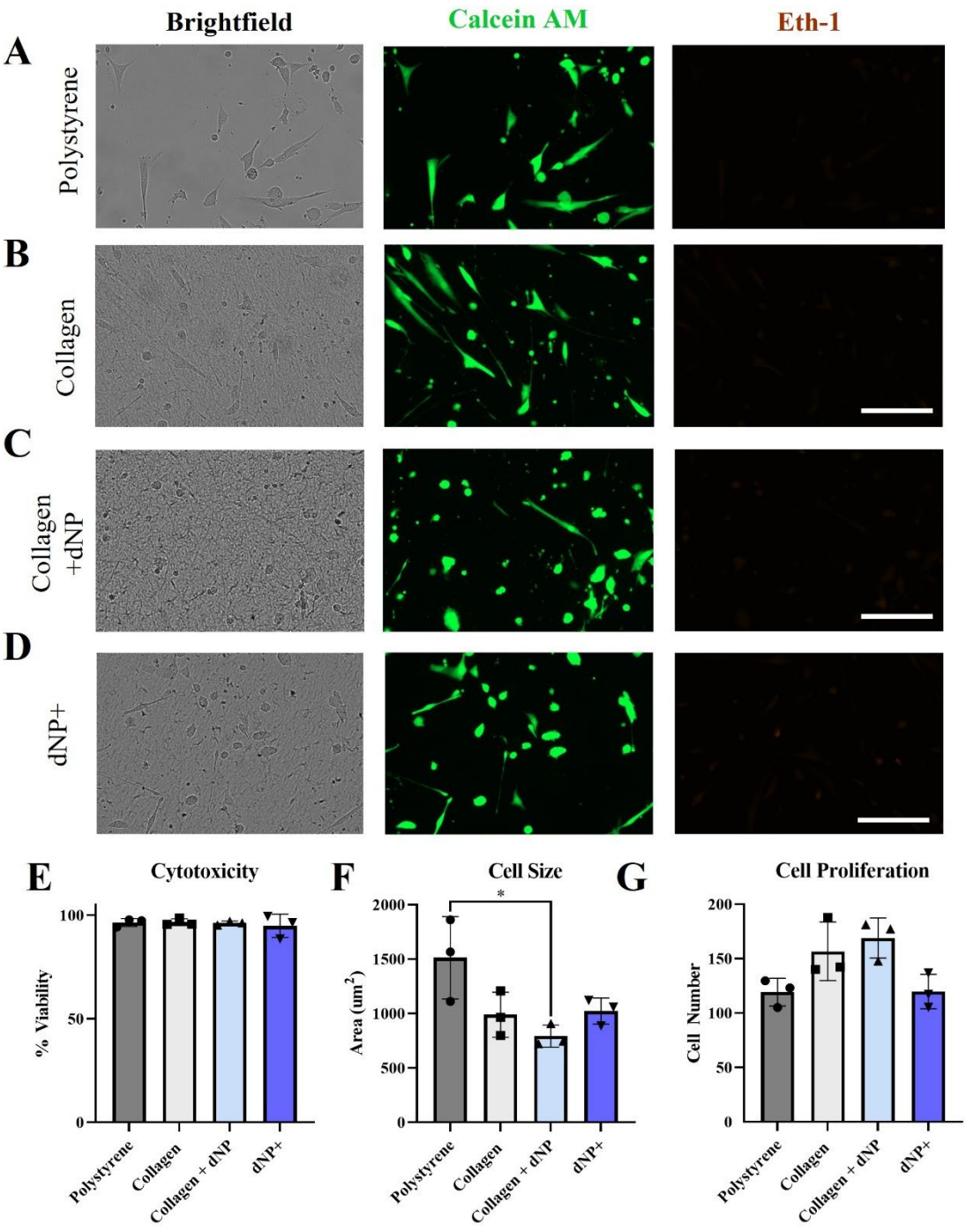
Brightfield
Calcein AM
Eth-1
A
Polystyrene
B
Collagen
C
Collagen +dNP
D
dNP+
E
Cytotoxicity
% Viability
100
50
0
F
Cell Size
Area (um²)
2000
1500
1000
500
0
*
G
Cell Proliferation
Cell Number
200
150
100
50
0
Polystyrene
Collagen
Collagen + dNP
dNP+

Figur

Figure. 23. dNP+ is not cytotoxic. Representative images from the NP cell viability experiments **(A-D)**. NP cells exhibited a more elongated morphology on polystyrene compared to collagen, collagen + dNP, and dNP+ substrates. **(E)** Quantification of treatment cytotoxicity. All treatments exhibited minimal cytotoxicity with the lowest average viability occurring in the dNP+ treatment at 94.75%. **(F)** Quantification of cell size. Cells plated on polystyrene had significantly larger average area than those plated on collagen + dNP. **(G)** Quantification of total cell proliferation over the 48 hours of culture. No significant differences were detected between any treatment group. The average dNP+ treatment cell count was 66% that of collagen + dNP but this difference narrowly missed significance ($p < .052$). Data is shown as mean with standard deviation. Experiments consisted of three unique donors plated in triplicate ($n = 3$). Significance is denoted by * = $p < 0.05$

Animal study overview

Previously, we have described a rat model of disc-associated pain that develops robust axial hypersensitivity after disc injury [3]. This model was employed to evaluate the efficacy of dNP+ as a rescue treatment for disc-associated low back pain. This arm entailed three weeks of acclimation, injury surgery, eight weeks of data collection, treatment surgery, six weeks of data collection, and post-processing **(Fig. 24A)**. For the study, 36, female Sprague Dawley rats were split into three groups of equal size: sham – 12, PBS – 12, dNP+ - 12. One sham animal was euthanized prematurely due to surgical complications and one dNP+ animal was excluded due to incorrect treatment injection **(Fig. 24B)**. Animal pain-like development was assessed using two evoked pain-like behavior assays, grip strength and pressure algometry, and one spontaneous pain-like behavior assay, the open field test **(Fig 24C)**. Disc degeneration was induced at week 0 in PBS and dNP+ animals and involved mechanical injury of the L5-L6 IVD using a ventral approach (Fig. 24D). Sham discs were visualized only. The treatment surgery followed the same steps as the injury surgery to visualize the disc **(Fig. 24E)**. PBS and dNP+ animals discs were injected with 1X PBS or dNP+ respectively **(Fig. 24F)**. Sham discs were visualized only.

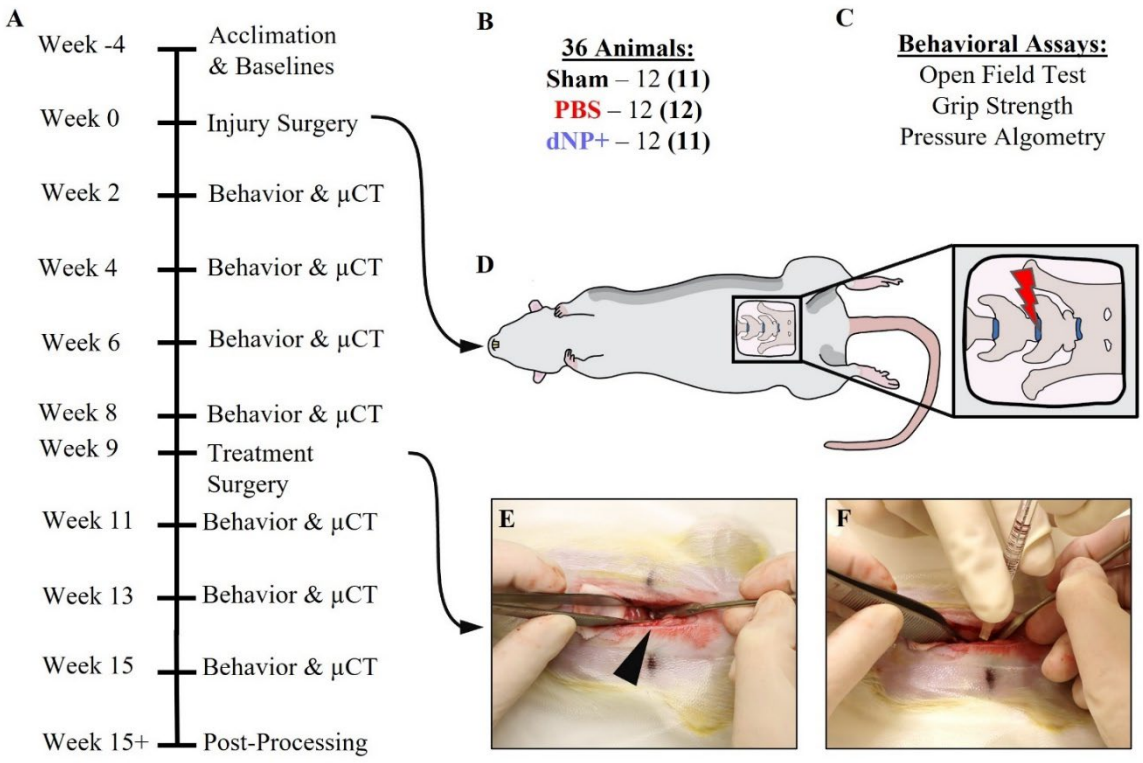

Figure. 24. Animal study overview. (A) Timeline of the *in vivo* assessment of dNP+. Animals were acclimated for three weeks before a week of baseline behavior and uCT measurements. Injury surgery was performed on week 0 and disc degeneration was allowed to progress for 8 weeks before treatment surgery on week 9. Following treatment surgery, behavior and uCT measurements were collected for 6 weeks. **(B)** For this study, 36, 18-week-old, female Sprague Dawley rats were split into three groups: sham, PBS and dNP+. One sham animal was terminated due to surgical complications and one dNP+ animal was excluded due to incorrect treatment injection. Final animal numbers are shown in bold in parenthesis. **(C)** Three assays were employed to measure the development and alleviated of pain-like behavior during the study. The open field test measured spontaneous pain-like behavior and grip strength and pressure algometry measured evoked pain-like behavior. **(D)** Graphical depiction of the injury surgery. The L5-L6 IVD was approached ventrally and injured using a microdissecting needle. **(E)** During treatment surgery, the L5-L6 disc was visualized in all animal groups. The disc can be seen at the tip of the black arrowhead. **(F)** Animals in the PBS group were injected with 1X PBS and animals in the dNP+ group were injected with dNP+.

dNP+ restores disc volume

Intervertebral disc volume was quantified at eight time points as a real time measurement of disc degeneration **(Fig. 25A&B)**. From weeks 2 to 8, both PBS and dNP+ groups exhibited significantly decreased disc volume compared to sham animals. After treatment, dNP+ disc volume returned to baseline and was not significantly different from sham at any time point from week 11 till study conclusion. Conversely, IVDs injected with 1X PBS remained at a sub baseline volume and were significantly different from sham and dNP+ at all time points. These data demonstrated dNP+ treatment restored disc volume 9 weeks after degeneration was initiated.

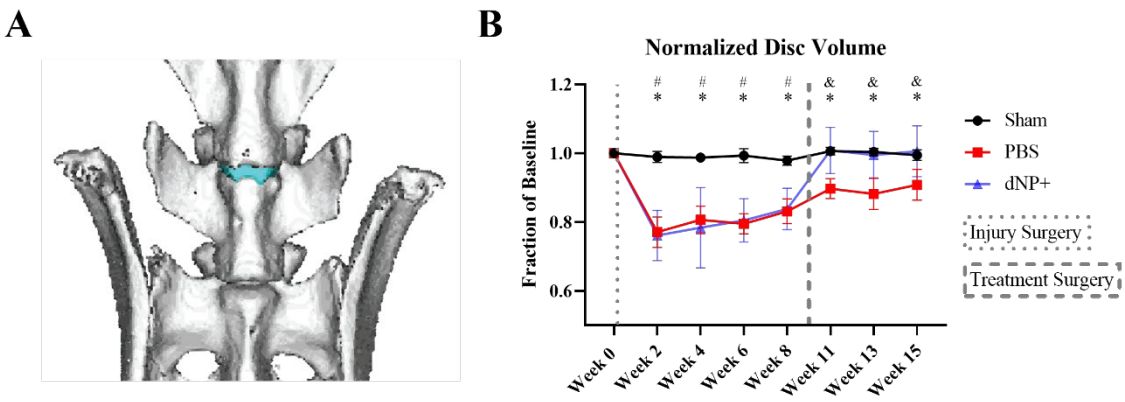

Figure. 25. dNP+ restores disc volume. (A) 3D rendering of a rat spine from L5 to S1. The L5-L6 IVD is colored in blue. **(B)** L5-L6 intervertebral disc volumes calculated from uCT data. The disc volume in both dNP+ and PBS animals significantly decreased after injury compared to sham animals. After treatment surgery, dNP+ treated animal disc volumes returned to baseline and were no longer significantly different from sham. Data is shown as mean with standard deviation (n = 11-12 per group). # = $p < 0.05$ sham vs. dNP+. * = $p < 0.05$ sham vs. PBS. & = $p < 0.05$ dNP+ vs. PBS.

dNP+ and diclofenac alleviate axial hypersensitivity

Evoked and spontaneous pain-like behavior were measured during the study to assess how pain-like behavior developed after injury and how dNP+ treatment affected pain-like behavior. Grip strength specifically measured hypersensitivity to axial strain, i.e., axial hypersensitivity **(Fig. 26A)**. From week 6 to 8, both PBS and dNP+ animal groups exhibited significantly decreased grip strength compared to sham animals. After treatment surgery, this decrease was ameliorated in animals injected with dNP+ whereas grip strength continued to decline in animals injected with 1X PBS. At weeks 13 and 15, dNP+ animals displayed significantly increased grip strengths compared to PBS animals and were not significantly different from sham. The grip strength data demonstrated the dNP+ treatment alleviated axial hypersensitivity and was effective for at least 6 weeks.

Deep pressure hypersensitivity as measured by the pressure algometry assay failed to detect differences between sham and dNP+ groups at any time point **(Fig. 26B)**. However, this assay was successful in detecting differences between PBS and sham animal groups at weeks 4, 8, 13, and 15. Also, animals in the PBS group displayed significantly decreased thresholds compared to dNP+ animals at week 13, 4 weeks after treatment surgery. Put together, data from this assay suggests dNP+ may have been effective in decreasing deep pressure hypersensitivity but the failure of dNP+ animals to develop deep pressure hypersensitivity prior to treatment, limits the interpretability of this data set.

The open field test measured changes in spontaneous pain-like behavior **(Fig. 26C)**. The only time point at which significant differences in total distance travel were observed was at week 11, 2 weeks after treatment surgery. At this point dNP+ animals

traveled significantly further than both PBS and sham groups. This highly significant difference, suggested the dNP+ treatment may have alleviated nociception evoked through movement, causing the animals to roam more.

Finally, an NSAID known to effectively treat acute low back pain in humans, diclofenac, was administered intraperitoneally to all animals in week 15 to determine if disc-associated pain could be alleviated in the animal model via drugs used in humans [46, 333-335] **(Fig. 26D)**. This evaluation was crucial for providing evidence of this model's predictive validity. After diclofenac administration, PBS animal grip strengths returned to baseline and were significantly different from week 15 pre-treatment evaluation. These data confirmed pain-like hypersensitivity in this model could be alleviated via approaches used in humans and that the increase in grip strength observed after treatment with dNP+ was likely due an alleviation of nociception in the degenerated disc tissue.

Altogether these pain-like measurements indicate dNP+ was effective at alleviating pain-like hypersensitivity and the effect of dNP+ was sustained for 6 weeks after treatment.

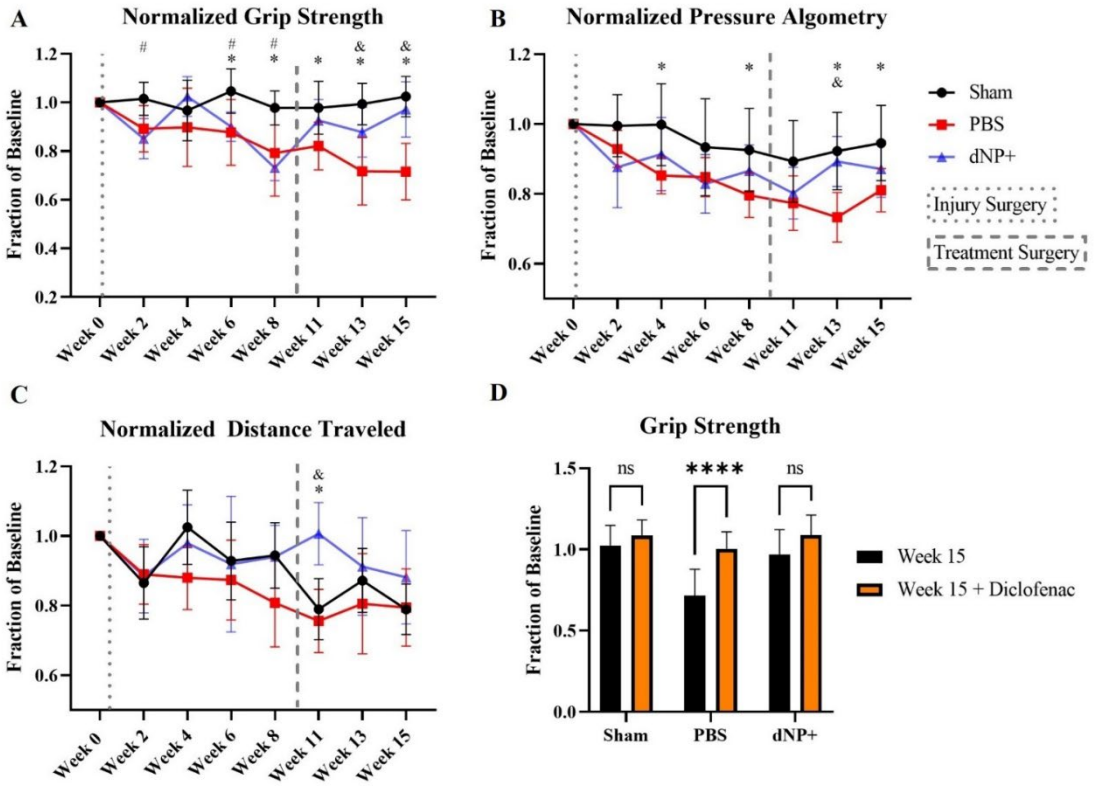

Figure. 26. dNP+ and diclofenac alleviate axial hypersensitivity. (A) Normalized grip strength data which measured axial hypersensitivity. Both PBS and dNP+ animals groups exhibited significantly decreased grip strength in weeks 6 and 8 compared to sham animals. After treatment surgery, grip strength increased in dNP+ animals and not significantly differ from sham animals for the remainder of the study. The grip strength of PBS animals continued to decline from week 11 onward and was significantly different from sham at all time points. PBS animals also exhibited significantly decreased grip strength compared to dNP+ treated animals at week 13 and 15. **(B)** Normalized pressure algometry which measure deep pressure hypersensitivity. PBS animals exhibited decreased pressure thresholds at week 4, 8, 13, and 15 compared to sham animals. Also, PBS animals exhibited lower thresholds compared to dNP+ animals at week 13. At no point did the dNP+ animal group significantly differ from sham animals. **(C)** Normalized distance traveled was a measure of spontaneous pain-like behavior. The only significant difference measured was at week 11 between dNP+ animals and both PBS and sham animals. **(D)** 15-week grip strength before and after treating with diclofenac. Diclofenac was effective at suppressing axial hypersensitivity as noted by the highly significant increase in animal grip strength after drug administration in PBS animals. (n = 11-12 per group). For longitudinal data, significant differences between groups were assessed using a two-way ANOVA. Drug treatment data was analyzed using a one-way ANOVA. # = $p < 0.05$ sham vs. dNP+. * = $p < 0.05$ sham vs. PBS. & = $p < 0.05$ dNP+ vs. PBS.

dNP+ alters motion segment rheological properties

At study conclusion, motion segments from six animals in each group were excised and potted using the same process as described in the *ex vivo* testing. A total of five motion segments (sham – 1, PBS – 1, dNP+ - 3), were removed from the sample pool due to desiccation during the potting process. The remaining motion segments were tested on a rheometer for storage and loss moduli to determine if segments from PBS or dNP+ treated animals were significantly different from sham motion segments **(Fig. 27)**. The storage modulus of PBS motion segments was significantly lower compared to sham. The loss modulus of PBS motion segments was also significantly lower than sham. These data indicated that resistance to strain mediated by both viscous and elastic properties declined due to injury. The moduli of dNP+ treated motion segments were not significantly different from sham nor PBS groups, but this may have been due to insufficient statistical power considering only three motion segments were included in the analysis. These data indicated injury and subsequent degeneration decreased the rheological properties of motion segments and the treatment with dNP+ resulted in motion segments that did not significantly differ from sham nor PBS injected motion segments.

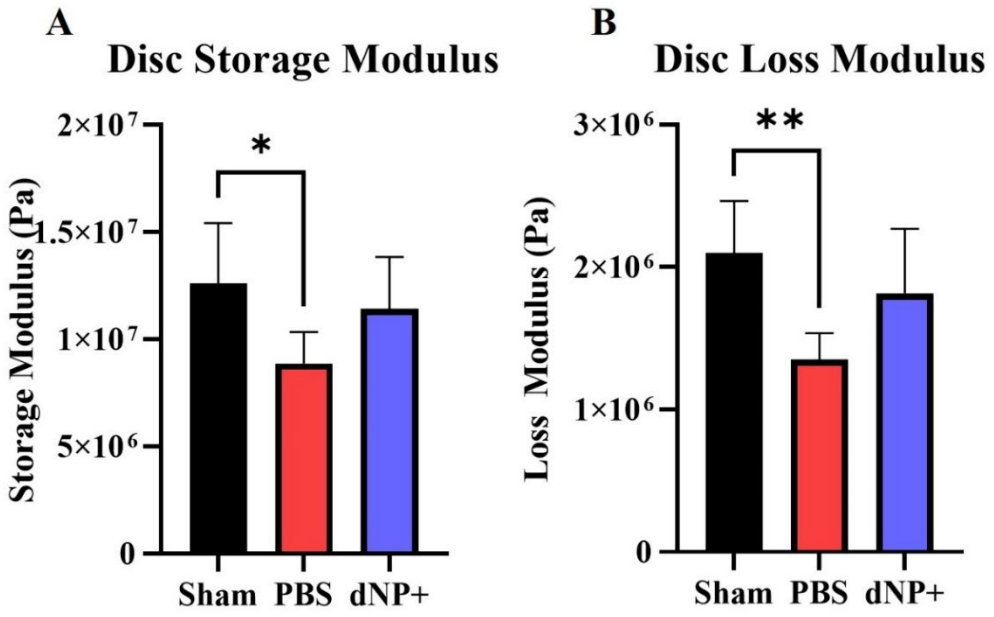

Figure. 27. dNP+ alters motion segments rheological properties. (A) Storage moduli of L5-L6 motion segments resected at the conclusion of the *in vivo* study. The average storage modulus for sham motion segments was significantly greater than PBS motion segments. **(B)** Loss moduli of L5-L6 motion segments resected at the conclusion of the *in vivo* study. The average loss modulus for sham motion segments was significantly greater than PBS motion segments. No significant differences were detected between dNP+ and the other treatment groups. A total of 5 motion segments were discarded due to desiccation during the potting process (sham: n = 5, PBS n = 5: dNP+: n = 3). Data was analyzed using a one-way ANOVA. * = $p < 0.05$

6.4 Discussion

This work provides evidence that a biomaterial composed of decellularized, healthy porcine NP, collagen, and genipin, could be an effective therapeutic for disc-associated low back pain. In our rat model, dNP+ treatment restored degenerated disc volume to baseline and this effect was maintained at all time points measured after treatment. Further, animals treated with dNP+ displayed remarkably diminished axial hypersensitivity which was maintained at all time points after the treatment surgery. Finally, motion segments resected at study conclusion from animals in the PBS group exhibited significantly lowered storage and loss moduli compared to sham. There was no

significant differences between sham and dNP+ motion segments nor PBS and dNP+ motion segments indicating the treatment was effective at augmenting mechanical properties.

Motivation to engineer the dNP+ therapeutic arose from observations made in our rodent model of disc degeneration. In this prior work, degenerated disc tissue routinely contained large fissures which radiated through the disc tissue. In most injured animals, these fissures presented as large swaths of annulus fibrosus tissue with no interconnection. Additionally, aberrant nerve sprouting localized around the fissures, implicating mechanical agitation as a potential source of nociception. Together, these observations strongly suggested that a therapeutic capable of annealing collagenous fissures and other microdefects could decrease deleterious loading patterns within the disc and decrease nociception, thereby alleviating pain. Based on prior work in our lab and published data[214, 336-340], we determined a hydrogel could be effective in treating disc degeneration and could potentially impact pain-like behavior as well[201, 341]. It was reasoned an injectable hydrogel could percolate into the tissue defects prior to completing fibrillogenesis. Moreover, the minimally invasive injection procedure would minimize surgical complications and facilitate delivery of the hydrogel to regions of the disc which could expand to accommodate the extra volume, like fissures.

To date, numerous research groups have treated disc degeneration in rodent models with varying degrees of success. These treatments have included cell transplantation, *in situ* gene therapy, and bioactive factors [202, 211-218]. However, the vast majority of models are limited by the administration of treatments prophylactic or concomitant with the initiation of degeneration. Further, the majority of publications that

evaluate treatments for disc degeneration fail to quantify pain-like behavior [219]. Clinically, patients do not seek treatment for disc degeneration unless the degeneration causes pain. This simple fact brings into question the validity of prior work because treatments are administered prior to pain-like manifestation which does not replicate how human patients are treated. As of 2021, no treatment in over 100 animal model publications has achieved FDA approval for the treatment of degenerative disc disease providing strong evidence that the prophylactic and concomitant treatment paradigms are inadequate [219]. With this knowledge, we decided that treating animals after disc degeneration and pain-like behavior had sufficiently developed would provide predictive validity far greater than the majority of prior work.

The hydrogel engineering process began by trialing different chemical crosslinking agents. It was hypothesized that a therapeutic would have greater potential to stabilize the disc if it covalently bound to the local tissue. In the past, covalent bonding of biomaterials doped with crosslinking agents has been studied as part of the development of bioadhesives likes GRF glue [240]. Lysyl oxidase, transglutaminase, and genipin were all tested but only genipin provided a dramatic increase in mechanical properties suggesting it had the greatest crosslinking capacity (data not shown). Having selected genipin as the crosslinker, experimentation to determine the optimal concentration commenced.

The first analysis assessed if the addition of genipin along with the changes to the dNP and collagen concentrations changed dNP gelation kinetics compared to prior work [235]. As part of this analysis, the time at which different concentrations of genipin began and completed crosslinking was also determined. It was revealed that the new

concentration of collagen and dNP and the addition of genipin did not dramatically change the onset time of collagen fibrillogenesis. From this data, 15 minutes was conservatively estimated as the time to fibrillogenesis completion *in vivo* fibrillogenesis. These data aligned with previously existing literature and indicated this process would occur during surgical recovery in the animal model [249].

With the inclusion of a chemical crosslinking agent, another major criterion was to avoid cellular cytotoxicity [245]. Work done by the Iatridis lab has suggested free genipin, rather than genipin bound in crosslinks, is responsible for cellular cytotoxicity [250]. Knowing lysine residues on collagen fibrils were the main target of genipin activity and that genipin transforms into genipin blue after becoming a crosslink, it was reasoned the absorbance assay could determine the genipin concentration at which all crosslinking sites were saturated. Unfortunately, at 610 nm absorbance, gels above 10 mM genipin reached absorbances above the linear response range of the plate reader. However, an absorbance greater than 1.0 was not reached at 405 nm and these values suggested there was diminishing return of genipin activity above 5 mM genipin. These data indicated that 2.5 mM genipin was a conservative concentration to use to avoid the presence of free genipin and in turn cytotoxicity.

All concentrations of genipin imparted an increase of storage and loss moduli to the hydrogels. Unexpectedly, the hydrogels suffered increasing variability at genipin concentrations of 5 mM and above. Experimental variability did not account for this change as duplicate gels were also variable. At 5 mM and above, the rheological properties increased at a faster rate than lower concentration suggesting the underlying crosslinking mechanisms were fundamentally different. Plotting concentration vs. storage

modulus revealed a non-linear relationship implying the mechanism of genipin crosslinking is not strictly stochastic and emergent aspects may come into play (data not shown). More work must be performed to discover why the hydrogels suffered this increased variability and why the rate of modulus increase changed at genipin concentrations of 5 mM and above.

Overall, the kinetic and rheological data indicated that 2.5 mM was the optimal concentration of genipin to achieve a rapidly gelling, cytocompatible, and consistent dNP hydrogel. This formulation was given the name dNP+.

As a proof of concept, motion segments excised from rat cadavers were treated with dNP+ after injury to establish that the hydrogel could be used as an injectable, mechanically enhancing, therapeutic. Motion segments treated with dNP+ exhibited significantly increased mechanical properties compared to pre-treatment values. The 15% increase in storage modulus represented around a 200,000 Pa increase, which was multiple orders of magnitude greater than the dNP+ gel alone. This increase may have resulted from the combinatorial effect of genipin on the existing tissue and annealing of the injury defect by dNP+. This analysis showed that dNP+ could be injected into a rat IVD and could increase IVD mechanical properties following injury.

DNP+ was further characterized by quantifying cellular cytotoxicity using a standard LIVE/DEAD assay. In this assay, dNP+ proved cytocompatible with primary human NP cells. This data complimented prior work done in our lab with dNP and collagen gels [235]. In this prior work, total cellular metabolic activity was greatest in collagen + dNP gels which parallels the high proliferation witnessed in our work. The fact that cellular proliferation in dNP+ narrowly avoided significance when compared to

collagen + dNP ($p < 0.052$) suggested any further increase of genipin would have significantly impacted cellular proliferation. Extrapolated further, higher concentrations might also have affected cell viability. This assay was limited by the equilibration step needed to ensure the gels were completely hydrated and at a uniform osmotic equilibrium prior to cell seeding. This step was limiting because it may have removed any free genipin from the gels, which could have increased cellular viability across the board. Having collected this data, we concluded 2.5 mM genipin represented the maximum concentration of genipin usable to guarantee minimal cytotoxicity.

Having chosen a 2.5 mM genipin, 6.0 mg/mL dNP and, 6.0 mg/mL collagen hydrogel as the best therapeutic candidate, work transitioned to testing *in vivo*. This arm entailed acquiring 36 animals, injuring 24, allowing degeneration to progress for 8 weeks and then treating 12 injured animals with 1X PBS and the other 12 with dNP+. Of all the work described in this manuscript the most time-consuming step was determining a method that ensured a consistent volume of liquid dNP+ precursor solution was injected into the disc. After trialing microinjectors, insulin syringes, and syringe pumps, it was found that microliter syringes manufactured for gas chromatography were ideal. The downside of these syringes was that they could not create sufficient back pressure to draw up the hydrogel solution. To solve this, each syringe was attached to a needle and the plunger was removed so that dNP+ could be filled from the back of the syringe. This technique also ensured that there was no dead volume in the needle hub. Further, rubber stoppers were affixed to the needle 2 mm from the needle tip to prevent overpenetration and increase the odds dNP+ was delivered to the NP space. Finally, the injection speed was limited to 5 uL/minute because it was discovered that IVDs could not handle rapid

volume injection and quick administration would force the gel to exude around the needle hub.

Disc volume was measured throughout the course of the study as a proxy for degeneration. Directly after surgery, the IVD volume of injured animals dramatically declined. After treatment surgery, dNP+ IVD volumes returned to baseline while PBS treated IVDs remained significantly lower than sham and dNP+ treated IVD volumes. This data provided compelling evidence that dNP+ successfully entered and remained in the IVD. The gradual increase of disc volume in all injured animals was due to radial expansion as noted in prior work. Interestingly, after treatment, dNP+ IVD volumes no longer exhibited this gradual increase indicating bony deposition caused by aberrant loading patterns may have been alleviated. Presuming that aberrant loading drives pain-like behavior, this indication was further supported by the behavioral data.

Similar to prior work, injured animals displayed a gradual decline in grip strength from week 2 to week 8 [291, 292]. For PBS treated animals, grip strength continued to decline after treatment surgery. Conversely, dNP+ treated animal grip strength increased after treatment surgery suggesting the treatment alleviated axial hypersensitivity. This axial analgesia reached significance compared to PBS animals at week 13 and 15. At week 15, the dNP+ grip strength was 26% higher than PBS treated animals. This difference is more than double the minimal clinically important difference (MCID) that has been recommended for low back pain treatment outcome measures [342]. The grip strength data provided strong evidence that dNP+ could be an effective treatment for axial pain caused by disc degeneration.

The pressure algometry data proved more difficult to interpret. At no time point did dNP+ animals significantly differ from sham animals. The failure to develop deep pressure hypersensitivity prior to the treatment surgery limited our understanding of the effect of dNP+ on deep pressure hypersensitivity. On the contrary, PBS animal thresholds were significantly lower than sham at multiple time points before and after surgery. Also at week 13, PBS thresholds were 16% lower than dNP+ animals which exceeded the MCID. This data indicated injury does produce deep pressure hypersensitivity but the variability of the assay, especially in dNP+ animals, limited our interpretation of the treatment effect.

The spontaneous pain-like behavior, as measured in the open field test, provided additional evidence that dNP+ treatment had an analgesic effect. This effect was manifested at week 11. This time point was 2-weeks after treatment surgery. Similar to week 2, which was 2 weeks after injury surgery, sham and PBS animals traveled less distance due to post-surgical effects like pain. Intriguingly, dNP+ animals traveled significantly more than both PBS and sham animals and this effect was highly significant ($p < .0029$ dNP+ vs. sham, $p < .0006$ dNP+ vs. PBS). We reason that dNP+ may have provided an analgesic effect that was greater than the inhibitory action of post-surgical effects causing the animals to roam more. Regardless of the cause, the increase in distance traveled did not continue into weeks 13 and 15. This data mirrors clinical interventions in humans for disc-associated low back where pain relief, as measured by the visual analog scale (VAS), is highest immediately after surgery and lessens as time goes on [343]. The open field test confirmed the dNP+ had an effect on spontaneous pain-like behavior but this effect was not significantly maintained.

Diclofenac was administered at week 15 primarily to verify the predictive validity of this model. Diclofenac is a non-steroidal anti-inflammatory drug (NSAID) that acts as an analgesic by inhibiting cyclooxygenase 1 and 2 (COX-1 and COX-2) [333]. This drug has proven efficacious in humans suffering acute episodes of low back pain and in animals model which exhibit mechanical hypersensitivity and decreased motor ability [334, 335, 344]. Similarly, diclofenac effectively reduced axial hypersensitivity in our model. This outcome confirmed that disc-associated pain in our model could be alleviated via mechanistic approaches applied in humans and indicated our model maintains a high degree of predictive validity.

In summary, these pain-like behavior assays determined dNP+ was effective at alleviating axial hypersensitivity and clearly augmented deep pressure hypersensitivity and spontaneous pain-like behavior.

The final data set collected in this study was motion segment rheological data. This was collected to evaluate if dNP+ treatment had an effect on disc mechanics as mechanics were hypothesized to contribute to disc-associated pain. Both storage and loss moduli of PBS animal motion segments were significantly lower than sham motion segments. The moduli of dNP+ segments did not differ from either PBS or sham. Looking at the dNP+ and sham storage modulus 95% confidence intervals, it was found that 82% of the intervals overlapped. This overlap in suggested the dNP+ and sham moduli were fairly equivalent.

This work has a few limitations additional to those already mentioned. First, only female animals were used, disallowing any insight into the role of sexual dimorphism on treatment effects. Second, an analysis of disc morphology and nerve sprouting was not

assessed leaving questions of how pain-like behavior was alleviated mechanistically. Work is ongoing to include male animals in treatment evaluation and to measure motion segments from this model concerning overall degeneration via hematoxylin and eosin staining and the presence and localization of nerves via immunohistochemistry.

Chronic low back pain is a tremendous burden on modern society. There is a great need for therapeutics which address the fundamental cause of pain. It has become increasingly clear in recent years that a reliance on central or systemic medicines like opioids and NSAIDs has only increased the societal burden of chronic low back pain. To this end, we have engineered a non-invasive, spontaneously assembling, therapeutic derived from healthy disc tissue that remarkably decreases pain-like behavior in animals suffering disc-associated low back pain. We hope this work will provide the basis of a next generation therapy for low back pain and will assist other research groups in developing similar treatments.

The work described in Chapter 6 will constitute a scientific paper. This paper will be titled “Extracellular Matrix Hydrogel Derived from Porcine Nucleus Pulposus Restores Disc Volume and Alleviates Axial Hypersensitivity” with authors DJ. Lillyman, KE. Ney, SM. Caparaso, E. Barnett, AL. Redwine, F. Lee, and RA. Wachs.

CHAPTER 7: Discussion and Future Directions

7.1 Chapter 4 Discussion and Future Directions

The first objective of this dissertation was to create a method to quantify the degenerative state of IVDs real-time in rats. The current gold standard for gauging degeneration real-time is the DHI method which entails measuring the IVD space and adjacent vertebral bone lengths using X-ray radiographs **(Fig. 28)** [158, 199, 203]. While this method seems straightforward in writing, X-ray images force the observer to make decisions about where a measurement stops and ends that are highly subjective. The reason for this subjectivity is because X-ray radiographs represent a projection of all dense objects in a sample onto a single plane. This projection creates many imaging artifacts especially around boney objects with complex structure, like the spinal column (**Fig. 29**). Further, X-ray machines lack sufficient spatial resolution to make precise measurements necessary for quantifying aspects of small structures like IVD height.

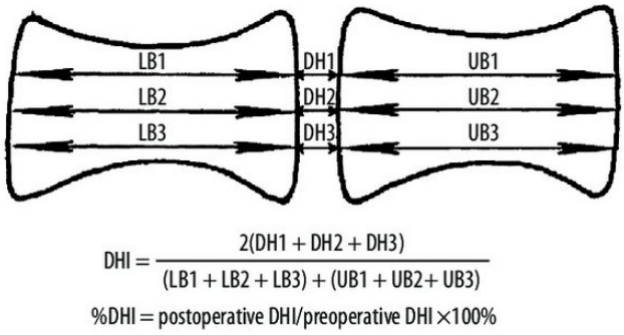

Figure 28. Overview of the DHI method [1]

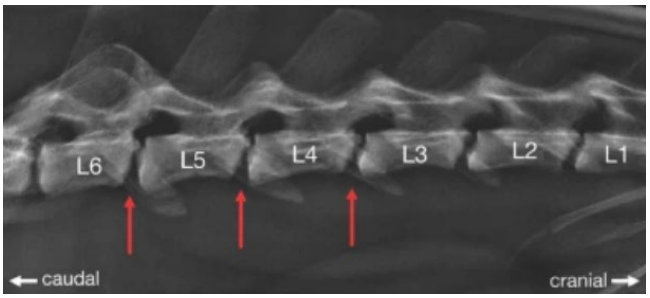

Figure 29. X-ray radiograph of a rat lumbar spine [2]

At the time DHI was being trialed, the Life Science Annex at UNL aqcuired a state of the art μCT (Quantum GX). Unlike X-ray imaging, μCT employs a rotating X-ray source and collector, permitting three dimensional scans. Additionally, the μCT

machine purchased was built for small animals, and thus had high spatial resolution, ideal for measuring a small structure like the disc.

Along with the μCT, post-processing software was included that allowed removal of soft tissue, creation of tissue density thresholds, and creation of unique objects within scans. For object maps, the software provided readouts like, average intensity, entropy, number of voxels, and volume. It was determined these object maps could be created for the IVD to approximate IVD volume. This rationale was enhanced by the fact that the IVD sits between bone, making the edges of segmentation straightforward.

In 2019, we performed a pilot study of disc degeneration using a different injury method than described in this dissertation. In this study, a early form of the disc volume method, which applied unique image algebra at each time point, was used to calculate the disc volume over the course of 21 weeks **(Fig. 30)**. Unfortunately, no differences between sham and injured animals were observed because the injury method did not induce disc degeneration. Despite this downside, it was abundantly clear the μCT method was highly precise because sham and injured animals were consistently equal with one another. Conversely, both sham and injured averages deviated from baseline, indicating this method might suffer low accuracy due to inter-experimental variabiltiy, i.e., the day animals were scanned influenced the outcomes. Initially, it was suspected the time of day and disc hydration state might explain this variation, but after testing a single threshold

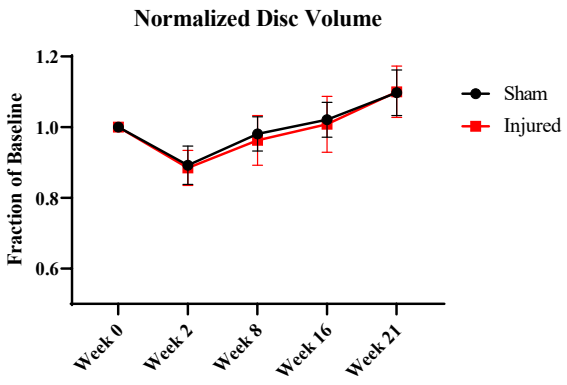

Figure 30. Normalized L5-L6 disc volume from the 2019 pilot study of disc degeneration

across multiple time points, it was determined that the post-processing imaging parameters were the source of inter-experimental variability. To remedy this source of error, imaging thresholds were standardized and kept consistent between imaging days.

Having established universal imaging thresholds, this final method was delineated in the methods paper described in Chapter 4. When compared to the DHI method, the disc volume method is superior in all ways except for time spent to analyze the data **(Fig. 9)**. The inclusion of multiple slice planes in the final measurement dramatically decreased the opportunity for observer bias to be introduced. Further, multiple slices also increased the quantity of data involved in the final measurement, increasing the precision of the estimate.

There are several factors that could improve the work described in Chapter 4. First, the scans gathered to calculate the disc volume collect a larger field of view (FOV) than necessary. Current scans include the lumbar region of the rat torsoe from L4 to S1. Because only the L5-L6 is injured and of interest, the current method includes a fair amount of extraneous data. Reducing the FOV would allow for greater spatial resolution and could further enhance the precision of the method. Additionally, an increased spatial resolution may permit alternate analyses pertinent to disc degeneration like degree of osteophyte formation, schmorl's node formation, etc. [345]. Furthermore, reducing the FOV could impart a sufficient increase in image quality that scan times could be reduced from two minutes to 18 seconds, which would dramatically decrease the X-ray dosing. In both animal models described in this dissertation, at least one animal developed a large tumor. Although tumor formation is part of the genetic predisposition of female Sprague Dawley rats, decreasing X-ray dosing stands to decrease the likelihood of tumor

formation [346]. In the future, the FOV can be reduced from 72 mm to 45 mm, which will decrease the voxel size from 144 μm to 90 μm. The smaller voxel size will allow for greater image resolution, and more precise disc volumes.

The disc volume method could also be validated to improve it's acceptability as a scientifically robust measure of IVD volume. This work would entail comparing the calculated disc volumes with volumes calculated using an alternate method. Because the disc is irregular in shape and elastic, it would be difficult to take physical measurements to approximate volume. One method to approximate the disc volume would be to collect its mass, and place it in liquids with linearly increasing densities to ascertain neutral bouyancy and in turn overall tissue density. Knowing the mass and density of the disc, the volume would be a trivial calculation.

In summary, Chapter 4 outlined a method for quantifying disc degeneration realt-time and non-invasively. Given the profound accuracy, precision, and consistency of this method, we believe it was an overhwelming success. Further work could be done to improve the method and validate the outcomes.

7.2 Chapter 5 Discussion and Future Directions

The second objective of this dissertation was to create an animal model of disc-associated pain. This objective was motivated by a lack of valid animal models of pure disc-associated pain and the desire to establish an in-house model for therapeutic testing. The first animal study occurred in 2019, but failed to induce disc degeneration and manifest a pain-like phenotype. However, this study was tremendously useful to acclimate experimenters to animal procedures and assays. Furthermore, this pilot study assisted in cementing assays, like the open field test, used in later studies.

In 2020, the COVID-19 pandemic allowed ample time to re-develop the animal model from first principles. During this time, a thorough investigation of rat neuroanatomy revealed rat IVD innervation is complex, un-intuitive, and involves DRG projections from multiple levels [180, 295]. It was discovered the dorsal side of the rat IVD is innervated by nerve fibers originating in adjacent DRGs, wherease the ventral side of the IVD is innervated by nerve fibers originating in DRGs multiple spinal levels higher. This neuroanatomy implied the location of injury and subsequent degeneration could affect the pain-like phenotype which emerges because distinct DRG were implicated in ventral and dorsal focused damage. In fact, the dichotomous innervation may explain the disparity in the results across all rat models of disc degeneration as some models induce more comprehensive degeneration than others [199, 200].

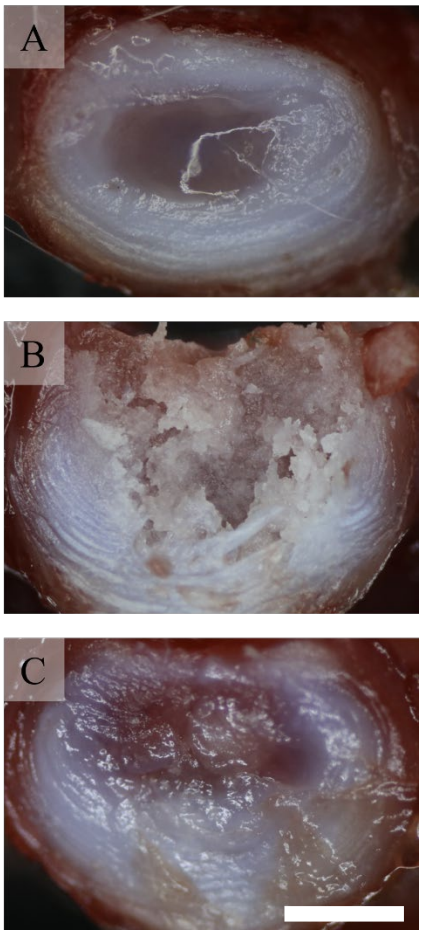

Figure 31. Overview of the injury refinement. **(A)** Undamaged IVD. **(B)** Over damaged IVD. **(C)** Ideally damaged IVD. Scale bar = 3 mm.

Provided the knowledge of IVD and rat whole body innervation, an injury procedure was created that would result in comprehensive, IVD-wide, tissue disruption. To accomplish this, an array of injury procedures were trialed on rat cadavers, starting with syringe puncture and progressing to puncture and scrape with a dissecting needle **(Fig. 31)**. The refinement process entailed damaging 85 motion segments to various degrees using needles of various diameter and mechanical agitation.

The outcomes from this process were evaluated using a semi-quantitative measurement scheme for total disc damage. The semi-quantitative analysis measured aspects of the injury like, NP damage, ventral AF damage, dorsal AF, damage, and end plate damage to determine a procedure that minimized damage to the end plate and maintained damage to the NP and AF. At the end of this process, the 1-scrape and 6-scrape methods were chosen because they caused comprehensive tissue damage, did not core the tissue, and posed little risk to errantly damage the end plates. Confirming this choice, the 1-scrape and 6-scrape injury were highly effective in the animal model at inducing disc degeneration, with all injured animals exhibiting a dramatic loss of disc volume after surgery **(Fig. 32)**.

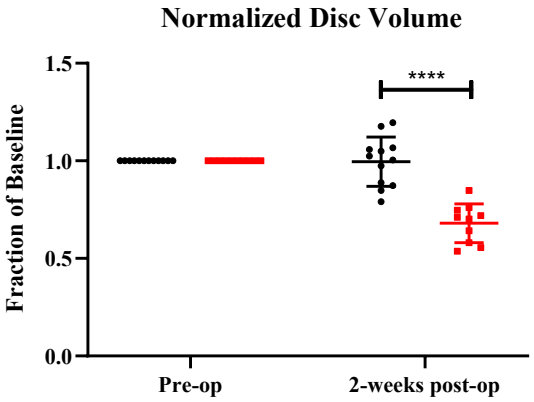

Figure 32. Normalized disc volume from the model of disc-associated pain before and after injury surgery

Concommitant with the initiation of this 2020 animal study, alternate assays of measuring pain-like behavior were considered to increase the chance that pain-like differences could be detected. Evidence in the literature in mouse models of spontaneous and induced disc-associated pain suggested grip strength could be useful [291, 292]. Thus, this assay was added as an additional pain-like assay to those employed in the 2019 pilot study. Complimenting the prior work in mice, the grip strength assay proved highly sensitive at detecting axial hypersensitivity due to disc degeneration in rats in our model **(Fig. 33)**. Intuitively, it may not be clear how IVD degeneration results in decreased forelimp grip strength. However, its reasonable to assume that increasing axial strain on

the IVD causes mechanically sensitive nociceptors to depolarize. This increase in pain likely has inhibitory effects on the maximum grip strength an animal is willing to endure, causing them to release the grip plate at a lower force. To our knowledge, this work was the first to describe persistent increased axial hypersensitivity in rats caused by disc injury and degeneration. It could be valuable in the future to also collect hindlimb grip strength considering the hindlimps are closer to the level of degeneration, however, this may prove more difficult as rats are less apt to reliably grip the plate in this manner [347].

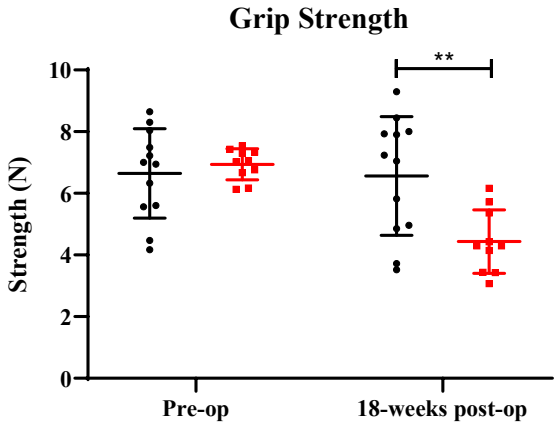

Figure 33. Raw grip strength from the model of disc-associated pain before injury surgery and 18-weeks after

Another major goal of this 2020 animal study was to measure degenerative changes in the disc. Two important assessments were the analysis of nerve sprouting and macrophage infiltration in the degenerated IVD tissue. Existing literature indicated there would be nerve sprouting in degenerated tissue but the quality of this prior evidence and a lack of consensus suggested there was value in confirming nerve sprouting in our model [71, 79, 118, 348]. Complimenting prior literature, widespread nerve sprouting was visualized in degenerated tissue, especially around the site of needle insertion [310]. Furthermore, a significant correlation between axial hypersensitivity, as measured by the grip strength assay, and the degree of nerve sprouting, was imputed, suggesting nerve sprouting plays a causal role in the manifestation of disc-associated pain. Evidence in the literature also implied that macrophages would be abundant in degenerated disc tissue

[349-351]. Suprisingly, little evidence of macrophages was found in degenerated IVD tissue despite using multiple antibody targets and concentrations. However, macrophages were visualized in skin tissue which indicated the antibodies worked. These observations indicated there were indeed no macrophages in degenerated disc tissue at the terminal timepoint in our study, however, macrophages may have been present at earlier time points and diminished over the 18-week post injury. This finding was of personal interest because early work in this Ph.D. had been spent trying to modulate macrophage phenotype using decellularized tissue with the end goal of using decellularized tissue to treat macrophages implicated in disc degeneration. This discovery caused a realization of three things. First, scientific literature is not always correct and the most robust data is that which has been replicated across multiple groups. Second, *in vitro* analyses do not always replicate how processes unfold *in vivo*. Third, macrophages do not play a large role in late stage disc degeneration in our model, and thus, do not represent a therapeutic target for disc-associated pain at chronic time points.

There are several aspects of this animal model that could be expanded or improved in future work. First, spontaneous pain-like behavior assays could be improved and more could be included. Because we only detected differences in evoked pain-like behavior, there is still a strong need for a spontaneous measure of pain-like behavior. Data from the Open Field Test was highly variable, limiting the power to detect differences, if there were any. One source of error noted in the first animal study, was uneven overhead lighting cause by imperfect alignment of the arenas' centerpoint with the overhead light source. The uneven overhead lighting caused asymmetric lighting among the four arenas which animals were placed. In half of the arenas, a large portion of

the floor was dark, causing the animals to preferentially reside in this area replicating a light-box dark-box experiment. Because this phenomenon only occurred in two of the four arenas, bias was introduced into the outcome. However, this factor was removed in the treatment study. Another source of error that could be removed in future studies from the open field test is the presence of human observers in the room during data collection. Due to the allocation of a single room, all behavior had to be performed in one location. For this reason, animals in the open field test were exposed to human talking, human smells, doors closing, and other animal vocalizations during data collection. These factors may have had a larger impact on animal spontaneous behavior than the pain caused by disc degeneration.

In future work, additional measures of spontaneous pain-like behavior like gait, grimace, and operant conditioning could be included [141]. If these methods are pursued, the power analysis used to determined n size should be computed using the assay with the largest standard deviation to improve the likelihood that significant differences can be detected.

Another aspect of pain-like data that should be addressed involves error in evoked assays. Evoked pain-like behavior assays are imperfect in animal studies because they involve an experimenter which subjects outcomes to unintentional bias. An interesting aspect in the collection of evoked pain-like behavior is the balance between experimenter empathy and apathy. Experimenter empathy is required because animals perform best under relaxed conditions [352]. For this reason, an experimenters ability to appraise animal affect, and treat the animal gently to minimize stress is imperative for behavioral data collection. Conversely, experimenters are also asked to subject animals to chronic

pain and disallow the pain-like suffering in animals from biasing how an animal is treated. Maintaining unbiased measurements of animals can be particularly difficult, especially when animals display overt signs of distress. For example, some animals during the grip strength assay, especially those which are injured, exhibit heightened fear responses to the assay apparatus. This manifests as erratic, energetic, and desparate avoidance of the grip plate. However, a grip strength must be collected so these animals are subjected repeatedly to the grip plate, further amplifying the stress. This forced reapplication of animals, despite overt signs of suffering, requires apathy from the experimenter to complete. It stands to reason that differences between animals which willingly grip the force plate and animals which exhibit aversive behavior are amplified due to the experimenters empathetic desire to minimize animal suffering. Furthermore, over the course of any animal study, experimenters become familiar with invididual animals, and may develop individualized relationships. However, at study conclusion, experimenters may be asked to personally euthanize these animals and treat them as a biological sample, resulting in cognitive dissonance. The requirement for experimenters to exhibit both empathy and apathy, which are diametric, necessitates further use of spontaneous pain-like assays in animal models.

Analysis of degenerated IVD tissue sections could also be expanded in the future to greatly benefit our understanding of pathomechanisms of disc degeneration. The preponderance of cellularized granulation tissue along the degenerated IVD's perimeter raises questions as to the cell type, inflammatory state, and function of this tissue. Additionally, IHC processing or more careful analysis in H&E could shed more light on these unknowns. Further, modes of nociception could be revealed by determining the

type of nerve fiber present in the disc using markers specific for fiber types, like IB4, CGRP, SP, etc [79]. Furthermore, the origin of these nerve fibers, i.e., whether some might be extensions of the sympathetic nervous system, could be determined by staining for tyrosine hydroxylase [353]. Finally, it would be useful to understand if the hypocellularity of the disc is a result of necrosis, apoptosis or a combination. This could be accomplished using IHC, to measure markers of apotosis and necrosis like Annexin V and receptor-interacting serine/threonine-protein kinase 3 (RIPK3), respectively [354, 355]. Understanding this aspect of degeneration would provide insights into whether deleterious loading or nutrient deficiency plays the predominant role in driving cell death.

In summary, Chapter 5 outlines a robust model of disc-associated cLBP. This model came to fruition through lessons learned in a failed pilot study, evidence in literature, and understanding of rat neuroanatomy. The manifestation of overt disc degeneration, chronic pain-like behavior, and nerve sprouting cements this as a leading model. As always, more could be done to improve the model's readouts and to explore more pathomechanisms of disc-associated pain.

7.3 Chapter 6 Discussion and Future Directions

The final Chapter of this dissertation described the engineering of a therapeutic for low back pain *in vitro* and its capacity to alleviate disc-associated pain *in vivo*. This final study represented the culmination of all the work completed from the start of the Ph.D. to the end. Critical motivation for this work arose from observations made during the establishment of the disc-associated pain model. After staining and imaging with H&E, it became clear that degeneration resulted in widespread loss of tissue integrity **(Fig. 34)**. Because we witnessed consistent staining of nerve fibers around annular

fissures and other tissue disruptions, we hypothesized altered biomechanics may drive nociception and in turn pain. The basis for this hypothesis was that mechanically sensitive nerve fibers located in sites of tissue integrity loss, may be subjected to deleterious loading, resulting in depolarization and nociception. Supporting this hypothesis, grip strength, which indirectly strained the disc and may have imparted deleterious loading, was the most sensitive measure of pain-like behavior.

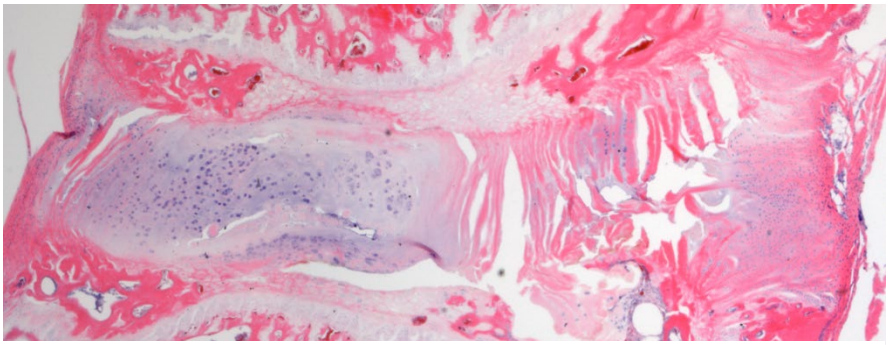

Figure 34. H&E stained section of an injured IVD from the rat model of disc-associated pain. Notice the loss of tissue integrity on the right side (ventral AF).

At the conclusion of the disc-associated model study, our lab also published data on a biomaterial derived from decellularized healthy NP tissue. In this paper, the biomaterial was amenable to injection, not cytotoxic, and partially neuroinhibitory [235]. Establishing the methods for fabricating this biomaterial and measuring its properties comprised the first two years of my Ph.D. Having worked with this biomaterial extensively, and knowing mechanics might be at the core of disc-associated pain, it was decided to re-engineer this biomaterial specifically for tissue integration and IVD stabalization.

In early work, it was realized that fabricating a hydrogel soley from decellularized tissue was not feasible, with early formulations unable to form a complete hydrogel. Collagen was added to the formulation to amplify fibrillogenesis and mechanical properties. An iteration of dNP supplemented with collagen comprised what was

described in the biomaterial paper we published. However, this biomaterial was deemed suboptimal for treating disc-associated pain *in vivo* because it would not robustly integrate with existing tissue, decreasing its capacity to augment deleterious loading. To resolve this limitation, the dNP biomaterial was supplemented with a crosslinking agent to promote integration.

The first crosslinking agent tested was lysyl oxidase (LOX), an endogenous enzyme known to crosslink collagen [244]. This enzyme is known to play a key role in tissue sclerotization, and therefore seemed a great candidate for integrating the biomaterial and rigidifying the IVD. Unfortunately, LOX only increased the mechanical properties of dNP hydrogel by around 30% after prolonged exposure, indicating the cross-linking activity was either too low or not rapid enough to ensure biomaterial integration. Genipin was next to be evaluated and exhibited a remarkable capacity to increase dNP mechanical properties **(Fig. 35)** [251]. Further, genipin completed 90% of its crosslinking in under 12 hours meaning tissue integration would be rapid. Various concentrations of genipin were then tested to find an amount that got close to saturating all crosslinking sites while maintaining low risk of free genipin as free genipin is thought to be cytotoxic [250]. The 2.5 mM concentration was an optimal choice because it minimized the risk of free

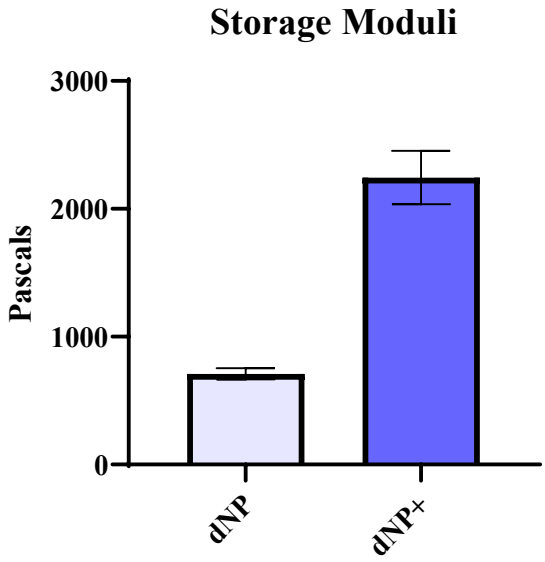

Figure 35. Storage moduli of dNP (0 mM genipin and dNP+ (2.5 mM genipin)

genipin, exhibited cytocompatibility, and still dramatically increased dNP mechanical properties suggesting there was a high degree of crosslinking activity.

Having chosen the final formulation, dNP+, the next problem solved was the injection procedure. This process was refined using trial and error on rat cadavers and involved insulin syringes, syringe pumps, microinjectors, and gas chromatography microliter syringes. Insulin syringes could not adequately control the small injection volume, syringe pumps were too wasteful because of hydrogel lost in the pump line and the microinjector was not feasible because of it's size and requirement for a new syringe for each injection. With these limitations, the gas chromotography syringe represented the only viable option for controlled, minimally wasteful, injections. However, dNP+ was too viscous to be drawn up by these syringes making them unusable. A solution was found by removing the syringe plunger and injecting the gel from the back end of the syringe. Next, to ensure the dNP+ was delivered to the middle of the disc, and did not overpenetrate, the syringe needles used for injection were affixed with a rubber stopper on the needle to control the injection depth. Initially, this final system did not reliably adminster dNP+ to the disc but rather leaked dNP+ around the needle hub. After more trial and error, we realized that the injection speed had to be slowed to allow time for the disc to expand and accommodate the gel. In future work, air-tight syringes with luer-locking hubs may further decrease the risk of injectate extrusion around the needle hub and provide more consistent injectate volumes.

Another major decision concerned the time at which degenerated IVDs would be treated *in vivo*. DNP+ was viewed as a treatment that might be used for humans suffering chronic disc-associated pain. Therefore, we reasoned the only permissible time to treat

IVDs with dNP+ would be at a chronic time point, after pain-like behavior had developed. In our model, this occurred by week 8, so treatment was administered at week 9. This treatment strategy contrasted nearly all work that has been done in animal models of chronic low back pain where most treatments occur concomittant or shortly after degeneration induction [221].

Given all the work developing the biomaterial and refining the injection procedure, it appeared dNP+ might be capable of treating disc-associated pain despite the overwhelming majority of treatments from other groups failing in animal models. Confirming this outlook, the treatment worked, restoring disc volume and alleviating axial hypersensitivity at all time points after administration. Further, at study conclusion, mechanics of dNP+ treated discs did not significantly differ from sham discs while sham discs did significantly differ from discs treated with PBS. Currently, it is not clear what caused this increase in mechanical properties because dNP+ was orders of magnitude weaker than disc tissue meaning that the addition of dNP+ alone could not have increased disc mechanics dramatically. The current hypothesis is that dNP+ reconnected tissue disruptions, permitting migration and localization of cells like fibroblasts to these sites which deposited new matrix to stabalize the disc. The dNP+ treatment may have also worked through an immunomodulatory capacity to promote tissue anabolism considering it is derived from healthy, decellularized tissue [226-229]. An alternative explaination is that genipin diffused from the hydrogel and crosslinked existing, degenerated tissue, stabalizing it. Overall, this process may have resolved deleterious loading and transformed the disc from unstable catabolism to stable, fibrotic, homeostasis. These

results indicated that mechanics may have underpinned the decrease in axial hypersensitivity.

This study has several areas that could be expanded or refined in future work. First, the cytocompatibility assessment *in vitro* did not entirely evaluate the effect of free genipin released from dNP+ hydrogels. Because dNP+ required eight hours to complete crosslinking, it was not feasible to plate cells on top of it prior to gelation completion. Additionally, during the incubation window there was some concern the gels could partially dry, resulting in erroneous outcomes. These two factors made it so the plates had to be coated with gels, incubated for 8 hours and then equilibrated with 1X PBS overnight prior to cell seeding. The 1X PBS equilibration step may have removed a significant fraction of free genipin, if there was any. In the future, cells could be cultured in proximity of dNP+ gels made separately or the dNP+ coated wells could be equilibrated with 1X PBS containing 2.5 mM genipin to address this limitation.

Another process that could be refined is the potting and mechanical evaluation of rat motion segments. For all mechanics, we simply measured motion segments using an amplitude sweep which measured the resistance to an increasing torsional strain. This method does not answer questions involving the neutral zone, stress-relaxation, nor creep behavior of the motion segments. Considering there is evidence in the literature that these aspects of motion segments change with degeneration, they represent valuable, quantifiable metrics of motion segement mechanics [75, 156, 168, 174]. In the future, tension displacement curves could be collected on a rheometer and analyzed to determine torsional stiffness, torque range, tosional hysteresis, and neutral zone [2, 325]. These data could provide insight into functional changes which coincide IVD degeneration and

provide targets for treatments. Furthermore, the potting process could be refined by making uniform cuts in the vertebral bone, a preset distance away from the IVD. Uniformity in this process would ensure that all motion segments are potted in a similar manner and that they are all of equal length. In the treatment study, a significant portion of the motion segments had to be discarded because the vertebral bodies were cut far from the IVD, making them unstable during the potting process. This instability caused these motion segments to detach from the pot, prolonging the potting process, eventually leading to tissue dessication which made collecting mechanical properties not feasible.

Finally, considerable work must yet be done processing motion segments into tissue sections to evaluate morphological and other aspects of degenerated and sham IVDs in this study. The first and foremost of the next steps should be H&E analysis. H&E will provide invaluable insight about the location of dNP+ within the degenerated tissue and may shed light on the effects dNP+ had on tissue necrosis and granulation deposition. IHC for nerve fibers may also be pursued to determine if dNP+ maintained neuroinhibitory capacity *in vivo* and prevented further nerve sprouting, or in best case, caused dieback of nerve sprouts.

In conclusion, this final chapter, explored the utility of a decellularized biomaterial, doped with collagen and genipin, as a treatment for disc-associated pain in an animal model. After thorough engineering, the dNP+ therapeutic proved viable as an injectable treatment that was spontaneously fibrillogenic and not cytotoxic. When applied to animals suffering disc-associated pain, dNP+ restored disc volume and alleviated axial hypersensitivity. These observations indicate that dNP+ is an effective treatment for disc-

associated cLBP in an animal model, but further work must be completed prior to disseminating these results or pursuring further animal trials.

CHAPTER 8: Personal Summary

Taken together, the chapters of this dissertation represent the distillation of five years of failure, learning, and success. Chapter 4 was the first exploration into animal models and animal data. From this I learned how to understand animals, work with variability inherent with *in vivo* data, and how to refine processes to provide maximum utility. Chapter 5 built upon the experience gathered in Chapter 4 and facilitated growth in managing timelines, groups of people, and complex, time-constrained, procedures. Chapter 5 also marked the turning point of my Ph.D., where I took on the projects personally, and the burden of success or failure became my own. Chapter 6 was the culmination of all that was learned throughout the pursuit of a Ph.D. This final work blended all the experience I had gathered into one task. Without all the past success, failures, and learning experiences, I would not have been equipped to attempt, much less succeed, in this final Chapter. I am grateful to have collected this experience and knowledge over the course of this Ph.D. I hope the work accomplished in and outside of this dissertation has expanded the frontier of understanding and will provide utility for future scientific work.

CHAPTER 9: Conclusion

The primary goal of this dissertation was to engineer a therapeutic for disc-associated low back pain. To do this, a method for quantifying disc degeneration real-time and a model of disc-associated pain were established in female Sprague Dawley rats. After this foundational work, a biomaterial, derived from decellularized porcine IVD tissue, was created and tested *in vitro* and *in vivo*.

Chapter 4 described a method for processing three-dimensional μCT data to create three-dimensional renderings of intervertebral discs. This method was extremely sensitive in detecting changes of the IVD and provided a state of the art means to monitor disc degeneration real time.

Chapter 5 established a novel and robust model of disc-associated pain. This model manifested consistent and increasing chronic axial hypersensitivity and deep pressure hypersensitivity at the L5-L6 level. Furthermore, this was the first rat model to demonstrate nerve fibers penetrating deep into degenerated disc tissue and the first to positively associate nerve sprouting with pain-like hypersensitivity. The presence of pain-like behavior across two assays in concert with aberrant nerve sprouting solidified this model as a leader in the field of biomedical research.

Chapter 6 outlined the creation of a biomaterial derived from decellularized, healthy NP tissue, supplemented with collagen and genipin. In our animal model, this novel biomaterial treatment increased exploratory behavior in the open field test, decreased axial hypersensitivity, and prevented the development of deep pressure hypersensitivity. Additionally, immediately after treatment, disc volumes in treated

animals returned to baseline and remained at baseline for the remainder of the study, suggesting complete tissue-biomaterial integration.

In sum, this dissertation outlines a platform for evaluating therapeutics and provides a strong treatment candidate for disc-associated pain.

REFERENCES

[1] K. Gui, W. Ren, Y. Yu, X. Li, J. Dong, W. Yin, Inhibitory effects of platelet-rich plasma on intervertebral disc degeneration: a preclinical study in a rabbit model, Medical Science Monitor: International Medical Journal of Experimental and Clinical Research 21 (2015) 1368.
[2] G.E. Mosley, M. Wang, P. Nasser, A. Lai, D.A. Charen, B. Zhang, J.C. Iatridis, Males and females exhibit distinct relationships between intervertebral disc degeneration and pain in a rat model, Scientific Reports 10(1) (2020) 15120.
[3] D.J. Lillyman, F.S. Lee, E.C. Barnett, T.J. Miller, M.L. Alvaro, H.C. Drvol, R.A. Wachs, Axial hypersensitivity is associated with aberrant nerve sprouting in a novel model of disc degeneration in female Sprague Dawley rats, JOR SPINE n/a(n/a) (2022) e1212.
[4] S.N. Raja, D.B. Carr, M. Cohen, N.B. Finnerup, H. Flor, S. Gibson, F. Keefe, J.S. Mogil, M. Ringkamp, K.A. Sluka, The revised IASP definition of pain: Concepts, challenges, and compromises, Pain 161(9) (2020) 1976.
[5] S.P. Cohen, L. Vase, W.M. Hooten, Chronic pain: an update on burden, best practices, and new advances, The Lancet 397(10289) (2021) 2082-2097.
[6] D.J. Gaskin, P. Richard, The Economic Costs of Pain in the United States, The Journal of Pain 13(8) (2012) 715-724.
[7] D.J. Gaskin, P. Richard, Appendix C: The economic costs of pain in the United States, Relieving Pain in America: A Blueprint for Transforming Prevention, Care, Education, and Research (2011) 1-22.
[8] G.J. Macfarlane, The epidemiology of chronic pain, Pain 157(10) (2016) 2158-2159.
[9] A.M. Elliott, B.H. Smith, K.I. Penny, W.C. Smith, W.A. Chambers, The epidemiology of chronic pain in the community, The lancet 354(9186) (1999) 1248-1252.
[10] H.I. Andersson, G. Ejlertsson, I. Leden, C. Rosenberg, Chronic pain in a geographically defined general population: studies of differences in age, gender, social class, and pain localization, Clin J Pain 9(3) (1993) 174-82.
[11] C.J. Murray, C. Atkinson, K. Bhalla, G. Birbeck, R. Burstein, D. Chou, R. Dellavalle, G. Danaei, M. Ezzati, A. Fahimi, D. Flaxman, Foreman, S. Gabriel, E. Gakidou, N. Kassebaum, S. Khatibzadeh, S. Lim, S.E. Lipshultz, S. London, Lopez, M.F. MacIntyre, A.H. Mokdad, A. Moran, A.E. Moran, D. Mozaffarian, T. Murphy, M. Naghavi, C. Pope, T. Roberts, J. Salomon, D.C. Schwebel, S. Shahraz, D.A. Sleet, Murray, J. Abraham, M.K. Ali, C. Atkinson, D.H. Bartels, K. Bhalla, G. Birbeck, R. Burstein, H. Chen, M.H. Criqui, Dahodwala, Jarlais, E.L. Ding, E.R. Dorsey, B.E. Ebel, M. Ezzati, Fahami, S. Flaxman, A.D. Flaxman, D. Gonzalez-Medina, B. Grant, H. Hagan, H. Hoffman, N. Kassebaum, S. Khatibzadeh, J.L. Leasher, J. Lin, S.E. Lipshultz, R. Lozano, Y. Lu, L. Mallinger, M.M. McDermott, R. Micha, T.R. Miller, A.A. Mokdad, A.H. Mokdad, D. Mozaffarian, M. Naghavi, K.M. Narayan, S.B. Omer, P.M. Pelizzari, D. Phillips, D. Ranganathan, F.P. Rivara, T. Roberts, U. Sampson, E. Sanman, A. Sapkota, D.C. Schwebel, S. Sharaz, R. Shivakoti, G.M. Singh, D. Singh, M. Tavakkoli, J.A. Towbin, J.D. Wilkinson, A. Zabetian, Murray, J. Abraham, M.K. Ali, M. Alvardo, C. Atkinson, L.M. Baddour, E.J. Benjamin, K. Bhalla, G. Birbeck, I. Bolliger, R. Burstein, E. Carnahan, D. Chou, S.S. Chugh, A. Cohen, K.E. Colson, L.T. Cooper, W. Couser, M.H. Criqui, K.C. Dabhadkar, R.P. Dellavalle, Jarlais, D. Dicker, E.R. Dorsey,

H. Duber, B.E. Ebel, R.E. Engell, M. Ezzati, D.T. Felson, M.M. Finucane, S. Flaxman, A.D. Flaxman, T. Fleming, Foreman, M.H. Forouzanfar, G. Freedman, M.K. Freeman, E. Gakidou, R.F. Gillum, D. Gonzalez-Medina, R. Gosselin, H.R. Gutierrez, H. Hagan, R. Havmoeller, H. Hoffman, K.H. Jacobsen, S.L. James, R. Jasrasaria, S. Jayarman, N. Johns, N. Kassebaum, S. Khatibzadeh, Q. Lan, J.L. Leasher, S. Lim, S.E. Lipshultz, S. London, Lopez, R. Lozano, Y. Lu, L. Mallinger, M. Meltzer, G.A. Mensah, C. Michaud, T.R. Miller, C. Mock, T.E. Moffitt, A.A. Mokdad, A.H. Mokdad, A. Moran, M. Naghavi, K.M. Narayan, R.G. Nelson, C. Olives, S.B. Omer, K. Ortblad, B. Ostro, P.M. Pelizzari, D. Phillips, M. Raju, H. Razavi, B. Ritz, T. Roberts, R.L. Sacco, J. Salomon, U. Sampson, D.C. Schwebel, S. Shahraz, K. Shibuya, D. Silberberg, J.A. Singh, K. Steenland, J.A. Taylor, G.D. Thurston, M.S. Vavilala, T. Vos, G.R. Wagner, M.A. Weinstock, M.G. Weisskopf, S. Wulf, Murray, The state of US health, 1990-2010: burden of diseases, injuries, and risk factors, Jama 310(6) (2013) 591-608.
[12] T.S. Vrbanić, [Low back pain--from definition to diagnosis], Reumatizam 58(2) (2011) 105-7.
[13] S. Rozenberg, [Chronic low back pain: definition and treatment], La Revue du praticien 58(3) (2008) 265-72.
[14] S. Dagenais, J. Caro, S. Haldeman, A systematic review of low back pain cost of illness studies in the United States and internationally, The spine journal 8(1) (2008) 8-20.
[15] J. Mathew, S.B. Singh, S. Garis, A.D. Diwan, Backing up the stories: The psychological and social costs of chronic low-back pain, Int J Spine Surg 7 (2013) e29-e38.
[16] H. Bahouq, F. Allali, H. Rkain, N. Hajjaj-Hassouni, Discussing sexual concerns with chronic low back pain patients: barriers and patients' expectations, Clinical rheumatology 32(10) (2013) 1487-1492.
[17] F. Bailly, V. Foltz, S. Rozenberg, B. Fautrel, L. Gossec, The impact of chronic low back pain is partly related to loss of social role: a qualitative study, Joint Bone Spine 82(6) (2015) 437-441.
[18] I. Jimenez-Rodríguez, J.M. Garcia-Leiva, B.M. Jimenez-Rodriguez, E. Condés-Moreno, F. Rico-Villademoros, E.P. Calandre, Suicidal ideation and the risk of suicide in patients with fibromyalgia: a comparison with non-pain controls and patients suffering from low-back pain, Neuropsychiatr Dis Treat 10 (2014) 625-630.
[19] K.R.R. Krishnan, R.D. France, S. Pelton, U.D. McCann, J. Davidson, B.J. Urban, Chronic pain and depression. I. Classification of depression in chronic low back pain patients, Pain 22(3) (1985) 279-287.
[20] N.K. Tang, K.J. Wright, P.M. Salkovskis, Prevalence and correlates of clinical insomnia co-occurring with chronic back pain, Journal of sleep research 16(1) (2007) 85-95.
[21] N.K. Tang, C. Crane, Suicidality in chronic pain: a review of the prevalence, risk factors and psychological links, Psychological medicine 36(5) (2006) 575-586.
[22] M.J. DePalma, J.M. Ketchum, T. Saullo, What is the source of chronic low back pain and does age play a role?, Pain medicine 12(2) (2011) 224-233.
[23] A.C. Schwarzer, C.N. Aprill, R. Derby, J. Fortin, G. Kine, N. Bogduk, The prevalence and clinical features of internal disc disruption in patients with chronic low back pain, Spine 20(17) (1995) 1878-1883.

[24] A.C. Schwarzer, C.N. Aprill, N. Bogduk, The sacroiliac joint in chronic low back pain, Spine (Phila Pa 1976) 20(1) (1995) 31-7.
[25] N. Kavita, A. Kimberly, L. Manchikanti, Age-related prevalence of facet-joint involvement in chronic neck and low back pain, Pain physician 11(1) (2008) 67-75.
[26] R.A. Deyo, S.F. Dworkin, D. Amtmann, G. Andersson, D. Borenstein, E. Carragee, J. Carrino, R. Chou, K. Cook, A. DeLitto, C. Goertz, P. Khalsa, J. Loeser, S. Mackey, J. Panagis, J. Rainville, T. Tosteson, D. Turk, M. Von Korff, D.K. Weiner, Report of the NIH Task Force on research standards for chronic low back pain, The journal of pain : official journal of the American Pain Society 15(6) (2014) 569-585.
[27] R. Baron, A. Binder, N. Attal, R. Casale, A.H. Dickenson, R.D. Treede, Neuropathic low back pain in clinical practice, European Journal of Pain 20(6) (2016) 861-873.
[28] A. Dower, M.A. Davies, A. Ghahreman, Pathologic basis of lumbar radicular pain, World neurosurgery 128 (2019) 114-121.
[29] F. Balagué, A.F. Mannion, F. Pellisé, C. Cedraschi, Non-specific low back pain, The Lancet 379(9814) (2012) 482-491.
[30] K.M. Cheung, J. Karppinen, D. Chan, D.W. Ho, Y.-Q. Song, P. Sham, K.S. Cheah, J.C. Leong, K.D. Luk, Prevalence and pattern of lumbar magnetic resonance imaging changes in a population study of one thousand forty-three individuals, Spine 34(9) (2009) 934-940.
[31] N. Todd, The surgical treatment of non-specific low back pain, The bone & joint journal 99(8) (2017) 1003-1005.
[32] M. VAN KLEEF, G. Barendse, S.K. BULSTRA, W. WEBER, M.E. SLUIJTER, Percutaneous intradiscal radio-frequency thermocoagulation in chronic non-specific low back, The Pain Clinic 9(3) (1996) 259-68.
[33] A.J. Vora, K.D. Doerr, L.R. Wolfer, Functional Anatomy and Pathophysiology of Axial Low Back Pain: Disc, Posterior Elements, Sacroiliac Joint, and Associated Pain Generators, Physical Medicine and Rehabilitation Clinics of North America 21(4) (2010) 679-709.
[34] J. Scholz, R.J. Mannion, D.E. Hord, R.S. Griffin, B. Rawal, H. Zheng, D. Scoffings, A. Phillips, J. Guo, R.J. Laing, A novel tool for the assessment of pain: validation in low back pain, PLoS medicine 6(4) (2009) e1000047.
[35] W. Brinjikji, F.E. Diehn, J.G. Jarvik, C.M. Carr, D.F. Kallmes, M.H. Murad, P.H. Luetmer, MRI Findings of Disc Degeneration are More Prevalent in Adults with Low Back Pain than in Asymptomatic Controls: A Systematic Review and Meta-Analysis, American Journal of Neuroradiology 36(12) (2015) 2394.
[36] H. Crock, A reappraisal of intervertebral disc lesions, Medical Journal of Australia 1(20) (1970) 983-989.
[37] M. Galve Villa, T. S Palsson, A. Cid Royo, C. R Bjarkam, S.A. Boudreau, Digital Pain Mapping and Tracking in Patients With Chronic Pain: Longitudinal Study, J Med Internet Res 22(10) (2020) e21475-e21475.
[38] I. Holm, A. Friis, K. Storheim, J.I. Brox, Measuring self-reported functional status and pain in patients with chronic low back pain by postal questionnaires: a reliability study, Spine 28(8) (2003) 828-833.
[39] P. Malliou, A. Gioftsidou, A. Beneka, G. Godolias, Measurements and evaluations in low back pain patients, Scandinavian Journal of Medicine & Science in Sports 16(4) (2006) 219-230.

[40] W. Alston, K.E. Carlson, D.J. Feldman, Z. Grimm, E. Gerontinos, A quantitative study of muscle factors in the chronic low back syndrome, Journal of the American Geriatrics Society 14(10) (1966) 1041-1047.
[41] K.L. Barker, H. Dawes, P. Hansford, D. Shamley, Perceived and measured levels of exertion of patients with chronic back pain exercising in a hydrotherapy pool, Archives of physical medicine and rehabilitation 84(9) (2003) 1319-1323.
[42] M. Bayramoglu, M.N. Akman, S. Klnç, N. Çetin, N. Yavuz, R. Özker, Isokinetic measurement of trunk muscle strength in women with chronic low-back pain, American journal of physical medicine & rehabilitation 80(9) (2001) 650-655.
[43] K.M. Malik, S.P. Cohen, D.R. Walega, H.T. Benzon, Diagnostic criteria and treatment of discogenic pain: a systematic review of recent clinical literature, The Spine Journal 13(11) (2013) 1675-1689.
[44] Z.L. McCormick, V.T. Lehman, C.T. Plastaras, D.R. Walega, P. Huddleston, III, C. Moussallem, J.R. Geske, J.T. Verdoorn, D.J. Kennedy, T.P. Maus, C.M. Carr, Low-Pressure Lumbar Provocation Discography According to Spine Intervention Society/International Association for the Study of Pain Standards Does Not Cause Acceleration of Disc Degeneration in Patients With Symptomatic Low Back Pain: A 7-Year Matched Cohort Study, Spine 44(19) (2019).
[45] E.J. Carragee, A.S. Don, E.L. Hurwitz, J.M. Cuellar, J. Carrino, R. Herzog, 2009 ISSLS prize winner: does discography cause accelerated progression of degeneration changes in the lumbar disc: a ten-year matched cohort study, Spine 34(21) (2009) 2338-2345.
[46] W.T.M. Enthoven, P. Roelofs, R.A. Deyo, M.W. van Tulder, B.W. Koes, Non-steroidal anti-inflammatory drugs for chronic low back pain, Cochrane Database of Systematic Reviews (2) (2016).
[47] G.A. Green, Understanding NSAIDs: From aspirin to COX-2, Clinical Cornerstone 3(5) (2001) 50-59.
[48] D.C. Cherkin, K.J. Wheeler, W. Barlow, R.A. Deyo, Medication use for low back pain in primary care, Spine 23(5) (1998) 607-614.
[49] L. Kuritzky, G.P. Samraj, Nonsteroidal anti-inflammatory drugs in the treatment of low back pain, J Pain Res 5 (2012) 579-590.
[50] L. Zhao, L. Manchikanti, A.D. Kaye, A. Abd-Elsayed, Treatment of Discogenic Low Back Pain: Current Treatment Strategies and Future Options-a Literature Review, Curr Pain Headache Rep 23(11) (2019) 86.
[51] M. Van Middelkoop, S.M. Rubinstein, T. Kuijpers, A.P. Verhagen, R. Ostelo, B.W. Koes, M.W. van Tulder, A systematic review on the effectiveness of physical and rehabilitation interventions for chronic non-specific low back pain, European Spine Journal 20(1) (2011) 19-39.
[52] M. Van Middelkoop, S.M. Rubinstein, A.P. Verhagen, R.W. Ostelo, B.W. Koes, M.W. van Tulder, Exercise therapy for chronic nonspecific low-back pain, Best practice & research Clinical rheumatology 24(2) (2010) 193-204.
[53] T. Thompson, S. Dias, D. Poulter, S. Weldon, L. Marsh, C. Rossato, J.I. Shin, J. Firth, N. Veronese, E. Dragioti, Efficacy and acceptability of pharmacological and non-pharmacological interventions for non-specific chronic low back pain: a protocol for a systematic review and network meta-analysis, Systematic reviews 9(1) (2020) 1-11.
[54] H. McQuay, Opioids in pain management, The Lancet 353(9171) (1999) 2229-2232.

[55] C. Zöllner, C. Stein, Opioids, in: C. Stein (Ed.), Analgesia, Springer Berlin Heidelberg, Berlin, Heidelberg, 2007, pp. 31-63.
[56] R. Kanjhan, OPIOIDS AND PAIN, Clinical and Experimental Pharmacology and Physiology 22(6-7) (1995) 397-403.
[57] A.D. Wasan, G. Davar, R. Jamison, The association between negative affect and opioid analgesia in patients with discogenic low back pain, Pain 117(3) (2005) 450-461.
[58] R.A. Deyo, M. Von Korff, D. Duhrkoop, Opioids for low back pain, BMJ (Clinical research ed.) 350 (2015) g6380-g6380.
[59] N. Vadivelu, A.M. Kai, V. Kodumudi, J. Sramcik, A.D. Kaye, The Opioid Crisis: a Comprehensive Overview, Current Pain and Headache Reports 22(3) (2018) 16.
[60] P. Fritzell, O. Hägg, P. Wessberg, A. Nordwall, S.L.S.S. Group, 2001 Volvo Award Winner in Clinical Studies: Lumbar fusion versus nonsurgical treatment for chronic low back pain: a multicenter randomized controlled trial from the Swedish Lumbar Spine Study Group, Spine 26(23) (2001) 2521-2532.
[61] P. Fritzell, O. Hägg, P. Wessberg, A. Nordwall, S.L.S.S. Group, Chronic low back pain and fusion: a comparison of three surgical techniques: a prospective multicenter randomized study from the Swedish lumbar spine study group, Spine 27(11) (2002) 1131-1141.
[62] A. Beschloss, T. Ishmael, C. Dicindio, C. Hendow, A. Ha, P. Louie, J. Lombardi, A. Pugely, A. Ozturk, V. Arlet, C. Saifi, The Expanding Frontier of Outpatient Spine Surgery, Int J Spine Surg 15(2) (2021) 266-273.
[63] R.A. Deyo, D.T. Gray, W. Kreuter, S. Mirza, B.I. Martin, United States trends in lumbar fusion surgery for degenerative conditions, Spine 30(12) (2005) 1441-1445.
[64] H. Nakashima, N. Kawakami, T. Tsuji, T. Ohara, Y. Suzuki, T. Saito, A. Nohara, R. Tauchi, K. Ohta, N. Hamajima, Adjacent segment disease after posterior lumbar interbody fusion, Spine 40(14) (2015) E831-E841.
[65] M.K. Cox, R. Serra, Development of the Intervertebral Disc, in: I.M. Shapiro, M.V. Risbud (Eds.), The Intervertebral Disc: Molecular and Structural Studies of the Disc in Health and Disease, Springer Vienna, Vienna, 2014, pp. 33-51.
[66] J.P.G. Urban, S. Roberts, J.R. Ralphs, The Nucleus of the Intervertebral Disc from Development to Degeneration1, American Zoologist 40(1) (2000) 53-061.
[67] M.V. Risbud, E. Schipani, I.M. Shapiro, Hypoxic regulation of nucleus pulposus cell survival: from niche to notch, The American journal of pathology 176(4) (2010) 1577-1583.
[68] J.C. Iatridis, J.J. MacLean, M. O'Brien, I.A.F. Stokes, Measurements of proteoglycan and water content distribution in human lumbar intervertebral discs, Spine 32(14) (2007) 1493-1497.
[69] P.L. Chandran, F. Horkay, Aggrecan, an unusual polyelectrolyte: review of solution behavior and physiological implications, Acta Biomater 8(1) (2012) 3-12.
[70] H. Rauvala, M. Paveliev, J. Kuja-Panula, N. Kulesskaya, Inhibition and enhancement of neural regeneration by chondroitin sulfate proteoglycans, Neural regeneration research 12(5) (2017) 687.
[71] A.M.R. Groh, D.E. Fournier, M.C. Battié, C.A. Séguin, Innervation of the Human Intervertebral Disc: A Scoping Review, Pain Medicine 22(6) (2021) 1281-1304.
[72] R.J. Moore, The vertebral end-plate: what do we know?, Eur Spine J 9(2) (2000) 92-6.

[73] Y. Lanir, Mechanisms of residual stress in soft tissues, Journal of biomechanical engineering 131(4) (2009).
[74] M.A. Adams, W. Hutton, The effect of posture on the role of the apophysial joints in resisting intervertebral compressive forces, The Journal of bone and joint surgery. British volume 62(3) (1980) 358-362.
[75] T. Guehring, F. Unglaub, H. Lorenz, G. Omlor, H.-J. Wilke, M.W. Kroeber, Intradiscal pressure measurements in normal discs, compressed discs and compressed discs treated with axial posterior disc distraction: an experimental study on the rabbit lumbar spine model, Eur Spine J 15(5) (2006) 597-604.
[76] H. Schmidt, A. Kettler, F. Heuer, U. Simon, L. Claes, H.J. Wilke, Intradiscal pressure, shear strain, and fiber strain in the intervertebral disc under combined loading, Spine (Phila Pa 1976) 32(7) (2007) 748-55.
[77] H.J. Wilke, P. Neef, M. Caimi, T. Hoogland, L.E. Claes, New in vivo measurements of pressures in the intervertebral disc in daily life, Spine (Phila Pa 1976) 24(8) (1999) 755-62.
[78] I.A. Stokes, M. Gardner-Morse, D. Churchill, J.P. Laible, Measurement of a spinal motion segment stiffness matrix, Journal of biomechanics 35(4) (2002) 517-521.
[79] J. García-Cosamalón, M.E. del Valle, M.G. Calavia, O. García-Suárez, A. López-Muñiz, J. Otero, J.A. Vega, Intervertebral disc, sensory nerves and neurotrophins: who is who in discogenic pain?, Journal of anatomy 217(1) (2010) 1-15.
[80] N. Bogduk, The innervation of the lumbar spine, Spine (Phila Pa 1976) 8(3) (1983) 286-93.
[81] G.J. Groen, B. Baljet, J. Drukker, Nerves and nerve plexuses of the human vertebral column, American journal of anatomy 188(3) (1990) 282-296.
[82] R.V. Haberberger, C. Barry, N. Dominguez, D. Matusica, Human dorsal root ganglia, Frontiers in cellular neuroscience (2019) 271.
[83] N. Ahimsadasan, V. Reddy, A. Kumar, Neuroanatomy, dorsal root ganglion, (2018).
[84] B.P. Bean, The action potential in mammalian central neurons, Nature Reviews Neuroscience 8(6) (2007) 451-465.
[85] J.C. Tuthill, E. Azim, Proprioception, Current Biology 28(5) (2018) R194-R203.
[86] T. Yamashita, Y. Minaki, I. Oota, K. Yokogushi, S. Ishii, Mechanosensitive afferent units in the lumbar intervertebral disc and adjacent muscle, Spine (Phila Pa 1976) 18(15) (1993) 2252-6.
[87] S. Neumann, T.P. Doubell, T. Leslie, C.J. Woolf, Inflammatory pain hypersensitivity mediated by phenotypic switch in myelinated primary sensory neurons, Nature 384(6607) (1996) 360-4.
[88] C.L. Stucky, IB4-Positive Neurons, Role in Inflammatory Pain, in: R.F. Schmidt, W.D. Willis (Eds.), Encyclopedia of Pain, Springer Berlin Heidelberg, Berlin, Heidelberg, 2007, pp. 952-955.
[89] W.H. Sun, C.C. Chen, Roles of Proton-Sensing Receptors in the Transition from Acute to Chronic Pain, Journal of Dental Research 95(2) (2015) 135-142.
[90] D.J. Cavanaugh, H. Lee, L. Lo, S.D. Shields, M.J. Zylka, A.I. Basbaum, D.J. Anderson, Distinct subsets of unmyelinated primary sensory fibers mediate behavioral responses to noxious thermal and mechanical stimuli, Proc Natl Acad Sci U S A 106(22) (2009) 9075-80.

[91] G. Stephan, L. Huang, Y. Tang, S. Vilotti, E. Fabbretti, Y. Yu, W. Nörenberg, H. Franke, F. Gölöncsér, B. Sperlágh, A. Dopychai, R. Hausmann, G. Schmalzing, P. Rubini, P. Illes, The ASIC3/P2X3 cognate receptor is a pain-relevant and ligand-gated cationic channel, Nat Commun 9(1) (2018) 1354.
[92] J. Levine, H. Fields, A. Basbaum, Peptides and the primary afferent nociceptor, The Journal of Neuroscience 13(6) (1993) 2273-2286.
[93] T. Ozawa, S. Ohtori, G. Inoue, Y. Aoki, H. Moriya, K. Takahashi, The degenerated lumbar intervertebral disc is innervated primarily by peptide-containing sensory nerve fibers in humans, Spine (Phila Pa 1976) 31(21) (2006) 2418-22.
[94] R. Greco, C. Tassorelli, G. Sandrini, P. Di Bella, S. Buscone, G. Nappi, Role of calcitonin gene-related peptide and substance P in different models of pain, Cephalalgia : an international journal of headache 28(2) (2008) 114-26.
[95] W.S. Schou, S. Ashina, F.M. Amin, P.J. Goadsby, M. Ashina, Calcitonin gene-related peptide and pain: a systematic review, The Journal of Headache and Pain 18(1) (2017) 34.
[96] D. Vardeh, J.F. Naranjo, Peripheral and Central Sensitization, in: R.J. Yong, M. Nguyen, E. Nelson, R.D. Urman (Eds.), Pain Medicine: An Essential Review, Springer International Publishing, Cham, 2017, pp. 15-17.
[97] S. Davidson, B.A. Copits, J. Zhang, G. Page, A. Ghetti, R.W. Gereau IV, Human sensory neurons: Membrane properties and sensitization by inflammatory mediators, PAIN® 155(9) (2014) 1861-1870.
[98] V. Gangadharan, R. Kuner, Pain hypersensitivity mechanisms at a glance, Dis Model Mech 6(4) (2013) 889-895.
[99] D. Fornasari, Pain mechanisms in patients with chronic pain, Clinical drug investigation 32(1) (2012) 45-52.
[100] Z. Sun, M. Zhang, X.-H. Zhao, Z.-H. Liu, Y. Gao, D. Samartzis, H.-Q. Wang, Z.-J. Luo, Immune cascades in human intervertebral disc: the pros and cons, International journal of clinical and experimental pathology 6(6) (2013) 1009.
[101] M.A. Adams, P. Dolan, Intervertebral disc degeneration: evidence for two distinct phenotypes, Journal of Anatomy 221(6) (2012) 497-506.
[102] D. Chan, Y. Song, P. Sham, K.M. Cheung, Genetics of disc degeneration, European spine journal 15(3) (2006) 317-325.
[103] A.G. Hadjipavlou, M.N. Tzermiadianos, N. Bogduk, M.R. Zindrick, The pathophysiology of disc degeneration, The Journal of bone and joint surgery. British volume 90-B(10) (2008) 1261-1270.
[104] S.J. Millward-Sadler, P.W. Costello, A.J. Freemont, J.A. Hoyland, Regulation of catabolic gene expression in normal and degenerate human intervertebral disc cells: implications for the pathogenesis of intervertebral disc degeneration, Arthritis Research & Therapy 11(3) (2009) R65.
[105] D. Purmessur, B.A. Walter, P.J. Roughley, D.M. Laudier, A.C. Hecht, J. Iatridis, A role for TNFα in intervertebral disc degeneration: A non-recoverable catabolic shift, Biochemical and Biophysical Research Communications 433(1) (2013) 151-156.
[106] C.L. Le Maitre, A.J. Freemont, J.A. Hoyland, The role of interleukin-1 in the pathogenesis of human intervertebral disc degeneration, Arthritis Res Ther 7(4) (2005) R732-45.

[107] J. Hoyland, C. Le Maitre, A. Freemont, Investigation of the role of IL-1 and TNF in matrix degradation in the intervertebral disc, Rheumatology 47(6) (2008) 809-814.
[108] K.L.E. Phillips, K. Cullen, N. Chiverton, A.L.R. Michael, A.A. Cole, L.M. Breakwell, G. Haddock, R.A.D. Bunning, A.K. Cross, C.L. Le Maitre, Potential roles of cytokines and chemokines in human intervertebral disc degeneration: interleukin-1 is a master regulator of catabolic processes, Osteoarthritis and Cartilage 23(7) (2015) 1165-1177.
[109] M.V. Risbud, I.M. Shapiro, Role of cytokines in intervertebral disc degeneration: pain and disc content, Nature Reviews Rheumatology 10 (2013) 44.
[110] H.E. Gruber, G.L. Hoelscher, J.A. Ingram, S. Bethea, H.J. Norton, E.N. Hanley, Production and expression of RANTES (CCL5) by human disc cells and modulation by IL-1-β and TNF-α in 3D culture, Experimental and Molecular Pathology 96(2) (2014) 133-138.
[111] C.Q. Zhao, Y.H. Zhang, S.D. Jiang, H. Li, L.S. Jiang, L.Y. Dai, ADAMTS-5 and intervertebral disc degeneration: the results of tissue immunohistochemistry and in vitro cell culture, J Orthop Res 29(5) (2011) 718-25.
[112] J. Rutges, J.A. Kummer, F.C. Oner, A.J. Verbout, R.J.M. Castelein, H.J.A. Roestenburg, W.J.A. Dhert, L.B. Creemers, Increased MMP-2 activity during intervertebral disc degeneration is correlated to MMP-14 levels, The Journal of Pathology 214(4) (2008) 523-530.
[113] M.D. Martin, C.M. Boxell, D.G. Malone, Pathophysiology of lumbar disc degeneration: a review of the literature, Neurosurgical focus 13(2) (2002) 1-6.
[114] N.V. Vo, R.A. Hartman, T. Yurube, L.J. Jacobs, G.A. Sowa, J.D. Kang, Expression and regulation of metalloproteinases and their inhibitors in intervertebral disc aging and degeneration, Spine J 13(3) (2013) 331-41.
[115] B. Peng, W. Wu, S. Hou, P. Li, C. Zhang, Y. Yang, The pathogenesis of discogenic low back pain, The Journal of bone and joint surgery. British volume 87(1) (2005) 62-67.
[116] A.L.A. Binch, A.A. Cole, L.M. Breakwell, A.L.R. Michael, N. Chiverton, L.B. Creemers, A.K. Cross, C.L. Le Maitre, Nerves are more abundant than blood vessels in the degenerate human intervertebral disc, Arthritis Research & Therapy 17(1) (2015) 370.
[117] D. Purmessur, A.J. Freemont, J.A. Hoyland, Expression and regulation of neurotrophins in the nondegenerate and degenerate human intervertebral disc, Arthritis Res Ther 10(4) (2008) R99.
[118] M.H. Coppes, E. Marani, R.T. Thomeer, G.J. Groen, Innervation of "painful" lumbar discs, Spine (Phila Pa 1976) 22(20) (1997) 2342-9; discussion 2349-50.
[119] I. Ashton, S. Roberts, D. Jaffray, J. Polak, S. Eisenstein, Neuropeptides in the human intervertebral disc, Journal of orthopaedic research 12(2) (1994) 186-192.
[120] A.J. Freemont, T.E. Peacock, P. Goupille, J.A. Hoyland, J. O'Brien, M.I.V. Jayson, Nerve ingrowth into diseased intervertebral disc in chronic back pain, The Lancet 350(9072) (1997) 178-181.
[121] H. Yoshizawa, J.P. O'Brien, W.T. Smith, M. Trumper, The neuropathology of intervertebral discs removed for low-back pain, J Pathol 132(2) (1980) 95-104.
[122] H. Shinohara, [Lumbar disc lesion, with special reference to the histological significance of nerve endings of the lumbar discs], Nihon Seikeigeka Gakkai zasshi 44(8) (1970) 553-70.

[123] D.K. Sengupta, H. Fan, The basis of mechanical instability in degenerative disc disease: a cadaveric study of abnormal motion versus load distribution, Spine 39(13) (2014) 1032-1043.
[124] U. Quint, H.-J. Wilke, Grading of degenerative disk disease and functional impairment: imaging versus patho-anatomical findings, European Spine Journal 17(12) (2008) 1705-1713.
[125] V. Palepu, M. Kodigudla, V.K. Goel, Biomechanics of disc degeneration, Adv Orthop 2012 (2012) 726210-726210.
[126] T.S. Jensen, R. Baron, M. Haanpää, E. Kalso, J.D. Loeser, A.S. Rice, R.-D. Treede, A new definition of neuropathic pain, Pain 152(10) (2011) 2204-2205.
[127] M. Shacklock, M. Rade, S. Poznic, A. Marčinko, M. Fredericson, H. Kröger, M. Kankaanpää, O. Airaksinen, Treatment of Sciatica and Lumbar Radiculopathy with an Intervertebral Foramen Opening Protocol: Pilot Study in a Hospital Emergency and In-patient Setting, Physiotherapy Theory and Practice (2022) 1-11.
[128] E. Krock, D.H. Rosenzweig, A.-J. Chabot-Doré, P. Jarzem, M.H. Weber, J.A. Ouellet, L.S. Stone, L. Haglund, Painful, degenerating intervertebral discs up-regulate neurite sprouting and CGRP through nociceptive factors, Journal of Cellular and Molecular Medicine 18(6) (2014) 1213-1225.
[129] H. Brisby, Pathology and Possible Mechanisms of Nervous System Response to Disc Degeneration, JBJS 88(suppl_2) (2006).
[130] N. Voilley, J. de Weille, J. Mamet, M. Lazdunski, Nonsteroid Anti-Inflammatory Drugs Inhibit Both the Activity and the Inflammation-Induced Expression of Acid-Sensing Ion Channels in Nociceptors, The Journal of Neuroscience 21(20) (2001) 8026-8033.
[131] J. Fairbank, H. Frost, J. Wilson-MacDonald, L.-M. Yu, K. Barker, R. Collins, Randomised controlled trial to compare surgical stabilisation of the lumbar spine with an intensive rehabilitation programme for patients with chronic low back pain: the MRC spine stabilisation trial, Bmj 330(7502) (2005) 1233.
[132] S.K. Mirza, R.A. Deyo, Systematic review of randomized trials comparing lumbar fusion surgery to nonoperative care for treatment of chronic back pain, Spine 32(7) (2007) 816-823.
[133] L.M. Parker, S.E. Murrell, S.D. Boden, W.C. Horton, The outcome of posterolateral fusion in highly selected patients with discogenic low back pain, Spine 21(16) (1996) 1909-1916.
[134] R. Sarafadeen, S.O. Ganiyu, A.A. Ibrahim, Effects of spinal stabilization exercise with real-time ultrasound imaging biofeedback in individuals with chronic nonspecific low back pain: a pilot study, J Exerc Rehabil 16(3) (2020) 293-299.
[135] S. Chung, J. Lee, J. Yoon, Effects of stabilization exercise using a ball on mutifidus cross-sectional area in patients with chronic low back pain, J Sports Sci Med 12(3) (2013) 533-541.
[136] A.H. Buck, A reference handbook of the medical sciences: embracing the entire range of scientific and practical medicine and allied science, W. Wood1885.
[137] D.C. Keyes, E.L. Compere, The normal and pathological physiology of the nucleus pulposus of the intervertebral disc: an anatomical, clinical, and experimental study, JBJS 14(4) (1932) 897-938.

[138] C. Daly, P. Ghosh, G. Jenkin, D. Oehme, T. Goldschlager, A review of animal models of intervertebral disc degeneration: pathophysiology, regeneration, and translation to the clinic, BioMed research international 2016 (2016).
[139] A. Lai, A. Moon, D. Purmessur, B. Skovrlj, D.M. Laudier, B.A. Winkelstein, S.K. Cho, A.C. Hecht, J.C. Iatridis, Annular puncture with tumor necrosis factor-alpha injection enhances painful behavior with disc degeneration in vivo, The Spine Journal 16(3) (2016) 420-431.
[140] T. Oichi, Y. Taniguchi, K. Soma, S.H. Chang, F. Yano, S. Tanaka, T. Saito, A Mouse Intervertebral Disc Degeneration Model by Surgically Induced Instability, Spine 43(10) (2018) E557-E564.
[141] J.R. Deuis, L.S. Dvorakova, I. Vetter, Methods Used to Evaluate Pain Behaviors in Rodents, Front Mol Neurosci 10 (2017) 284-284.
[142] D.J. Nuckley, P.A. Kramer, A. Del Rosario, N. Fabro, S. Baran, R.P. Ching, Intervertebral disc degeneration in a naturally occurring primate model: Radiographic and biomechanical evidence, Journal of Orthopaedic Research 26(9) (2008) 1283-1288.
[143] C. Daly, P. Ghosh, G. Jenkin, D. Oehme, T. Goldschlager, A Review of Animal Models of Intervertebral Disc Degeneration: Pathophysiology, Regeneration, and Translation to the Clinic, BioMed Research International 2016 (2016) 5952165.
[144] C. Abboud, A. Duveau, R. Bouali-Benazzouz, K. Massé, J. Mattar, L. Brochoire, P. Fossat, E. Boué-Grabot, W. Hleihel, M. Landry, Animal models of pain: Diversity and benefits, Journal of Neuroscience Methods 348 (2021) 108997.
[145] H.E. Carlsson, S.J. Schapiro, I. Farah, J. Hau, Use of primates in research: a global overview, American Journal of Primatology: Official Journal of the American Society of Primatologists 63(4) (2004) 225-237.
[146] G.E. Mosley, T.W. Evashwick-Rogler, A. Lai, J.C. Iatridis, Looking beyond the intervertebral disc: the need for behavioral assays in models of discogenic pain, Ann N Y Acad Sci 1409(1) (2017) 51-66.
[147] J.P. Norcross, G.E. Lester, P. Weinhold, L.E. Dahners, An in vivo model of degenerative disc disease, Journal of Orthopaedic Research 21(1) (2003) 183-188.
[148] S. Ohtori, G. Inoue, M. Miyagi, K. Takahashi, Pathomechanisms of discogenic low back pain in humans and animal models, The spine journal 15(6) (2015) 1347-1355.
[149] C. Shi, S. Qiu, S.M. Riester, V. Das, B. Zhu, A.A. Wallace, A.J. van Wijnen, F. Mwale, J.C. Iatridis, D. Sakai, G. Votta-Velis, W. Yuan, H.-J. Im, Animal models for studying the etiology and treatment of low back pain, J Orthop Res 36(5) (2018) 1305-1312.
[150] L. Carbone, Do “Prey Species” Hide Their Pain? Implications for Ethical Care and Use of Laboratory Animals, Journal of Applied Animal Ethics Research 2(2) (2020) 216-236.
[151] J.S. Mogil, Animal models of pain: progress and challenges, Nature Reviews Neuroscience 10(4) (2009) 283-294.
[152] A. Kettler, L. Liakos, B. Haegele, H.J. Wilke, Are the spines of calf, pig and sheep suitable models for pre-clinical implant tests?, European Spine Journal 16(12) (2007) 2186-2192.
[153] P.E. Riches, N. Dhillon, J. Lotz, A.W. Woods, D.S. McNally, The internal mechanics of the intervertebral disc under cyclic loading, J Biomech 35(9) (2002) 1263-71.

[154] Y.W. Kuo, J.L. Wang, Rheology of intervertebral disc: an ex vivo study on the effect of loading history, loading magnitude, fatigue loading, and disc degeneration, Spine (Phila Pa 1976) 35(16) (2010) E743-52.
[155] M. Nikkhoo, R. Kargar, K. Khalaf, Biphasic Rheology of Different Artificial Degenerated Intervertebral Discs, World Congress on Medical Physics and Biomedical Engineering 2018, Springer, 2019, pp. 671-674.
[156] J.C. Beckstein, S. Sen, T.P. Schaer, E.J. Vresilovic, D.M. Elliott, Comparison of animal discs used in disc research to human lumbar disc: axial compression mechanics and glycosaminoglycan content, Spine (Phila Pa 1976) 33(6) (2008) E166-73.
[157] K.H. Lin, Q. Wu, D.J. Leib, S.Y. Tang, A novel technique for the contrast-enhanced microCT imaging of murine intervertebral discs, Journal of the Mechanical Behavior of Biomedical Materials 63 (2016) 66-74.
[158] A. Lai, D.H.K. Chow, W.S. Siu, A.D. Holmes, F.H. Tang, Reliability of radiographic intervertebral disc height measurement for in vivo rat-tail model, Medical Engineering & Physics 29(7) (2007) 814-819.
[159] S. Roberts, H. Evans, J. Trivedi, J. Menage, Histology and pathology of the human intervertebral disc, JBJS 88(suppl_2) (2006) 10-14.
[160] A. Lai, J. Gansau, S.E. Gullbrand, J. Crowley, C. Cunha, S. Dudli, J.B. Engiles, M. Fusellier, R.M. Goncalves, D. Nakashima, Development of a standardized histopathology scoring system for intervertebral disc degeneration in rat models: An initiative of the ORS spine section, JOR Spine (2021) e1150.
[161] C.L. Le Maitre, C.L. Dahia, M. Giers, S. Illien-Junger, C. Cicione, D. Samartzis, G. Vadala, A. Fields, J. Lotz, Development of a standardized histopathology scoring system for human intervertebral disc degeneration: an Orthopaedic Research Society Spine Section Initiative, JOR SPINE 4(2) (2021) e1167.
[162] I.P. Melgoza, S.S. Chenna, S. Tessier, Y. Zhang, S.Y. Tang, T. Ohnishi, E.J. Novais, G.J. Kerr, S. Mohanty, V. Tam, Development of a standardized histopathology scoring system using machine learning algorithms for intervertebral disc degeneration in the mouse model—An ORS spine section initiative, JOR spine 4(2) (2021) e1164.
[163] S.E. Gullbrand, B.G. Ashinsky, A. Lai, J. Gansau, J. Crowley, C. Cunha, J.B. Engiles, M. Fusellier, C. Muehleman, M. Pelletier, Development of a standardized histopathology scoring system for intervertebral disc degeneration and regeneration in rabbit models-An initiative of the ORS spine section, JOR spine 4(2) (2021) e1147.
[164] V.Y.L. Leung, W.C.W. Chan, S.-C. Hung, K.M.C. Cheung, D. Chan, Matrix Remodeling During Intervertebral Disc Growth and Degeneration Detected by Multichromatic FAST Staining, Journal of Histochemistry & Cytochemistry 57(3) (2008) 249-256.
[165] H. Gruber, J. Ingram, E.H. Jr, An improved staining method for intervertebral disc tissue, Biotechnic & histochemistry 77(2) (2002) 81-83.
[166] I.A. Stokes, J.C. Iatridis, Mechanical conditions that accelerate intervertebral disc degeneration: overload versus immobilization, Spine 29(23) (2004) 2724.
[167] G.E. Mosley, R.C. Hoy, P. Nasser, T. Kaseta, A. Lai, T.W. Evashwick-Rogler, M. Lee, J.C. Iatridis, Sex Differences in Rat Intervertebral Disc Structure and Function Following Annular Puncture Injury, Spine 44(18) (2019) 1257-1269.
[168] K. Fujii, A. Lai, N. Korda, W.W. Hom, T.W. Evashwick-Rogler, P. Nasser, A.C. Hecht, J.C. Iatridis, Ex-vivo biomechanics of repaired rat intervertebral discs using

genipin crosslinked fibrin adhesive hydrogel, Journal of Biomechanics 113 (2020) 110100.
[169] R.G. Long, S.G. Rotman, W.W. Hom, D.J. Assael, S. Illien-Jünger, D.W. Grijpma, J.C. Iatridis, In vitro and biomechanical screening of polyethylene glycol and poly(trimethylene carbonate) block copolymers for annulus fibrosus repair, J Tissue Eng Regen Med 12(2) (2018) e727-e736.
[170] A. Cappozzo, Compressive loads in the lumbar vertebral column during normal level walking, Journal of orthopaedic research 1(3) (1983) 292-301.
[171] J.I. Boxberger, J.D. Auerbach, S. Sen, D.M. Elliott, An in vivo model of reduced nucleus pulposus glycosaminoglycan content in the rat lumbar intervertebral disc, Spine 33(2) (2008) 146-154.
[172] D.M. Elliott, C.S. Yerramalli, J.C. Beckstein, J.I. Boxberger, W. Johannessen, E.J. Vresilovic, The Effect of Relative Needle Diameter in Puncture and Sham Injection Animal Models of Degeneration, Spine 33(6) (2008).
[173] E.M. Leimer, M.G. Gayoso, L. Jing, S.Y. Tang, M.C. Gupta, L.A. Setton, Behavioral Compensations and Neuronal Remodeling in a Rodent Model of Chronic Intervertebral Disc Degeneration, Scientific Reports 9(1) (2019) 3759.
[174] S. Ohtori, G. Inoue, M. Miyagi, K. Takahashi, Pathomechanisms of discogenic low back pain in humans and animal models, Spine J 15(6) (2015) 1347-55.
[175] H. Cui, J. Zhang, Z. Li, F. Chen, H. Cui, X. Du, H. Liu, J. Wang, A.D. Diwan, Z. Zheng, Growth differentiation factor-6 attenuates inflammatory and pain-related factors and degenerated disc-induced pain behaviors in rat model, Journal of Orthopaedic Research® 39(5) (2021) 959-970.
[176] Z. Li, H. Liu, H. Yang, J. Wang, H. Wang, K. Zhang, W. Ding, Z. Zheng, Both expression of cytokines and posterior annulus fibrosus rupture are essential for pain behavior changes induced by degenerative intervertebral disc: an experimental study in rats, Journal of orthopaedic research 32(2) (2014) 262-272.
[177] M.-A.A. Rousseau, J.A. Ulrich, E.C. Bass, A.G. Rodriguez, J.J. Liu, J.C. Lotz, Stab Incision for Inducing Intervertebral Disc Degeneration in the Rat, Spine 32(1) (2007).
[178] G.E. Mosley, T.W. Evashwick-Rogler, A. Lai, J.C. Iatridis, Looking beyond the intervertebral disc: the need for behavioral assays in models of discogenic pain, Ann N Y Acad Sci 1409(1) (2017) 51.
[179] Y. Takahashi, T. Chiba, M. Kurokawa, Y. Aoki, Dermatomes and the central organization of dermatomes and body surface regions in the spinal cord dorsal horn in rats, Journal of Comparative Neurology 462(1) (2003) 29-41.
[180] T. Morinaga, K. Takahashi, M. Yamagata, T. Chiba, K. Tanaka, Y. Takahashi, S.-i. Nakamura, K. Suseki, H. Moriya, Sensory innervation to the anterior portion of lumbar intervertebral disc, Spine 21(16) (1996) 1848-1851.
[181] A.P. Malykhina, C. Qin, B. Greenwood-van Meerveld, R.D. Foreman, F. Lupu, H.I. Akbarali, Hyperexcitability of convergent colon and bladder dorsal root ganglion neurons after colonic inflammation: mechanism for pelvic organ cross-talk, Neurogastroenterology & Motility 18(10) (2006) 936-948.
[182] E.E. Ustinova, M.O. Fraser, M.A. Pezzone, Colonic irritation in the rat sensitizes urinary bladder afferents to mechanical and chemical stimuli: an afferent origin of pelvic organ cross-sensitization, American Journal of Physiology-Renal Physiology 290(6) (2006) F1478-F1487.

[183] S. Ohtori, K. Takahashi, H. Moriya, Calcitonin gene-related peptide immunoreactive DRG neurons innervating the cervical facet joints show phenotypic switch in cervical facet injury in rats, European Spine Journal 12(2) (2003) 211-215.
[184] B. Beland, M. Fitzgerald, Influence of peripheral inflammation on the postnatal maturation of primary sensory neuron phenotype in rats, The Journal of Pain 2(1) (2001) 36-45.
[185] S. Ohtori, K. Takahashi, T. Chiba, M. Yamagata, H. Sameda, H. Moriya, Phenotypic inflammation switch in rats shown by calcitonin gene-related peptide immunoreactive dorsal root ganglion neurons innervating the lumbar facet joints, Spine 26(9) (2001) 1009-1013.
[186] M.F. Shamji, K.D. Allen, S. So, L. Jing, S.B. Adams, Jr., R. Schuh, J. Huebner, V.B. Kraus, A.H. Friedman, L.A. Setton, W.J. Richardson, Gait abnormalities and inflammatory cytokines in an autologous nucleus pulposus model of radiculopathy, Spine 34(7) (2009) 648-654.
[187] M.L. LaCroix-Fralish, V.L. Tawfik, J.A. DeLeo, The organizational and activational effects of sex hormones on tactile and thermal hypersensitivity following lumbar nerve root injury in male and female rats, Pain 114(1-2) (2005) 71-80.
[188] M. Miyagi, T. Ishikawa, H. Kamoda, M. Suzuki, Y. Sakuma, S. Orita, Y. Oikawa, Y. Aoki, T. Toyone, K. Takahashi, G. Inoue, S. Ohtori, Assessment of Pain Behavior in a Rat Model of Intervertebral Disc Injury Using the Catwalk Gait Analysis System, Spine 38(17) (2013).
[189] R.N. Walsh, R.A. Cummins, The Open-Field Test: a critical review, Psychological bulletin 83(3) (1976) 482-504.
[190] Y. Fujioka, A. Stahlberg, M. Ochi, K. Olmarker, Expression of Inflammation/Pain-Related Genes in the Dorsal Root Ganglion following Disc Puncture in Rats, Journal of Orthopaedic Surgery 24(1) (2016) 106-112.
[191] D. Fukui, M. Kawakami, M. Yoshida, S.-i. Nakao, T. Matsuoka, H. Yamada, Gait abnormality due to spinal instability after lumbar facetectomy in the rat, European Spine Journal 24(9) (2015) 2085-2094.
[192] H. Cui, J. Zhang, Z. Li, J. Long, F. Chen, H. Cui, X. Du, H. Liu, J. Wang, H. Wang, Growth differentiation factor-6 attenuates inflammatory and pain-related factors and degenerated disc-induced pain behaviors in rat model, Journal of Orthopaedic Research®.
[193] S. Saleem, H.M. Aslam, M.A.K. Rehmani, A. Raees, A.A. Alvi, J. Ashraf, Lumbar disc degenerative disease: disc degeneration symptoms and magnetic resonance image findings, Asian Spine J 7(4) (2013) 322-334.
[194] M. Teraguchi, N. Yoshimura, H. Hashizume, S. Muraki, H. Yamada, A. Minamide, H. Oka, Y. Ishimoto, K. Nagata, R. Kagotani, N. Takiguchi, T. Akune, H. Kawaguchi, K. Nakamura, M. Yoshida, Prevalence and distribution of intervertebral disc degeneration over the entire spine in a population-based cohort: the Wakayama Spine Study, Osteoarthritis and Cartilage 22(1) (2014) 104-110.
[195] A. Muralidharan, T.S.W. Park, J.T. Mackie, L.G.S. Gimenez, A. Kuo, J.R. Nicholson, L. Corradini, M.T. Smith, Establishment and Characterization of a Novel Rat Model of Mechanical Low Back Pain Using Behavioral, Pharmacologic and Histologic Methods, Frontiers in pharmacology 8 (2017) 493-493.

[196] T.S.W. Park, N. Khan, A. Kuo, J.R. Nicholson, L. Corradini, M.T. Smith, J-2156, a somatostatin receptor type 4 agonist, alleviates mechanical hyperalgesia in a rat model of chronic low back pain, Biomedicine & Pharmacotherapy 117 (2019) 109056.
[197] A. Kuo, J. Lourdesamy, J.R. Nicholson, L. Corradini, M.T. Smith, Assessment of the anti-hyperalgesic efficacy of J-2156, relative to clinically available analgesic/adjuvant agents in a rat model of mild to moderate chronic mechanical low back pain (LBP), Clinical and Experimental Pharmacology and Physiology 47(12) (2020) 1912-1922.
[198] J.D. Glaeser, W. Tawackoli, D.G. Ju, J.H. Yang, L.E.A. Kanim, K. Salehi, V. Yu, E. Saidara, J.-P. Vit, Z. Khnkoyan, Z. NaPier, L.S. Stone, H.W. Bae, D. Sheyn, Optimization of a rat lumbar IVD degeneration model for low back pain, JOR SPINE 3(2) (2020) e1092.
[199] A. Lai, A. Moon, D. Purmessur, B. Skovrlj, B.A. Winkelstein, S.K. Cho, A.C. Hecht, J.C. Iatridis, Assessment of functional and behavioral changes sensitive to painful disc degeneration, J Orthop Res 33(5) (2015) 755-764.
[200] A. Muralidharan, T.S. Park, J.T. Mackie, L.G. Gimenez, A. Kuo, J.R. Nicholson, L. Corradini, M.T. Smith, Establishment and characterization of a novel rat model of mechanical low back pain using behavioral, pharmacologic and histologic methods, Frontiers in pharmacology 8 (2017) 493.
[201] I.L.M. Isa, S.A. Abbah, M. Kilcoyne, D. Sakai, P. Dockery, D.P. Finn, A. Pandit, Implantation of hyaluronic acid hydrogel prevents the pain phenotype in a rat model of intervertebral disc injury, Science Advances 4(4) (2018) eaaq0597.
[202] T. Evashwick-Rogler, A. Lai, H. Watanabe, J. Salandra, B. Winkelstein, S. Cho, Inhibiting tumor necrosis factor-alpha at time of induced intervertebral disc injury limits long-term pain and degeneration in a rat model. JOR Spine. 2018; 1 (2).
[203] A. Lai, L. Ho, T.W. Evashwick-Rogler, H. Watanabe, J. Salandra, B.A. Winkelstein, D. Laudier, A.C. Hecht, G.M. Pasinetti, J.C. Iatridis, Dietary polyphenols as a safe and novel intervention for modulating pain associated with intervertebral disc degeneration in an in-vivo rat model, PLOS ONE 14(10) (2019) e0223435.
[204] T.W. Evashwick-Rogler, A. Lai, H. Watanabe, J.M. Salandra, B.A. Winkelstein, S.K. Cho, A.C. Hecht, J.C. Iatridis, Inhibiting tumor necrosis factor-alpha at time of induced intervertebral disc injury limits long-term pain and degeneration in a rat model, JOR Spine 1(2) (2018).
[205] I. Altun, Cytokine profile in degenerated painful intervertebral disc: variability with respect to duration of symptoms and type of disease, The Spine Journal 16(7) (2016) 857-861.
[206] M.-A.A. Rousseau, J.A. Ulrich, E.C. Bass, A.G. Rodriguez, J.J. Liu, J.C. Lotz, Stab incision for inducing intervertebral disc degeneration in the rat, Spine 32(1) (2007) 17-24.
[207] N. Willems, A.R. Tellegen, N. Bergknut, L.B. Creemers, J. Wolfswinkel, C. Freudigmann, K. Benz, G.C.M. Grinwis, M.A. Tryfonidou, B.P. Meij, Inflammatory profiles in canine intervertebral disc degeneration, BMC Veterinary Research 12(1) (2016) 10.
[208] T. TANriVErDi, M. HANC, Catabolic cytokine expressions in patients with degenerative disc disease, Turkish neurosurgery 20(4) (2010) 492-499.
[209] M. Lee, B.-J. Kim, E.J. Lim, S.K. Back, J.-H. Lee, S.-W. Yu, S.-H. Hong, J.H. Kim, S.-H. Lee, W.-W. Jung, D. Sul, H.S. Na, Complete Freund's Adjuvant-Induced

Intervertebral Discitis as an Animal Model for Discogenic Low Back Pain, Anesthesia & Analgesia 109(4) (2009).
[210] Q. Liu, X. Wang, Y. Hua, G. Kong, X. Wu, Z. Huang, Z. Huang, J. Liu, Z. Yang, Q. Zhu, Estrogen deficiency exacerbates intervertebral disc degeneration induced by spinal instability in rats, Spine 44(9) (2019) E510-E519.
[211] G. Crevensten, A.J. Walsh, D. Ananthakrishnan, P. Page, G.M. Wahba, J.C. Lotz, S. Berven, Intervertebral disc cell therapy for regeneration: mesenchymal stem cell implantation in rat intervertebral discs, Annals of biomedical engineering 32(3) (2004) 430-434.
[212] A.A. Allon, N. Aurouer, B.B. Yoo, E.C. Liebenberg, Z. Buser, J.C. Lotz, Structured coculture of stem cells and disc cells prevent disc degeneration in a rat model, The Spine Journal 10(12) (2010) 1089-1097.
[213] C.-Z. Liang, H. Li, Y.-Q. Tao, X.-P. Zhou, Z.-R. Yang, F.-C. Li, Q.-X. Chen, The relationship between low pH in intervertebral discs and low back pain: a systematic review, Arch Med Sci 8(6) (2012) 952-956.
[214] F. Wang, L.-p. Nan, S.-f. Zhou, Y. Liu, Z.-y. Wang, J.-c. Wang, X.-m. Feng, L. Zhang, Injectable hydrogel combined with nucleus pulposus-derived mesenchymal stem cells for the treatment of degenerative intervertebral disc in rats, Stem cells international 2019 (2019).
[215] J. Ge, Q. Yan, Y. Wang, X. Cheng, D. Song, C. Wu, H. Yu, H. Yang, J. Zou, IL-10 delays the degeneration of intervertebral discs by suppressing the p38 MAPK signaling pathway, Free Radical Biology and Medicine 147 (2020) 262-270.
[216] A.J. Walsh, D.S. Bradford, J.C. Lotz, In vivo growth factor treatment of degenerated intervertebral discs, Spine 29(2) (2004) 156-163.
[217] H. Zhang, L. Wang, J.B. Park, P. Park, V.C. Yang, S.J. Hollister, F. La Marca, C.-Y. Lin, Intradiscal injection of simvastatin retards progression of intervertebral disc degeneration induced by stab injury, Arthritis research & therapy 11(6) (2009) 1-10.
[218] G. Marfia, R. Campanella, S.E. Navone, I. Zucca, A. Scotti, M. Figini, C. Di Vito, G. Alessandri, L. Riboni, E. Parati, Potential use of human adipose mesenchymal stromal cells for intervertebral disc regeneration: a preliminary study on biglycan-deficient murine model of chronic disc degeneration, Arthritis research & therapy 16(5) (2014) 1-13.
[219] D.S. Mern, T. Walsen, A. Beierfuß, C. Thomé, Animal models of regenerative medicine for biological treatment approaches of degenerative disc diseases, Experimental Biology and Medicine 246(4) (2020) 483-512.
[220] K. Akeda, K. Ohishi, K. Masuda, W.C. Bae, N. Takegami, J. Yamada, T. Nakamura, T. Sakakibara, Y. Kasai, A. Sudo, Intradiscal injection of autologous platelet-rich plasma releasate to treat discogenic low back pain: a preliminary clinical trial, Asian Spine J 11(3) (2017) 380.
[221] Y.C. Huang, Y. Hu, Z. Li, K.D. Luk, Biomaterials for intervertebral disc regeneration: Current status and looming challenges, J Tissue Eng Regen Med 12(11) (2018) 2188-2202.
[222] R.a. Markets, Biomaterials Market Size, Share & Trends Analysis Report by Product (Natural, Metallic, Polymer), by Application (Cardiovascular, Orthopedics, Plastic Surgery), by Region, and Segment Forecasts, 2020 - 2027, Biomaterials Market (2020).

[223] J.M. Morais, F. Papadimitrakopoulos, D.J. Burgess, Biomaterials/tissue interactions: possible solutions to overcome foreign body response, The AAPS journal 12(2) (2010) 188-196.
[224] M.D. Swartzlander, C.A. Barnes, A.K. Blakney, J.L. Kaar, T.R. Kyriakides, S.J. Bryant, Linking the foreign body response and protein adsorption to PEG-based hydrogels using proteomics, Biomaterials 41 (2015) 26-36.
[225] A.D. Lynn, T.R. Kyriakides, S.J. Bryant, Characterization of the in vitro macrophage response and in vivo host response to poly (ethylene glycol)-based hydrogels, Journal of Biomedical Materials Research Part A: An Official Journal of The Society for Biomaterials, The Japanese Society for Biomaterials, and The Australian Society for Biomaterials and the Korean Society for Biomaterials 93(3) (2010) 941-953.
[226] J.M. Aamodt, D.W. Grainger, Extracellular matrix-based biomaterial scaffolds and the host response, Biomaterials 86 (2016) 68-82.
[227] X. Lin, X. Fang, Q. Wang, Z. Hu, K. Chen, Z. Shan, S. Chen, J. Wang, J. Mo, J. Ma, W. Xu, A. Qin, S. Fan, Decellularized allogeneic intervertebral disc: natural biomaterials for regenerating disc degeneration, Oncotarget 7(11) (2016) 12121-12136.
[228] N. Mehrban, C. Pineda Molina, L.M. Quijano, J. Bowen, S.A. Johnson, J. Bartolacci, J.T. Chang, D.A. Scott, D.N. Woolfson, M.A. Birchall, S.F. Badylak, Host macrophage response to injectable hydrogels derived from ECM and α-helical peptides, Acta Biomaterialia 111 (2020) 141-152.
[229] H. Cui, Y. Chai, Y. Yu, Progress in developing decellularized bioscaffolds for enhancing skin construction, Journal of Biomedical Materials Research Part A 107(8) (2019) 1849-1859.
[230] S. Illien-Jünger, D.D. Sedaghatpour, D.M. Laudier, A.C. Hecht, S.A. Qureshi, J.C. Iatridis, Development of a bovine decellularized extracellular matrix-biomaterial for nucleus pulposus regeneration, Journal of orthopaedic research 34(5) (2016) 876-888.
[231] M.C. Cramer, S.F. Badylak, Extracellular matrix-based biomaterials and their influence upon cell behavior, Annals of biomedical engineering 48(7) (2020) 2132-2153.
[232] J.J. Mercuri, S.S. Gill, D.T. Simionescu, Novel tissue-derived biomimetic scaffold for regenerating the human nucleus pulposus, Journal of biomedical materials research Part A 96(2) (2011) 422-435.
[233] L.K. Chan, V.Y. Leung, V. Tam, W.W. Lu, K. Sze, K.M. Cheung, Decellularized bovine intervertebral disc as a natural scaffold for xenogenic cell studies, Acta biomaterialia 9(2) (2013) 5262-5272.
[234] Z. Huang, B. Kohl, M. Kokozidou, S. Arens, G. Schulze-Tanzil, Establishment of a cytocompatible cell-free intervertebral disc matrix for chondrogenesis with human bone marrow-derived mesenchymal stromal cells, Cells Tissues Organs 201(5) (2016) 354-365.
[235] L.M. Piening, D.J. Lillyman, F.S. Lee, A.M. Lozano, J.R. Miles, R.A. Wachs, Injectable decellularized nucleus pulposus tissue exhibits neuroinhibitory properties, JOR SPINE n/a(n/a) (2022) e1187.
[236] E.A. Growney Kalaf, M. Pendyala, J.G. Bledsoe, S.A. Sell, Characterization and restoration of degenerated IVD function with an injectable, in situ gelling alginate hydrogel: An in vitro and ex vivo study, Journal of the Mechanical Behavior of Biomedical Materials 72 (2017) 229-240.

[237] K. Nam, A. Kishida, Application of the Collagen as Biomaterials, Biomedical Materials and Diagnostic Devices (2012) 1-17.
[238] X. Zhou, J. Wang, X. Huang, W. Fang, Y. Tao, T. Zhao, C. Liang, J. Hua, Q. Chen, F. Li, Injectable decellularized nucleus pulposus-based cell delivery system for differentiation of adipose-derived stem cells and nucleus pulposus regeneration, Acta Biomaterialia 81 (2018) 115-128.
[239] S. Mohanty, R. Pinelli, P. Pricop, T.J. Albert, C.L. Dahia, Chondrocyte-like nested cells in the aged intervertebral disc are late-stage nucleus pulposus cells, Aging cell 18(5) (2019) e13006.
[240] H.-W. Sung, D.-M. Huang, W.-H. Chang, R.-N. Huang, J.-C. Hsu, Evaluation of gelatin hydrogel crosslinked with various crosslinking agents as bioadhesives: In vitro study, Journal of Biomedical Materials Research 46(4) (1999) 520-530.
[241] R.M. Dunn, Cross-Linking in Biomaterials: A Primer for Clinicians, Plastic and Reconstructive Surgery 130(5S-2) (2012).
[242] H.S. Abandansari, M.H. Ghanian, F. Varzideh, E. Mahmoudi, S. Rajabi, P. Taheri, M.R. Nabid, H. Baharvand, In situ formation of interpenetrating polymer network using sequential thermal and click crosslinking for enhanced retention of transplanted cells, Biomaterials 170 (2018) 12-25.
[243] H. Tan, C.R. Chu, K.A. Payne, K.G. Marra, Injectable in situ forming biodegradable chitosan–hyaluronic acid based hydrogels for cartilage tissue engineering, Biomaterials 30(13) (2009) 2499-2506.
[244] A.A. Athens, E.A. Makris, J.C. Hu, Induced Collagen Cross-Links Enhance Cartilage Integration, PLOS ONE 8(4) (2013) e60719.
[245] N. Reddy, R. Reddy, Q. Jiang, Crosslinking biopolymers for biomedical applications, Trends in biotechnology 33(6) (2015) 362-369.
[246] H.W. Sung, W.H. Chang, C.Y. Ma, M.H. Lee, Crosslinking of biological tissues using genipin and/or carbodiimide, Journal of Biomedical Materials Research Part A: An Official Journal of The Society for Biomaterials, The Japanese Society for Biomaterials, and The Australian Society for Biomaterials and the Korean Society for Biomaterials 64(3) (2003) 427-438.
[247] A. Bigi, G. Cojazzi, S. Panzavolta, N. Roveri, K. Rubini, Stabilization of gelatin films by crosslinking with genipin, Biomaterials 23(24) (2002) 4827-4832.
[248] H.W. Sung, I.L. Liang, C.N. Chen, R.N. Huang, H.F. Liang, Stability of a biological tissue fixed with a naturally occurring crosslinking agent (genipin), Journal of Biomedical Materials Research: An Official Journal of The Society for Biomaterials, The Japanese Society for Biomaterials, and The Australian Society for Biomaterials and the Korean Society for Biomaterials 55(4) (2001) 538-546.
[249] Y.-J. Hwang, J. Larsen, T.B. Krasieva, J.G. Lyubovitsky, Effect of Genipin Crosslinking on the Optical Spectral Properties and Structures of Collagen Hydrogels, ACS Applied Materials & Interfaces 3(7) (2011) 2579-2584.
[250] R.M. Schek, A.J. Michalek, J.C. Iatridis, Genipin-crosslinked fibrin hydrogels as a potential adhesive to augment intervertebral disc annulus repair, European cells & materials 21 (2011) 373-383.
[251] H.G. Sundararaghavan, G.A. Monteiro, N.A. Lapin, Y.J. Chabal, J.R. Miksan, D.I. Shreiber, Genipin-induced changes in collagen gels: Correlation of mechanical properties

to fluorescence, Journal of Biomedical Materials Research Part A 87A(2) (2008) 308-320.
[252] S. Tarafder, G.Y. Park, J. Felix, C.H. Lee, Bioadhesives for musculoskeletal tissue regeneration, Acta Biomaterialia 117 (2020) 77-92.
[253] S.L. James, D. Abate, K.H. Abate, S.M. Abay, C. Abbafati, N. Abbasi, H. Abbastabar, F. Abd-Allah, J. Abdela, A. Abdelalim, Global, regional, and national incidence, prevalence, and years lived with disability for 354 diseases and injuries for 195 countries and territories, 1990–2017: a systematic analysis for the Global Burden of Disease Study 2017, The Lancet 392(10159) (2018) 1789-1858.
[254] L. Hestbaek, C. Leboeuf-Yde, C. Manniche, Low back pain: what is the long-term course? A review of studies of general patient populations, European Spine Journal 12(2) (2003) 149-165.
[255] B.I. Martin, R.A. Deyo, S.K. Mirza, J.A. Turner, B.A. Comstock, W. Hollingworth, S.D. Sullivan, Expenditures and health status among adults with back and neck problems, Jama 299(6) (2008) 656-664.
[256] M. Racine, Chronic pain and suicide risk: A comprehensive review, Progress in Neuro-Psychopharmacology and Biological Psychiatry 87 (2018) 269-280.
[257] A. Shmagel, R. Foley, H. Ibrahim, Epidemiology of Chronic Low Back Pain in US Adults: Data From the 2009-2010 National Health and Nutrition Examination Survey, Arthritis Care Res (Hoboken) 68(11) (2016) 1688-1694.
[258] I.M. Shapiro, M.V. Risbud, Intervertebral Disc, Springer2016.
[259] C.M. De Geer, Intervertebral Disk Nutrients and Transport Mechanisms in Relation to Disk Degeneration: A Narrative Literature Review, J Chiropr Med 17(2) (2018) 97-105.
[260] J.F. Griffith, Y.-X.J. Wang, G.E. Antonio, K.C. Choi, A. Yu, A.T. Ahuja, P.C. Leung, Modified Pfirrmann grading system for lumbar intervertebral disc degeneration, Spine 32(24) (2007) E708-E712.
[261] D.D. Sun, K.W. Leong, A nonlinear hyperelastic mixture theory model for anisotropy, transport, and swelling of annulus fibrosus, Annals of biomedical engineering 32(1) (2004) 92-102.
[262] H. Inoue, K. Ohmori, K. Miyasaka, H. Hosoe, Radiographic evaluation of the lumbosacral disc height, Skeletal radiology 28(11) (1999) 638-643.
[263] K.H. Lin, S.Y. Tang, The quantitative structural and compositional analyses of degenerating intervertebral discs using magnetic resonance imaging and contrast-enhanced micro-computed tomography, Annals of biomedical engineering 45(11) (2017) 2626-2634.
[264] G.D. O'Connell, E.J. Vresilovic, D.M. Elliott, Comparison of animals used in disc research to human lumbar disc geometry, Spine 32(3) (2007) 328-333.
[265] M.D. Newton, A.A. Marek, M. Planalp, D.K. Park, K.C. Baker, T. Maerz, Longitudinal characterization of intervertebral disc remodeling following acute annular injury in a rat model of degenerative disc disease, Connective tissue research 61(6) (2020) 568-576.
[266] A. Sasov, D. Van Dyck, Desktop X-ray microscopy and microtomography, Journal of microscopy 191(2) (1998) 151-158.

[267] G. Delling, M. Hahn, U. Bonse, F. Busch, O. Günnewig, F. Beckmann, H. Uebbing, W. Graeff, New possibilities for structural analysis of bone biopsies using microcomputer tomography (muCT), Der Pathologe 16(5) (1995) 342-347.
[268] A. Behrooz, J.-C. Tseng, J. Meganck, M. Hopkinton, Image resolution in MicroCT: principles and characterization of the quantum FX and quantum GX systems, Preclin. Vivo Imaging (2016) 1-5.
[269] C. Cunha, S. Lamas, R.M. Gonçalves, M.A. Barbosa, Joint analysis of IVD herniation and degeneration by rat caudal needle puncture model, Journal of Orthopaedic Research 35(2) (2017) 258-268.
[270] H. Choi, S. Tessier, E.S. Silagi, R. Kyada, F. Yousefi, N. Pleshko, I.M. Shapiro, M.V. Risbud, A novel mouse model of intervertebral disc degeneration shows altered cell fate and matrix homeostasis, Matrix Biology 70 (2018) 102-122.
[271] R. Molteni, Prospects and challenges of rendering tissue density in Hounsfield units for cone beam computed tomography, Oral surgery, oral medicine, oral pathology and oral radiology 116(1) (2013) 105-119.
[272] N. Batawil, S. Sabiq, Hounsfield unit for the diagnosis of bone mineral density disease: a proof of concept study, Radiography 22(2) (2016) e93-e98.
[273] H.M. Sohn, J.W. You, J.Y. Lee, The Relationship between Disc Degeneration and Morphologic Changes in the Intervertebral Foramen of the Cervical Spine: A Cadaveric MRI and CT Study, jkms 19(1) (2004) 101-106.
[274] M.D. Newton, S.E. Hartner, K. Gawronski, E.J. Davenport, S.C. Timmons, K.C. Baker, T. Maerz, Nondestructive, indirect assessment of the biomechanical properties of the rat intervertebral disc using contrast-enhanced μCT, Journal of Orthopaedic Research® 36(7) (2018) 2030-2038.
[275] N. Holguin, G. Uzer, F.-P. Chiang, C. Rubin, S. Judex, Brief daily exposure to low-intensity vibration mitigates the degradation of the intervertebral disc in a frequency-specific manner, Journal of Applied Physiology 111(6) (2011) 1846-1853.
[276] C.G. Maher, Effective physical treatment for chronic low back pain, The Orthopedic clinics of North America 35(1) (2004) 57-64.
[277] Y. Lu, J.Z. Guzman, D. Purmessur, J.C. Iatridis, A.C. Hecht, S.A. Qureshi, S.K. Cho, Nonoperative management of discogenic back pain: a systematic review, Spine 39(16) (2014) 1314-1324.
[278] S. Mohanty, C.L. Dahia, Defects in intervertebral disc and spine during development, degeneration, and pain: New research directions for disc regeneration and therapy, Wiley Interdiscip Rev Dev Biol 8(4) (2019) e343-e343.
[279] B.-G. Peng, Pathophysiology, diagnosis, and treatment of discogenic low back pain, World J Orthop 4(2) (2013) 42-52.
[280] J.G. Burke, R.W. Watson, D. McCormack, F.E. Dowling, M.G. Walsh, J.M. Fitzpatrick, Intervertebral discs which cause low back pain secrete high levels of proinflammatory mediators, The Journal of bone and joint surgery. British volume 84(2) (2002) 196-201.
[281] O.-G. Berge, Predictive validity of behavioural animal models for chronic pain, British Journal of Pharmacology 164(4) (2011) 1195-1206.
[282] T. Denayer, T. Stöhr, M. Van Roy, Animal models in translational medicine: Validation and prediction, New Horizons in Translational Medicine 2(1) (2014) 5-11.

[283] G. Blackburn-Munro, Pain-like behaviours in animals–how human are they?, Trends in pharmacological sciences 25(6) (2004) 299-305.
[284] I. Levenfus, An efficient method for counting DAPI-stained cells using Fiji, GRIN Verlag2011.
[285] L. Jin, G. Balian, X.J. Li, Animal models for disc degeneration-an update, Histol Histopathol 33(6) (2018) 543-554.
[286] Y.X.J. Wáng, J.-Q. Wáng, Z. Káplár, Increased low back pain prevalence in females than in males after menopause age: evidences based on synthetic literature review, Quant Imaging Med Surg 6(2) (2016) 199-206.
[287] D.L. DeMoss, G.L. Wright, Sex and strain differences in whole skeletal development in the rat, Calcified tissue international 62(2) (1998) 153-7.
[288] H. Takeshita, K. Yamamoto, S. Nozato, T. Inagaki, H. Tsuchimochi, M. Shirai, R. Yamamoto, Y. Imaizumi, K. Hongyo, S. Yokoyama, M. Takeda, R. Oguro, Y. Takami, N. Itoh, Y. Takeya, K. Sugimoto, S.-I. Fukada, H. Rakugi, Modified forelimb grip strength test detects aging-associated physiological decline in skeletal muscle function in male mice, Scientific reports 7 (2017) 42323-42323.
[289] I. Urits, A. Burshtein, M. Sharma, L. Testa, P.A. Gold, V. Orhurhu, O. Viswanath, M.R. Jones, M.A. Sidransky, B. Spektor, Low back pain, a comprehensive review: pathophysiology, diagnosis, and treatment, Current pain and headache reports 23(3) (2019) 1-10.
[290] S.C. Lee, Percutaneous intradiscal treatments for discogenic pain, Acta Anaesthesiologica Taiwanica 50(1) (2012) 25-28.
[291] M. Millecamps, L.S. Stone, Delayed onset of persistent discogenic axial and radiating pain after a single-level lumbar intervertebral disc injury in mice, PAIN 159(9) (2018).
[292] M. Millecamps, M. Tajerian, L. Naso, E.H. Sage, L.S. Stone, Lumbar intervertebral disc degeneration associated with axial and radiating low back pain in ageing SPARC-null mice, Pain 153(6) (2012) 1167-1179.
[293] J.-J. Vatine, S.C. Shapira, F. Magora, D. Adler, A. Magora, Electronic pressure algometry of deep pain in healthy volunteers, Archives of Physical Medicine and Rehabilitation 74(5) (1993) 526-530.
[294] A.Y. Neziri, M. Curatolo, A. Limacher, E. Nüesch, B. Radanov, O.K. Andersen, L. Arendt-Nielsen, P. Jüni, Ranking of parameters of pain hypersensitivity according to their discriminative ability in chronic low back pain, PAIN® 153(10) (2012) 2083-2091.
[295] Y. Aoki, Y. Takahashi, K. Takahashi, T. Chiba, M. Kurokawa, T. Ozawa, H. Moriya, Sensory innervation of the lateral portion of the lumbar intervertebral disc in rats, The Spine Journal 4(3) (2004) 275-280.
[296] S. Ohtori, Y. Takahashi, K. Takahashi, M. Yamagata, T. Chiba, K. Tanaka, J. Hirayama, H. Moriya, Sensory innervation of the dorsal portion of the lumbar intervertebral disc in rats, Spine (Phila Pa 1976) 24(22) (1999) 2295-9.
[297] H. Hyodo, T. Sato, H. Sasaki, Y. Tanaka, Discogenic pain in acute nonspecific low-back pain, European Spine Journal 14(6) (2005) 573-577.
[298] S. Jay Lipson, H. Muir, Experimental intervertebral disc degeneration. Morphologic and proteoglycan changes over time, Arthritis & Rheumatism: Official Journal of the American College of Rheumatology 24(1) (1981) 12-21.

[299] M.E. Goldstein, S.B. House, H. Gainer, NF-L and peripherin immunoreactivities define distinct classes of rat sensory ganglion cells, Journal of neuroscience research 30(1) (1991) 92-104.
[300] M. Fornaro, J.M. Lee, S. Raimondo, S. Nicolino, S. Geuna, M. Giacobini-Robecchi, Neuronal intermediate filament expression in rat dorsal root ganglia sensory neurons: An in vivo and in vitro study, Neuroscience 153(4) (2008) 1153-1163.
[301] D.L. Hammond, L. Ackerman, R. Holdsworth, B. Elzey, Effects of spinal nerve ligation on immunohistochemically identified neurons in the L4 and L5 dorsal root ganglia of the rat, Journal of Comparative Neurology 475(4) (2004) 575-589.
[302] T.J. Price, M.D. Louria, D. Candelario-Soto, G.O. Dussor, N.A. Jeske, A.M. Patwardhan, A. Diogenes, A.A. Trott, K.M. Hargreaves, C.M. Flores, Treatment of trigeminal ganglion neurons in vitro with NGF, GDNF or BDNF: effects on neuronal survival, neurochemical properties and TRPV1-mediated neuropeptide secretion, BMC neuroscience 6(1) (2005) 1-15.
[303] H. Pionchon, M. Tommasi, J. Pialat, B. Bancel, J. Chazal, G. Escande, T. Scheye, G. Vanneuville, [Study of the innervation of the spinal ligaments at the lumbar level], Bulletin de l'Association des anatomistes 70(210) (1986) 63-7.
[304] C. Weiler, A.G. Nerlich, B.E. Bachmeier, N. Boos, Expression and Distribution of Tumor Necrosis Factor Alpha in Human Lumbar Intervertebral Discs: A Study in Surgical Specimen and Autopsy Controls, Spine 30(1) (2005).
[305] F.-J. Lyu, H. Cui, H. Pan, K. Mc Cheung, X. Cao, J.C. Iatridis, Z. Zheng, Painful intervertebral disc degeneration and inflammation: from laboratory evidence to clinical interventions, Bone Research 9(1) (2021) 7.
[306] O.L. Osti, B. Vernon-Roberts, R. Moore, R.D. Fraser, Annular tears and disc degeneration in the lumbar spine. A post-mortem study of 135 discs, The Journal of bone and joint surgery. British volume 74-B(5) (1992) 678-682.
[307] W.-e. Wang, R.L.M. Ho, B. Gatto, S.M. van der Veen, M.K. Underation, J.S. Thomas, A.B. Antony, S.A. Coombes, Cortical dynamics of movement-evoked pain in chronic low back pain, The Journal of Physiology 599(1) (2021) 289-305.
[308] S. Young, C. Aprill, M. Laslett, Correlation of clinical examination characteristics with three sources of chronic low back pain, The Spine Journal 3(6) (2003) 460-465.
[309] H.E. Gruber, B. Gordon, C. Williams, H.J. Norton, E.N. Hanley, Jr., Vertebral endplate and disc changes in the aging sand rat lumbar spine: cross-sectional analyses of a large male and female population, Spine (Phila Pa 1976) 32(23) (2007) 2529-36.
[310] B. Peng, J. Hao, S. Hou, W. Wu, D. Jiang, X. Fu, Y. Yang, Possible pathogenesis of painful intervertebral disc degeneration, Spine 31(5) (2006) 560-566.
[311] Q. Xu, H. Fang, L. Zhao, C. Zhang, L. Zhang, B. Tian, Mechano growth factor attenuates mechanical overload-induced nucleus pulposus cell apoptosis through inhibiting the p38 MAPK pathway, Bioscience reports 39(3) (2019) BSR20182462.
[312] R. He, Z. Wang, M. Cui, S. Liu, W. Wu, M. Chen, Y. Wu, Y. Qu, H. Lin, S. Chen, B. Wang, Z. Shao, HIF1A Alleviates compression-induced apoptosis of nucleus pulposus derived stem cells via upregulating autophagy, Autophagy 17(11) (2021) 3338-3360.
[313] Y. Zhuo, H. Wang, L. Zou, Y. Wang, Y. Hu, P. Li, Q. Zhou, SIRT1 Attenuates Apoptosis of Nucleus Pulposus Cells by Targeting Interactions between LC3B and Fas under High-Magnitude Compression, Oxid Med Cell Longev 2021 (2021) 2420969-2420969.

[314] O.M. Torre, V. Mroz, M.K. Bartelstein, A.H. Huang, J.C. Iatridis, Annulus fibrosus cell phenotypes in homeostasis and injury: implications for regenerative strategies, Ann N Y Acad Sci 1442(1) (2019) 61-78.
[315] P. Lama, C.L. Le Maitre, I.J. Harding, P. Dolan, M.A. Adams, Nerves and blood vessels in degenerated intervertebral discs are confined to physically disrupted tissue, Journal of anatomy 233(1) (2018) 86-97.
[316] S.M. Richardson, D. Purmessur, P. Baird, B. Probyn, A.J. Freemont, J.A. Hoyland, Degenerate human nucleus pulposus cells promote neurite outgrowth in neural cells, PloS one 7(10) (2012) e47735-e47735.
[317] M. Wang, D. Zhu, J. Zhu, R. Nussinov, B. Ma, Local and global anatomy of antibody-protein antigen recognition, J Mol Recognit 31(5) (2018) e2693-e2693.
[318] J. Hernandez-Lallement, P. Gómez-Sotres, M. Carrillo, Towards a unified theory of emotional contagion in rodents—A meta-analysis, Neuroscience & Biobehavioral Reviews (2020).
[319] J.C. Lotz, J.A. Ulrich, Innervation, inflammation, and hypermobility may characterize pathologic disc degeneration: review of animal model data, JBJS 88(suppl_2) (2006) 76-82.
[320] S.-Y. Ma, H.-D. Kim, The Efficacy of Spinal Decompression via DRX3000 Combined with a Spinal Mobilization and a Lumbar Stabilization Exercise Program for Patients with Discogenic Low Back Pain, Journal of Physical Therapy Science 22(4) (2010) 345-354.
[321] K. Olmarker, A. Gerward, B. Isberg, A. Lehmann, S. Berg, Translational Studies on Biologic Fusion of a Vertebral Segment as a Novel Treatment Modality for Low Back Pain, Spine 45(24) (2020) E1636-E1644.
[322] M. Zusman, Associative memory for movement-evoked chronic back pain and its extinction with musculoskeletal physiotherapy, Physical Therapy Reviews 13(1) (2008) 57-68.
[323] K. Wuertz, L. Haglund, Inflammatory mediators in intervertebral disk degeneration and discogenic pain, Global spine journal 3(3) (2013) 175-184.
[324] Z.I. Johnson, Z.R. Schoepflin, H. Choi, I.M. Shapiro, M.V. Risbud, Disc in flames: Roles of TNF-α and IL-1β in intervertebral disc degeneration, European cells & materials 30 (2015) 104.
[325] T. Di Pauli von Treuheim, O.M. Torre, G.E. Mosley, P. Nasser, J.C. Iatridis, Measuring the neutral zone of spinal motion segments: comparison of multiple analysis methods to quantify spinal instability, JOR spine 3(2) (2020) e1088.
[326] I.A. Stokes, D.F. Counts, J.W. Frymoyer, Experimental instability in the rabbit lumbar spine, Spine (Phila Pa 1976) 14(1) (1989) 68-72.
[327] K. Gong, W. Shao, H. Chen, Z. Wang, Z.-J. Luo, Rat model of lumbar facet joint osteoarthritis associated with facet-mediated mechanical hyperalgesia induced by intra-articular injection of monosodium iodoacetate, Journal of the Formosan Medical Association 110(3) (2011) 145-152.
[328] P. Suri, A. Miyakoshi, D.J. Hunter, J.G. Jarvik, J. Rainville, A. Guermazi, L. Li, J.N. Katz, Does lumbar spinal degeneration begin with the anterior structures? A study of the observed epidemiology in a community-based population, BMC Musculoskeletal Disorders 12(1) (2011) 202.

[329] M. Stefanakis, M. Al-Abbasi, I. Harding, P. Pollintine, P. Dolan, J. Tarlton, M.A. Adams, Annulus fissures are mechanically and chemically conducive to the ingrowth of nerves and blood vessels, Spine 37(22) (2012) 1883-1891.
[330] J.S. Cheng, C.B. Carr, C. Wong, A. Sharma, M.R. Mahfouz, R.D. Komistek, Altered spinal motion in low back pain associated with lumbar strain and spondylosis, Evid Based Spine Care J 4(1) (2013) 6-12.
[331] N. Gusi, A. Raimundo, A. Leal, Low-frequency vibratory exercise reduces the risk of bone fracture more than walking: a randomized controlled trial, BMC musculoskeletal disorders 7(1) (2006) 1-8.
[332] H. Yang, M.G. Jekir, M.W. Davis, T.M. Keaveny, Effective modulus of the human intervertebral disc and its effect on vertebral bone stress, J Biomech 49(7) (2016) 1134-1140.
[333] T.J. Gan, Diclofenac: an update on its mechanism of action and safety profile, Current medical research and opinion 26(7) (2010) 1715-31.
[334] M. Schattenkirchner, K. Milachowski, A double-blind, multicentre, randomised clinical trial comparing the efficacy and tolerability of aceclofenac with diclofenac resinate in patients with acute low back pain, Clinical rheumatology 22(2) (2003) 127-135.
[335] A. Ximenes, M. Robles, G. Sands, R. Vinueza, Valdecoxib is as efficacious as diclofenac in the treatment of acute low back pain, The Clinical journal of pain 23(3) (2007) 244-250.
[336] F. Hu, Z. Pan, C. Liu, X. Dong, Z. Zhang, Q. Ji, W. Hu, S. Zhang, Y. Zhang, Z. Sun, Identification of inflammatory regulation roles of thalidomide/ruxolitinib in nucleus pulposus and construction of polyelectrolyte nanocomplexes-impregnated injectable hydrogels for synergistic intervertebral disk degeneration treatment, Nano Today 44 (2022) 101462.
[337] G. Tang, B. Zhou, F. Li, W. Wang, Y. Liu, X. Wang, C. Liu, X. Ye, Advances of naturally derived and synthetic hydrogels for intervertebral disk regeneration, Frontiers in Bioengineering and Biotechnology 8 (2020) 745.
[338] S. Nakashima, Y. Matsuyama, K. Takahashi, T. Satoh, H. Koie, K. Kanayama, T. Tsuji, K. Maruyama, S. Imagama, Y. Sakai, Regeneration of intervertebral disc by the intradiscal application of cross-linked hyaluronate hydrogel and cross-linked chondroitin sulfate hydrogel in a rabbit model of intervertebral disc injury, Bio-medical materials and engineering 19(6) (2009) 421-429.
[339] H. Jia, X. Lin, D. Wang, J. Wang, Q. Shang, X. He, K. Wu, B. Zhao, P. Peng, H. Wang, Injectable hydrogel with nucleus pulposus-matched viscoelastic property prevents intervertebral disc degeneration, Journal of orthopaedic translation 33 (2022) 162-173.
[340] U.Y. Choi, H.P. Joshi, S. Payne, K.T. Kim, J.W. Kyung, H. Choi, M.J. Cooke, S.Y. Kwon, E.J. Roh, S. Sohn, An Injectable Hyaluronan–Methylcellulose (HAMC) Hydrogel combined with Wharton's jelly-derived mesenchymal Stromal cells (WJ-MSCs) promotes degenerative disc repair, International journal of molecular sciences 21(19) (2020) 7391.
[341] X. Huang, C. Zheng, W. Wang, X. Ye, C.-Y. Lin, Z. Wu, The Effect and Possible Mechanism of Intradiscal Injection of Simvastatin in the Treatment of Discogenic Pain in Rats, Frontiers in Neuroscience 15 (2021).

[342] C. Bombardier, J. Hayden, D.E. Beaton, Minimal clinically important difference. Low back pain: outcome measures, The Journal of Rheumatology 28(2) (2001) 431.
[343] H. Takahashi, Y. Aoki, M. Inoue, J. Saito, A. Nakajima, M. Sonobe, Y. Akatsu, K. Koyama, Y. Shiga, K. Inage, Y. Eguchi, S. Orita, S. Maki, T. Furuya, T. Akazawa, T. Abe, T. Funayama, H. Noguchi, K. Miura, K. Mataki, Y. Shibao, F. Eto, M. Kono, M. Koda, M. Yamazaki, S. Ohtori, K. Nakagawa, Characteristics of relief and residual low back pain after discectomy in patients with lumbar disc herniation: analysis using a detailed visual analog scale, BMC Musculoskeletal Disorders 22(1) (2021) 167.
[344] F. Ter Heegde, A.P. Luiz, S. Santana-Varela, I.P. Chessell, F. Welsh, J.N. Wood, C. Chenu, Noninvasive mechanical joint loading as an alternative model for osteoarthritic pain, Arthritis & Rheumatology 71(7) (2019) 1078-1088.
[345] C.W. Pfirrmann, D. Resnick, Schmorl nodes of the thoracic and lumbar spine: radiographic-pathologic study of prevalence, characterization, and correlation with degenerative changes of 1,650 spinal levels in 100 cadavers, Radiology 219(2) (2001) 368-374.
[346] L. Gross, Y. Dreyfuss, Spontaneous tumors in Sprague-Dawley and Long-Evans rats and in their F1 hybrids: carcinogenic effect of total-body x-irradiation, Proceedings of the National Academy of Sciences of the United States of America 76(11) (1979) 5910-5913.
[347] O.A. Meyer, H.A. Tilson, W.C. Byrd, M.T. Riley, A method for the routine assessment of fore- and hindlimb grip strength of rats and mice, Neurobehavioral toxicology 1(3) (1979) 233-6.
[348] E.H. Park, S.W. Moon, H.R. Suh, S. Hochman, M.-G. Lee, Y. Kim, I. Jang, H.C. Han, Disc degeneration induces a mechano-sensitization of disc afferent nerve fibers that associates with low back pain, Osteoarthritis and cartilage 27(11) (2019) 1608-1617.
[349] K.R. Nakazawa, B.A. Walter, D.M. Laudier, D. Krishnamoorthy, G.E. Mosley, K.L. Spiller, J.C. Iatridis, Accumulation and localization of macrophage phenotypes with human intervertebral disc degeneration, Spine J 18(2) (2018) 343-356.
[350] H. Yang, B. Liu, Y. Liu, D. He, Y. Xing, Y. An, W. Tian, Secreted factors from intervertebral disc cells and infiltrating macrophages promote degenerated intervertebral disc catabolism, Spine 44(9) (2019) E520-E529.
[351] Y. Yamamoto, Y. Kokubo, H. Nakajima, K. Honjoh, S. Watanabe, A. Matsumine, Distribution and Polarization of Hematogenous Macrophages Associated with the Progression of Intervertebral Disc Degeneration, Spine 47(4) (2022) E149-E158.
[352] J.S. Mogil, Laboratory environmental factors and pain behavior: the relevance of unknown unknowns to reproducibility and translation, Lab animal 46(4) (2017) 136-141.
[353] D.-S. Liu, T.-L. Xu, Cell-Type Identification in the Autonomic Nervous System, Neurosci Bull 35(1) (2019) 145-155.
[354] K. Newton, D.L. Dugger, K.E. Wickliffe, N. Kapoor, M.C. de Almagro, D. Vucic, L. Komuves, R.E. Ferrando, D.M. French, J. Webster, Activity of protein kinase RIPK3 determines whether cells die by necroptosis or apoptosis, Science 343(6177) (2014) 1357-1360.
[355] G. Niu, X. Chen, Apoptosis imaging: beyond annexin V, Journal of Nuclear Medicine 51(11) (2010) 1659-1662.